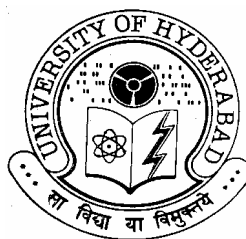# Interaction of major bovine seminal plasma protein, PDC-109 and its domain B with phospholipids and soluble ligands

A thesis
submitted for the degree of
DOCTOR OF PHILOSOPHY

By

Rajani Swarnalatha Damai

School of Chemistry
University of Hyderabad
Hyderabad – 500 046
INDIA
April 2008

CONTENTS

ABBREVIATIONS

ANS	-	8-anilino-1-naphthlene-sulfonic acid
Apo A1	-	Apolipoprotein A1
AR	-	Acrosome reaction
bis-ANS	-	4,4'-dianilino-1,1'-binaphthyl-5,5'-disulphonic acid
BSP	-	Bovine seminal plasma
C	-	Carbon
Ca^{2+}	-	Calcium ion
Cs^{+}	-	Cesium ion
cAMP	-	cyclic Adenosine mono phosphate
cDNA	-	Complementary DNA
CSA	-	Chemical shift anisotropy
CD	-	Circular dichroism
Chol.	-	Cholesterol
Da	-	Dalton
DEAE	-	Diethylaminoethyl
DMPA	-	1,2-dimyristoyl –*sn*-glycero-3-phosphatidic acid
DMPC	-	1,2-dimyristoyl –*sn*-glycero-3-phosphocholine
DMPE	-	1,2-dimyristoyl –*sn*-glycero-3-phosphoethanolamine
DMPG	-	1,2-dimyristoyl –*sn*-glycero-3-phosphoglycerol
DNA	-	Deoxyribonucleicacid

DOPC	-	1,2-dioleyl –*sn*-glycero-3-phosphocholine
DPG	-	Diphosphatidylglycerol
DPPG	-	1,2-dipalmitoyl –*sn*-glycero-3- phosphoglycerol
EDTA	-	Ethylenediamine tetra acetic acid
ESR	-	Electron spin resonance
Fn	-	Fibronectin
GAG	-	Glycosaminoglycans
HDL	-	High density lipoprotein
I$^-$	-	Iodide
ITC	-	Isothermal titration calorimetry
K_a	-	Association constant
Lyso-PC	-	Lysophosphatidylcholine
MLVs	-	Multilamellar vesicles
NaCl	-	Sodium chloride
PA	-	Phosphatidic acid
PAF	-	Platelet activating factor
PC	-	Phosphatidylcholine
PDC-109		Protein contains *N*-terminal asparatic acid, D and *C*-terminal cystine, C with 109 amino acids
PDC-109/B	-	Domain B of PDC-109
PE	-	Phosphatidylethanolamine
PI	-	Phosphatidylinositol

^{31}P-NMR	-	Phosphorous-31 Nuclear magnetic resonance
ppm	-	Parts per million
PrC	-	Phosphorylcholine
PS	-	Phosphatidylserine
REES	-	Red-edge excitation shift
SDS	-	Sodium dodecyl sulphate
SM	-	Sphingomyelin
sn	-	Stereo specific numbering
SPR	-	Surface plasmon resonance
SUV	-	Small unilamellar vesicles
TBS I	-	Tris buffer containing, 50 mM Tris, 0.15 M NaCl, 5 mM EDTA, 0.025% NaN$_3$, pH = 7.4
TBS II	-	Tris buffer containing, 25 mM Tris, 1 M NaCl, 0.025% NaN$_3$, pH = 6.4
Thr (T)	-	Threonine
TNS	-	2-(*p*-toluidino) naphthalene-6-sulfonic acid
Trp (W)	-	Tryptophan
Tyr (Y)	-	Tyrosine
ZP	-	Zona pellucida

Chapter 1

Introduction

1.1. Biomembrane

The cell is a highly organized entity with many functional units or organelles. Most of these units are limited by one or more membranes. Membranes play a central role in both the structure and function of prokaryotic and eukaryotic, plant and animal cells. Electron micrographs of mammalian cells reveal the wealth of membranous organelles which comprise a large part of the intracellular volume. The structural features for all these membranes are basically same [Robertson, 1959]. The diversity in membranes function is primarily due to the different functions of the proteins present in each membrane and to the way in which these proteins interact with each other as well as with cytoplasmic components. These interactions result in distinct morphologies, such as in the microvilli of the intestinal epithelium or the tubular endoplasmic reticulum, and may result in lateral inhomogeneities within a given membrane. Membranes are vital because they separate the cell from the outside world. They also separate compartments inside the cell to protect important processes and events. In essence membranes are essential for the integrity and function of the cell.

1.1.2. Functions of cell membrane

The most important functions of the cell membrane are the following:

1) Protection of the cellular constituents by providing a semi-permeable barrier which selectively allows only certain types of molecules/ions to pass through. In addition, a number of membrane-associated proteins regulate the passage of different types of molecules or ions into the cell or out of the cell. Selective permeability is essential for effective separation of a cell or organelle from its surroundings.

2) Allowing selective reception of information and signal transduction by providing transmembrane receptors that bind signaling molecules.

3) Cell recognition by the interaction of cell-surface receptors with complementary ligands on opposing cells.

4) Providing anchoring sites for cytoskeletal filaments or components of the extra cellular matrix, which lends strength to the plasma membrane and also allows the cell to maintain its shape.

5) Helping in compartmentalization of sub-cellular domains or micro-domains.

6) Providing a stable site for the binding and catalysis of enzymes. The inner mitochondrial membrane and the thylakoid membrane of chloroplasts contain complex system of many enzymes and proteins.

7) Regulating the fusion of the membrane with other membranes in the cell via special junctions.

8) Allowing directed cell or organelle motility.

1.2. Membrane structure

1.2.1 Historical background

In the middle of nineteenth century, it was recognized that plasma membrane is a discrete structure at the surface of cell. In 1925 Gorter and Grendel proposed that lipids in the erythrocyte membrane are arranged in the form of a bimolecular leaflet or lipid bilayer [Gorter et al., 1925]. The bilayer model was further elaborated in 1935 by Davson and Danielli in the 'paucimolecular' model, which postulated that proteins coat the surface of the lipid bilayer [Danielli & Davson, 1935]. Freeze-fracture electron microscopic studies revealed globular particles/proteins embedded within the membrane [Branton, 1966, 1971; Bullivant, 1974]. Spectroscopic

evidence also indicated that membrane proteins had an appreciable amount of α-helix and that they were likely to be globular rather than spread out in a monolayer on the lipid bilayer surface [Lenard & Singer, 1966; Wallach & Zahler, 1966]. The non-polar characteristics of membrane proteins [Green & Fleischer, 1963; Richardson et al., 1964] indicated that hydrophobic contacts between the proteins and the lipid bilayer interior must be contributing significantly to the overall interaction between the transmembrane proteins and the lipid bilayer.

1.2.2. Fluid mosaic model

In 1972, Singer and Nicolson combined the above ideas in to the fluid mosaic model, which basically pictures that the matrix, or continuous part of membrane, is a nonpolar lipid bilayer. The bilayer is fluid because the hydrophobic tails of its constituent lipids consist of an appropriate mixture of saturated and unsaturated fatty acids that is fluid at normal temperature of the cell. The term mosaic is consistent with the presence of a variety of molecules in the membrane including proteins, cholesterol, phospholipids, glycolipids etc. The Fluid-mosaic model proposes that the intrinsic or integral membrane proteins have hydrophobic amino acid R groups on their surfaces that interact with hydrophobic fatty acyl groups of the membrane lipid bilayer. On the other hand, peripheral or extrinsic proteins have essentially hydrophilic R groups on their surfaces, which are bound by electrostatic attraction to the hydrophilic, and electrically charged polar heads of the bilayer lipids. The integral membrane proteins, which include enzymes and transport systems, are inactive unless they are placed inside the hydrophobic core of the bilayer, which produces the proper three-dimensional conformation for their activity. Fig. 1.1 gives a schematic view of the fluid-mosaic model.
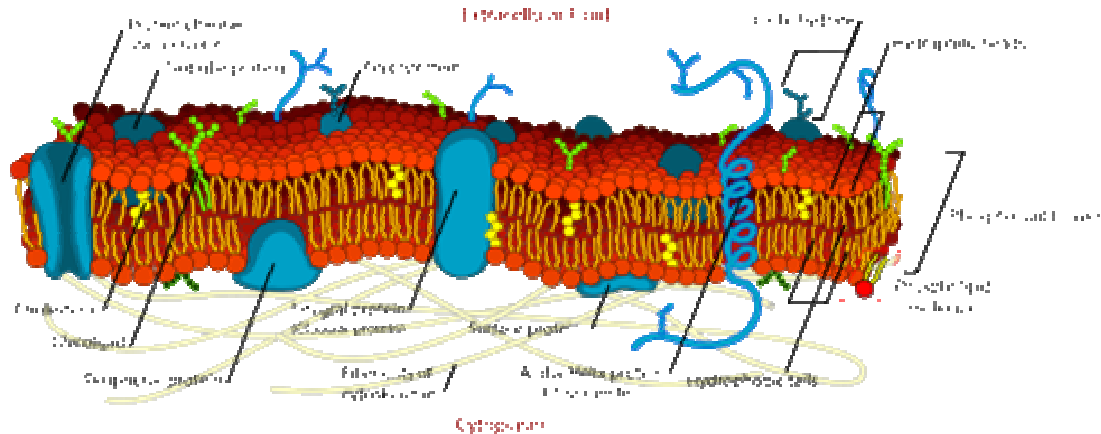
Fig. 1.1. Fluid mosaic structure of membrane (Taken from http://en.wikipedia.org/wiki/plasma_ membrane).

According to the fluid-mosaic model, individual phospholipids diffuse rapidly throughout the two-dimensional surface of the membrane. This model further allows the movement of proteins laterally through fluid-like phospholipid bilayer to varying degrees [Singer & Nicolson, 1972; Singer, 1974]. Membrane proteins diffuse throughout the membrane at a slower pace because of their massive size (the molecular weight of a phospholipid may be 650 Daltons), and a medium sized membrane protein can be about 100,000 Daltons). From time to time a given phospholipid can "flip-flop" through the membrane to the opposite side, but this is uncommon. This requires the hydrophilic head of the phospholipid to pass fully through the highly hydrophobic interior of the membrane, and for the hydrophobic tails to be exposed to the aqueous environment. Over the years the fluid mosaic model has undergone some modifications. In particular, it is now clear that membrane proteins do not all diffuse freely in the fluid lipid bilayer [Jacobson, 1983]. Also there is evidence for the presence of lateral domains within membrane, which are enriched with many kinds of lipids such as cholesterol, glycolipids, and

sphingolipids, present in cell membranes; these microdomains are currently being referred to as "lipid rafts" [Jain & White, 1977; Thompson & Tillack, 1985; Simons & van Meer, 1988; Simons & Toomre, 2000]. Moreover, some regions of biological membranes may not be arranged in the traditional bilayer form [Cullis et al., 1983].

1.3. Composition of membranes

A mosaic is a structure made up of many different parts. Likewise, the plasma membrane is composed of different kinds of macromolecules. The components of a plasma membrane are integral membrane proteins, peripheral membrane proteins, glycoproteins, phospholipids, glycolipids, cholesterol and lipoproteins. In addition to being composed of different components, the relative amounts of these components can vary from membrane to membrane. Table 1.1 shows some of the variation in protein, lipid and carbohydrate content of some membranes. Not only do membranes vary in the relative amount of lipid they contain, the kinds of lipids in membranes can also vary. Table 1.2 shows the proportions of various kinds of lipids in different membranes.

Table 1.1: Protein, lipid and carbohydrate composition of some membranes.*

Membrane	% protein	% lipid	% carbohydrate
Myelin	18	79	3
Human erythrocyte plasma membrane	49	43	8
Mitochondrial inner membrane	79	24	0
Amoeba plasma membrane	54	42	4

* Taken from http://academic.brooklyn.cuny.edu/biology/bio4fv/page/pm_mos.htm

Table 1.2: Different proportions of lipids in some membranes.*

Membrane	Cholesterol	Phosphotidyl-choline (PC)	Sphingomyelin (SM)	Phosphotidyl-serine (PS)	glyco-lipids
Rat liver plasma membrane	30	18	14	9	-
Rat liver RER	6	55	3	3	-
Rat liver nuclear membrane	10	55	3	3	-
Rat liver myelin	22	11	6	7	12

*Taken from http://academic.brooklyn.cuny.edu/biology/bio4fv/page/pm_mos.htm

1.3.1. Lipids

Lipids are a large and diverse group of naturally occurring organic compounds that are insoluble in aqueous solutions and soluble in organic solvents such as ether, chloroform, acetone and benzene. All lipids are predominantly hydrophobic because they consist largely of long hydrocarbon tails which are hydrophobic in nature. This group of molecules includes fats and oils, waxes, phospholipids, steroids (like cholesterol), and some other related compounds. In living organisms, lipids are used for energy storage, serve as structural components of cell membranes, and both lipids and lipid derivatives serve as vitamins and hormones. Lipids are found in all organisms including viruses. Lipids are generally classified into two types; i) *complex lipids*, which yield smaller molecules on hydrolyses such as fats and waxes, and ii) *simple lipids*, which cannot be hydrolyzed, such as cholesterol and other steroids.

1.3.2. Membrane lipids

The major components of membranes are proteins and lipids. The most striking feature of membrane lipids is their enormous diversity. The reasons for the heterogeneity are not clear, although there is an increasing awareness of the multiple roles of lipids in membranes. The most important function is that the lipid mixture must form a stable bilayer in which the proteins can function. Some lipids may be required because their shapes favor packing configurations that may be necessary to stabilize regions of high curvature, junctions between membranes, or optimal interactions with specific proteins [De Kruijff, 1987; Cullis et al., 1986]. Some lipids are important as regulatory agents, most notable being the derivatives of phosphotidylinositol in the plasma membrane of eukaryotic cells. The lipids in membranes are usually made up of a non-polar portion, mostly polymethylene chains and a polar portion, such as choline, glycerol, ethanolamine etc. Membranes contain three major kinds of lipids; they are phospholipids, glycolipids and sterols.

Phospholipids: The lipids in the plasma membrane are chiefly phospholipids. They can be of two types: glycerophospholipids (or phosphoglycerolipids) and phosphosphingolipids. Phospholipids are amphiphilic, contain a negatively charged phosphate moiety in the head group and two long, highly hydrophobic hydrocarbon chains (tails). The tails of the phospholipids orient towards each other creating a hydrophobic environment within the membrane. This leaves the charged phosphate groups facing out into the hydrophilic environment.

Glycerophospholipids are the major class of naturally occurring phospholipids found in biomembranes. One of the two primary hydroxyls of the glycerol is connected to a polar group via a phosphodiester linkage and the other two hydroxyls are linked to long hydrocarbon chains by ester- or ether linkages (Fig.
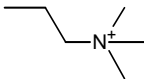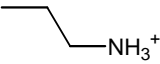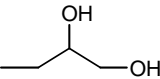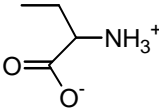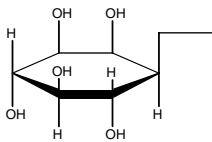
1.2).   Most phosphoglycerides have the phosphate group at *sn*-3 position of glycerol.   The phosphate is usually linked to one of the several groups as indicated in Table 1.3, including choline, ethanolamine, inositol, serine and glycerol.   The hydrocarbon chains vary widely in terms of length, branching and degree of unsaturation.
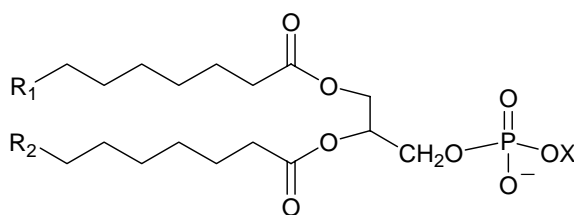
Fig. 1.2. The general structure of a glycerophospholipid.   Phospholipids are named after the head-group alcohol (X), with prefix "phosphatidyl".

Phosphatidic acid (PA), the simplest among glycerophospholipids, is only a minor membrane constituent.   Its principal role is as an intermediate in the synthesis of other glycerophospholipids.   Fig. 1.2 shows that the glycerophospholipids have polar head groups, all carrying some charge. Phosphatidylcholine is a major component in animal cell membranes, and phosphatidylethanolamine is often a major component in bacterial membranes.   The acyl chains mostly have an even number of carbon atoms, ranging from C14 to C24, most common being C16, C18 and C20.   The degree of unsatuaration also varies widely, but most common unsaturated acyl chains are 18:1, 18:2, 18:3 and 20:4.   Nearly all naturally occurring double bonds are *cis* rather than *trans,* resulting in a kink in the molecule which is generally disruptive of ordered packing of the chains in the bilayer [Gennis, 1989; Mathews et al., 2003].   Increasing the unsaturation in membrane lipids results in an increase in the membrane fluidity.

Table 1.3: List of head groups (X) attached to the phosphate moiety of glycerophospholipids.

Name of the Glycerophospholipid	-X
Phosphatidic acid	-H
Phosphatidylcholine (Lecithin)	
Phosphaitidylethanolamine (Cephalin)	
Phosphatidylglycerol	
Phosphatidylserine	
Phosphatidylinositol	
Diphosphatidylglycerol (Cardiolipin, DPG)	Phosphatidylglycerol

Plasmologens are phosphoglycerides where one of the hydrocarbon chains is linked via vinyl ether linkage. Ethanolamine plasmologens are an important component of myelin and of the cardiac sarcoplasmic reticulum [Gross, 1985]. *Cardiolipins* are essentially dimeric phospholipids. They are important component of the

mitochondrial inner membrane, chloroplast membrane and some bacterial membranes.

Sphingolipids and glycerosphingolipids are another major class of membrane constituents built on the long-chain amino alcohol sphingosine, rather than on glycerol.   They contain the same kind of polar head groups as in the glycerophospholipids, but the hydrophobic group is ceramide (Fig. 1.3). Sphingomyelin (ceramide 1-phosphorylcholine) is widely found in animal cell plasma membranes.
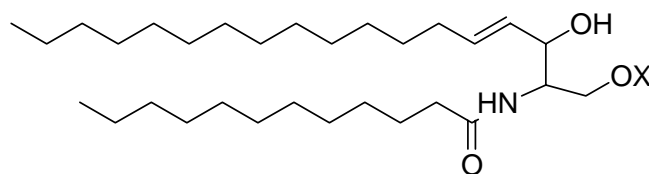
Fig. 1.3. The general structure of sphingolipid

Glycolipids have a glycosidic linkage to the terminal hydroxyl of ceramide. Monoglycosyl ceramides are generally known as cerebrosides.   The structure of glucosylcerebroside is given in Fig. 1.4.   Gangliosides are a class of anionic glycosphingolipids that contain one or more molecules of sialic acid linked to the sugar residues of ceramide oligosaccharides.   Glycolipids are found on the outer surface of the plasma membrane.   Glycosphingolipids in the erythrocyte membrane carry blood group antigens [Gardas, 1976; Dejter-Juszynski et al., 1978].
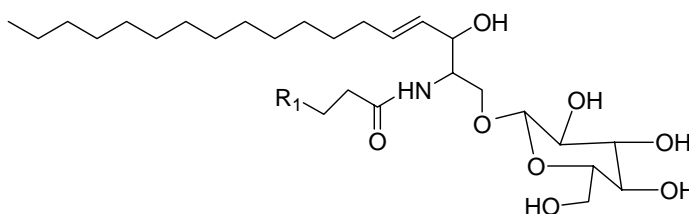
Fig. 1.4. Structure of glucosylcerebroside.

Sterols are found in many plant, animal and microbial membranes. Cholesterol is the most commonly found sterol in the animal tissues. It is a compact, polycyclic, rigid hydrophobic entity with a polar hydroxyl group. Cholesterol is present in animal plasma membrane, lysosomes, endosomes and golgi and constitutes about 30% of the mass of the membrane lipids [Evans & Hardison, 1985]. It is important in the metabolism of eukaryotic cells because it is a component of cell membrane and is involved in maintaining the membrane order (fluidity). It is a precursor to many steroid hormones. The hydroxyl group of cholesterol is oriented in the membrane such that it interacts with the water inside the cell or outside the cell. Other sterols, sitosterol and stigmasterol are found in higher plants [Jain, 1988].
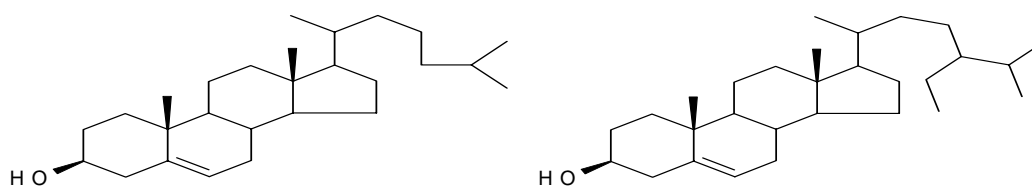
Fig. 1.5. Structure of cholesterol and stigmasterol.

1.3.3. Membrane proteins

Membranes contain between 20% and 80% (w/w) protein. Proteins are the biochemically active components of the membrane and provide the diversity of enzymes, transporters, receptors, pores, etc. which distinguish different membranes. The lipid bilayer carries two types of proteins in it. *Integral membrane proteins* or transmembrane proteins completely go through the lipid bilayer and their association with the membrane interior is well stabilized by hydrophobic interactions [Mathews et al., 2003]. Most of the initially characterized integral proteins contained α-helical transmembrane segments; however, more recently a number of transmembrane proteins have been shown to have a predominantly β-

sheet structure, e.g., the bacterial outermembrane proteins such as OmpA [Arora et al., 2001]. Many membrane proteins carry oligosaccharide groups (*glycoproteins*) that project into the surrounding aqueous medium [Roth, 1987; Hirschberg, 1987]. The two sides of the bilayer are usually different, both in lipid composition and in the placement and orientation of proteins and oligosaccharides. *Peripheral membrane proteins* are exposed at only one membrane face or the other. They mostly contain a large proportion of the positively charged lysine and arginine residues, and exhibit specific binding to negatively charged lipids. They are held to the membrane by ionic or other weak interaction with lipid heads or integral membrane proteins [Mathews et al., 2003]. An example of peripheral membrane protein is cytochrome *c* present in the electron transport chain. Peripheral proteins are generally water soluble and can be easily removed from membrane. Some peripheral proteins are derivatized by a fatty acyl chain, e.g. a palmitoyl chain which gets embedded into the hydrophobic interior of the membrane, this anchoring the protein to the membrane.
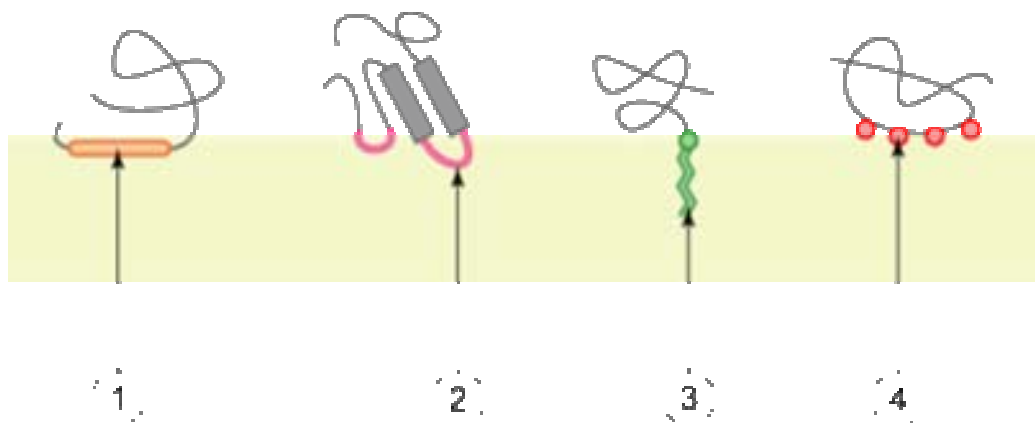
Fig. 1.6. Peripheral membrane proteins. (1) Interaction by an amphipathic α-helix parellel to the membrane plane (in plane membrane) **(2)** Interaction by a hydrophobic loop **(3)** Interaction by a covalently bound membrane lipid (lipidation) **(4)** Electrostatic or ionic interactions with membrane lipids. (Taken from http://en.wikipedia.org/wiki/peripheral_membrane_proteins)

(1)   **(2)**   **(3)**
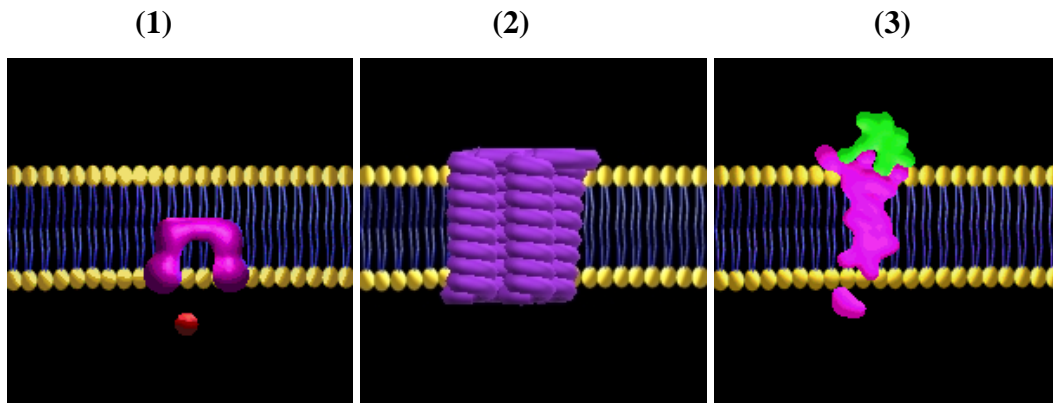
Fig. 1.7. Integral membrane proteins (1) carrier protein that regulates transport and diffusion **(2)** marker protein that identify cells to others **(3)** receptor protein that allow cell to receive instructions. (Taken from http://www.ibiblio.org/virtualcell/textbook/chapter3/cms2.htm)

Integral membrane proteins are largely buried within the hydrophobic regions of phospholipid bilayer but are usually exposed on both faces [Mathews et al., 2003]. The integral membrane proteins contain amino acid residues with hydrophobic side chains that interact with fatty acyl groups of the membrane lipids (e.g., bacteriorhodopsin) [Henderson & Unwin, 1975]. These proteins can only be removed from the membrane through harsh treatment with detergents or non-polar solvents [Helenius & Simons, 1975; Tanford & Reynolds, 1976]. Integral proteins are frequently involved in transmitting either specific substances or chemical signals through the membrane. Integral membrane proteins include Na^+- K^+ ATPase, glucose permease, hormone receptors, ion channels and gates, histocompatibility antigens, certain enzymes of the electron transport chains and gap junction proteins [Segrest et al., 1973; Foster et al., 1983; Engelman et al., 1982; Cheifetz et al., 1985]. The NADH-CoQ reductase complex of enzymes and cytochrome *c* reductase complex of enzymes are integral membrane proteins of the mitochondrial electron transport chain. Cytochrome *c* is a peripherial membrane protein because it is associated with the other integral membrane proteins but it does not penetrate into the inner mitochondrial membrane.

1.4. Self-aggregation of lipids

The lipids in the plasma membrane are chiefly phospholipids such as phosphatidylcholine and phosphatidylethanolamine and cholesterol. When the amphiphilic phospholipids are mixed with water, a variety of aggregates such as micells, bilayers and liposomes or vesicles are formed depending on the specific conditions such as temperature, pressure, ionic strength, pH and nature of the lipids used. The major thermodynamic driving force that stabilizes hydrated lipid aggregates is the hydrophobic force by which contact between the nonpolar portions of the lipid and water is minimized as hydrophobic acyl chains of the lipids come together such that only the hydrophilic head groups interact with water. Other stabilizing forces are short, weak *van der waals* forces between adjacent hydrocarbons chains. This attraction results from interactions between polarizable electrons and hydrogen bonding between polar head groups of some lipid molecules such as phosphatidylethanolamine.

1.4.1. Micelles

In polar media such as water, the hydrophobic part of the amphiphiles forming the micelle tends to locate away from the polar phase while the polar parts of the molecule (head groups) tend to locate at the polar micelle solvent interface. Such micelles may contain thousands of lipid molecules. A micelle may take several forms, depending on the conditions and composition of the system, such as distorted spheres, disks, or rods (Fig. 1.8.A). Micelles are also formed in nonpolar media such as benzene, where the amphiphiles cluster around small water droplets in the system, forming an assembly known as a reversed micelle.

(A)   **(B)**
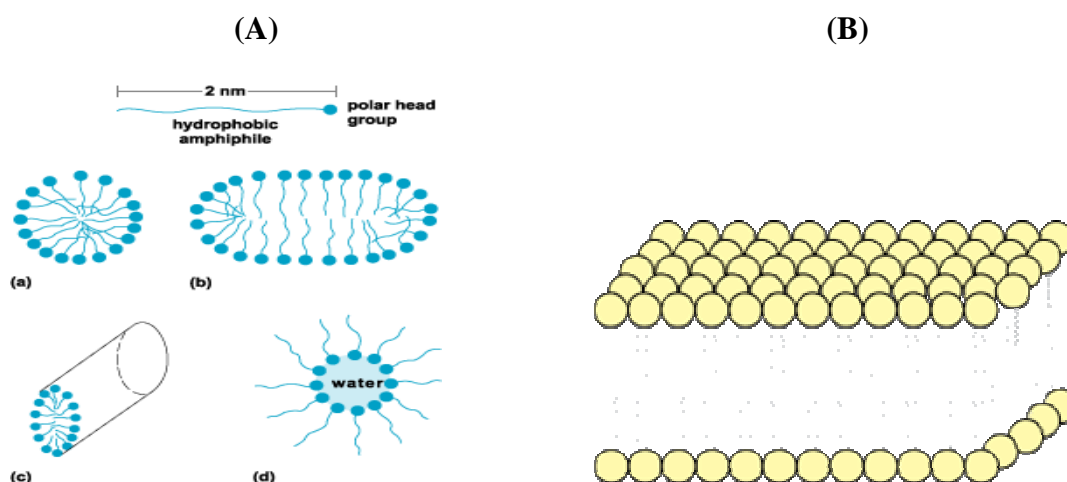
Fig. 1.8. (A) Form of an amphiphile and several forms of micelle: (a) spherical, (b) disk, (c) rod, and (d) reversed (Taken from sci-tech encyclopedia) **(B)** phospholipid bilayer (Taken from http://en.wikipedia.org/wiki/ plasma_membrane).

1.4.2. Bilayers

Polar lipids also spontaneously form very thin bilayers separating two aqueous compartments. In these structures the hydrocarbon tails of the lipid molecules extend inward from the two surfaces of water to form a continuous inner hydrocarbon core, and the hydrophilic heads face towards aqueous phases. Phospholipid bilayers are about 6-7 nm thick depending on the nature of fatty acids in the lipids (Fig. 1.8.B).

1.4.3. Monolayers

Polar lipids also spread spontaneously on the surface of aqueous solutions to form a layer one molecule thick, i.e., a *monolayer*. In such system the hydrocarbon tails of polar lipids are exposed to air, thus avoiding the water, and hydrophilic heads extend into the polar water phase.

1.4.4. Liposomes

A liposome is a spherical vesicle with a membrane composed of a phospholipid (or phospholipid/cholesterol) bilayer. Liposomes are used to deliver certain vaccines, enzymes, or drugs (e.g., insulin and some cancer drugs) to the body due to their unique properties.   A liposome encapsulates an aqueous solution inside a hydrophobic membrane; dissolved hydrophilic solutes can not readily pass through the lipids. Hydrophobic chemicals can be dissolved into the membrane, and in this way liposome can carry both hydrophobic molecules and hydrophilic molecules. Liposomes can be created by sonicating phospholipids in water, where low shear rates create multilamellar liposomes and continued high-shear sonication tends to form smaller unilamellar liposomes.

(A)   **(B)**
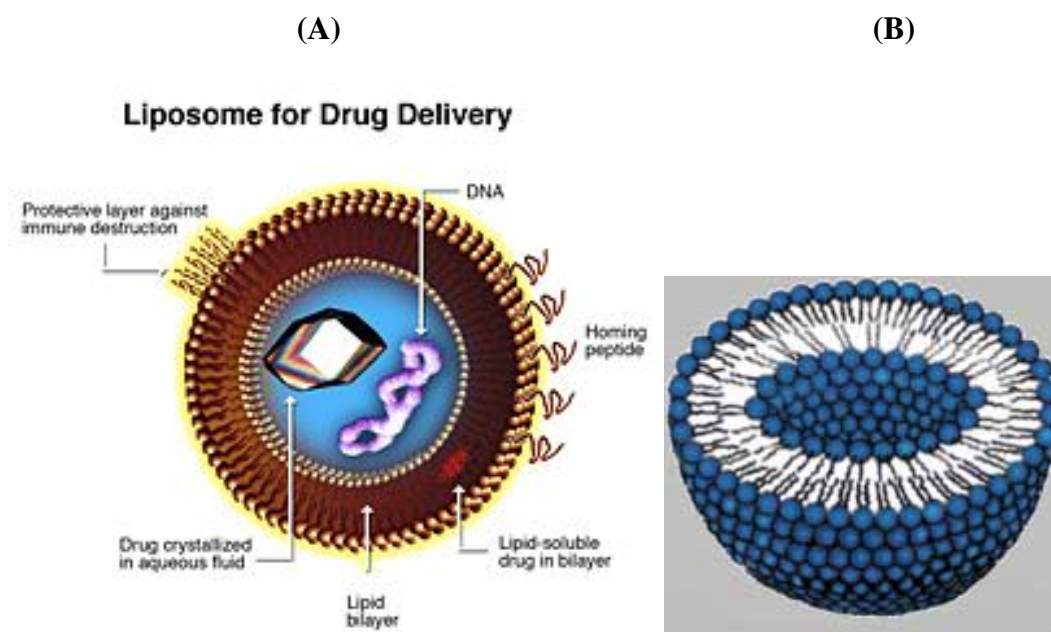
Fig. 1.9. Cross sectional views of liposomes **(A)** Taken from http://en.wikipedia.org/wiki/liposomes. **(B)** Taken from http://www.livonlabs/LV/apps/images/liptra2.JPG)

1.5. Lipid-protein interactions

Lipids and proteins are the major constituents of plasma membrane. Lipid-protein interactions are crucial for nearly all the functional properties of biological membranes. This is clearly evident from the fact that current estimates indicate that approximately 50% of drug targets correspond to membrane proteins [Terstappen & Reggiani, 2001]. In addition, newly synthesized peripheral proteins as well as large fraction of soluble proteins have to pass through one or more membranes during biosynthesis and during their journey from the site of synthesis to their final destination [Marsh, 1990]. It is therefore clear that lipid-protein interactions are an essential part of membrane structure and function. The functional activity of different membrane proteins may be modulated by the presence of specific lipids in their surrounding environment. On the other hand, the lipid dynamics (lateral diffusion, segmental motion as well as rotation around the axis) are affected by integral membrane proteins with which the lipid molecules interact [Marsh, 1990; Swamy et al., 2007].

1.6. Sperm structure

Sperm cell, or spermatozoon, or male gamete is a haploid cell. It is carried in a fluid called semen, and is capable of fertilizing an egg to form a zygote. Sperm cell contains half of the genetic information needed to create life. Antoni van Leuwenhoek first observed sperm cells under a microscope in 1679. Spermatozoa are formed from the spermatogenial sperm cells by a well organized process of cellular proliferation and differentiation known as spermatogenesis [Clermont et al., 1993; de Krester & Kerr, 1994].

The sperm cell (Fig. 1.10) consists of two principal parts; the head and the tail. The tail consists of four components; the neck, middle piece, principal piece and the end piece [Phillips, 1975]. The *sperm head* consists mainly of the nucleus and the acrosome. Its shape, size and structure vary greatly in different species of mammals [Guraya, 1965; Phillips, 1975; Gledhill, 1986]. The main characteristic of the sperm nucleus is the extremely condensed state of the nuclear material. The nucleus consists of DNA and proteins. The sperm nucleus contain the paternal genetic material (DNA) consisting of a haploid set of somatic chromosomes and in addition, one sex chromosome (X or Y). Mammalian spermatozoa have uniformly condensed chromatin, which is highly stable.

The *acrosome* plays an important role at the site of egg-zona pellucida (ZP) binding during the fertilization process. The acrosome, a unique exocytotic vesicle overlies the nucleus in the apical region of the sperm head [Eddy & O'Brein, 1994; Yanangimachi, 1994]. Acrosome is formed from Golgi apparatus during early stages of spermiogenesis. The acrosome contains structural, non-structural, enzymatic and non-enzymatic proteins. The acrosomal membrane can be subdivided into "outer" acrosomal membrane just underlying the plasma membrane and the "inner" acrosomal membrane overlying the nucleus, which becomes the plasma membrane after acrosome reaction. Acrosome contains enzymes such as acid glycohydrolases, proteases, acid phosphatases, aryl sulphatases, and estarases [Tulsiani et al., 1998a]. Powerful hydrolytic enzymes released during the acrosomal exocytosis, along with the enhanced thrust generated by the hyper activated beat pattern of the bound spermatozoa [Katz & Drobnis, 1990] are important factors that regulate the penetration of ZP and fusion of the gametes. The *neck* is a short, slightly constricted segment of the sperm located between the base

of the head and the first gyre of the mitochondrial helices of the mid piece [Sato & Oura, 1984].
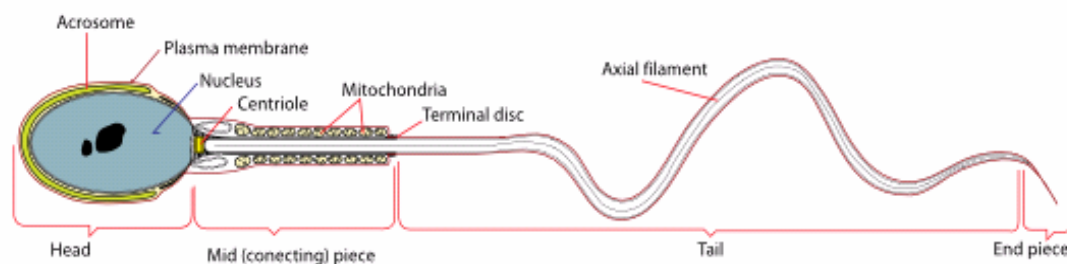
Fig. 1.10. Schematic diagram of mammalian sperm (Taken from http://en.wikipedia.org/wiki/ acrosome

The *mitochondrial sheath* and the outer ring of coarse fibers characterize the mammalian sperm mid-piece [Fawcett, 1975; Phillips, 1975]. It is the part of the flagellum, which lies between the neck and annulus and forms the most important site for various metabolic activities of the sperm. Mitochondrial sheath is believed to be the source of energy for the sperm motility. The size and the length of the mid-piece vary among different species of mammals. Mitochondrial sheath is particularly rich in phospholipids, most of which are bound to protein, suggesting that these endogenous lipids might be the source of the oxidative energy utilized for the sperm motility and the other metabolic activities including maturation [Guraya, 1971, 1973]. Phospholipids are also essential for the proper functioning of the mitochondria.

The major fraction of the lipids present in mammalian spermatozoa are phospholipids.   These include sphingomyelin, phosphatidylcholine, choline plasmalogen, ethanolamineplasmologen, phophotidylethanolamine, phosphotidylserine, gangliosides and cardiolipins [Mann & Lutwalk-Mann, 1981]. In most of the mammalian species studied so far, cholesterol forms the major

neutral lipid followed by the triglycerides [Sidhu & Guraya, 1985]. Changes in lipid and fatty acid composition of the sperm occur during migration through the reproductive tract [Johnson, 1970; Mann & Lutwalk-Mann, 1981].

1.6.1. Plasma membrane

All mammalian spermatozoa are surrounded by a plasma membrane that mediates many of the early events leading to fertilization. Glycan recognizing proteins, glycosyltransferases, which add sugar residues from the nucleotide sugar (donor) to the existing glycoprotein molecules, and glycohydrolases, which cleave sugar residues from the existing glycoproteins [Tulsiani et al., 1998a], and lectin like molecules are present on the plasma membrane [Skudlarek et al., 1992; Tulsiani, 1998b].

The plasma membrane on the surface of the sperm head is subdivided into well-defined regional domains such as (i) the marginal segment (apical segment) over the anterior region of the acrosome, (ii) the principal segment (acrosomal segment) over the major portion of the acrosome, and (iii) the equatorial segment over the posterior part of the acrosome (posterior acrosome). The marginal and principal segments are referred to as acrosome and acrosomal cap, respectively.

1.6.2. Capacitation

Unlike in lower animals, ejaculated sperm from mammals must undergo an activation process in order to fertilize an oocyte. Sperm become "fertilization competent" as they reside in the female reproductive tract through a series of physiological changes known as capacitation [Visconti et al., 1995; Fraser, 1995]. Capacitation has been referred to as changes that enable the sperm to undergo both the acrosome reaction and hyperactivation. However the molecular events involved

in sperm capacitation are not well understood, but ultrastructural and biochemical studies suggest that sperm undergoing capacitation exhibit a membrane remodeling process [Yanagamachi, 1994; Visconti et al., 1995; Patrat et al., 2000]. A decrease in the molar ratio of cholesterol to phospholipids, modification of the composition of surface adsorbed components, increased permeability to Ca^{2+}, and spatial redistribution of membrane proteins and lipids have been reported to take place during capacitation [Go & Wolf, 1983; Meizel 1985; Oliphant et al., 1985; Langlais & Roberts, 1985; Yanagamachi, 1994]. Capacitation has also been correlated with changes in sperm plasma membrane fluidity, metabolism and motility. Changes in sperm cyclic nucleotide metabolism and protein phosphorylation have also been implicated in sperm functions such as capacitation. Still, the molecular basis behind these events is poorly understood [Visconti et al., 1995].

1.6.3. Acrosome reaction (AR)

The sperm-egg binding is a carbohydrate-mediated process which initiates a signal transduction cascade resulting in the exocytosis of acrosomal contents i.e. acrosome reaction. There are many different inducers of the acrosome reaction (e.g., progesterone) [Yanagimachi, 1994; Roldan, 1994]. However, now ZP3 is accepted as the natural inducer that initiates the acrosome reaction [Bleil & Wassarman, 1983; Ward & Kopf, 1993, Darszon et al., 1996; Florman et al., 1998]. The binding of spermatozoa to the terminal sugar residues on ZP3 initiates two distinct signaling cascades resulting in exocytosis of acrosomal content, the G protein activation particularly G1- like proteins [Ward et al., 1992, 1994] and activation of ion channels [Florman, 1994; Arnoult et al., 1996; Florman et al., 1998]. Binding of ZP3 results in a depolarization of sperm membrane and intracellular Ca^{2+} elevation [Aranoult, 1996; Lievano, 1996]. Intracellular Ca^{2+} is necessary to initiate the acrosome reaction. ZP3-stimulated spermatozoa display an elevated pH in sperm,

which triggers the AR. Elevation of pH is believed to be regulated by several ion channels on sperm plasma membrane and outer acrosomal membrane [Tulsiani et al., 1998]. Recent reports have demonstrated that cholesterol efflux during sperm capacitation causes in increase of sperm pH [Arnoult et al., 1996; Florman et al., 1998].

1.6.4. Fertilization

Mammalian fertilization is the net result of a complex set of molecular events which allow the capacitated spermatozoa to recognize and bind to glycan residues on the extra-cellular coat of the ovum, the zona pellucida (ZP), following which they undergo the acrosome reaction and fuse with the egg plasma membrane [Gwatkin, 1977; Wasserman, 1987; Yanagamachi, 1994; Snell & White, 1996]. Sperm–ZP binding in mammals is believed to take place in two stages. First, capacitated (acrosome intact) spermatozoa loosely and reversibly adhere to the zona-intact ovum, followed by a tight, species-specific, irreversible binding. Both types of binding are thought to be mediated by the presence of glycan-binding proteins (receptors) on the sperm plasma membrane and their complementary bioactive glycan units (ligand) on the surface of the zona pellucida. Binding of sperm to zona pellucida initiates a signal transduction process, resulting in induction of the acrosome reaction (AR) [Wasserman, 1999].

1.7. Seminal plasma and its constituents

The seminal plasma is a mixture made up by the secretions from the testis, epididymus and accessory sex glands, in which spermatozoa are suspended. It is a complex fluid containing a variety of small molecules such as ions, organic acids, sugars, lipids and amino acids. The only high molecular weight biomolecules

present in seminal plasma are proteins whereas polysaccharides and nucleic acids are absent in it [Shivaji et al., 1990]. It serves as a carrier of sperm through the female reproductive tract. It contains decapacitation factors, which prevent spontaneous acrosome reactions. In addition to these inhibitory modulators, the seminal plasma also contains heparin binding proteins that bind to the surface of spermatozoa at ejaculation and plays a crucial role in membrane lipid modification events that occur during sperm capacitation which is an important step before acrosome reaction can occur [Miller et al., 1990; Manjunath et al., 1994; Thérien et al., 1995]. This finding provided evidence for a positive regulatory role of seminal plasma heparin-binding proteins in capacitation of bovine spermatozoa modulated by heparin-like glycosaminoglycans that are present in the female reproductive tract.

1.7.1. Bovine seminal plasma proteins

BSP-A1, BSP-A2, BSP-A3 and BSP-30 kDa are the major proteins of bovine seminal plasma (collectively called BSP proteins) which are acidic in nature [Majunath et al., 1987a; Manjunath et al., 1987b; Chandonnet et al., 1990]. These proteins are secretory products of seminal vesicles [Manjunath et al., 1987b; Schiet et al., 1988]. The primary structure and biochemical characteristics of these proteins have been reported [Seidah et al., 1987; Calvete et al., 1996a]. Cloning and cDNA corresponding to all BSP proteins have been reported [Schiet et al., 1988; Kemme et al., 1988; Desnoyers et al., 1992]. These are single chain polypeptides: BSP-A1, BSP-A2 and BSP-A3 have molecular weights ranging between 12 and 15 kDa, where as BSP 30 kDa protein has a molecular weight of ~30,000 Da [Manjunath et al., 1987a]. The amino acid sequence of BSP-A1 is identical to that of BSP-A2, but differs in the extent of glycosylation, the former is

glycosylated at Thr-11 [Calvete et al., 1994; Gerwig et al., 1996] and their mixture is also referred as PDC-109 [Esch et al., 1983].

BSP-A1/-A2 Proteins
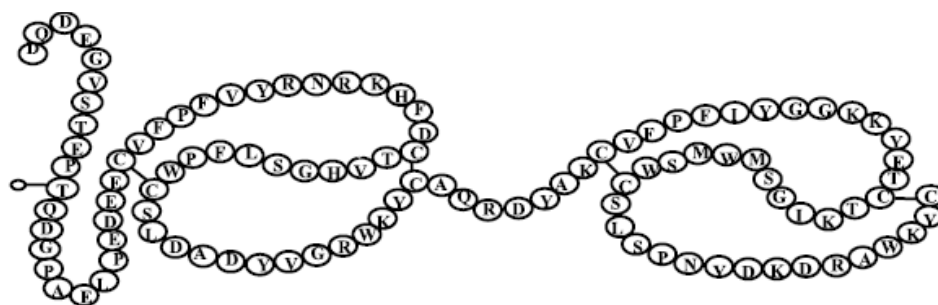
BSP-A3 protein
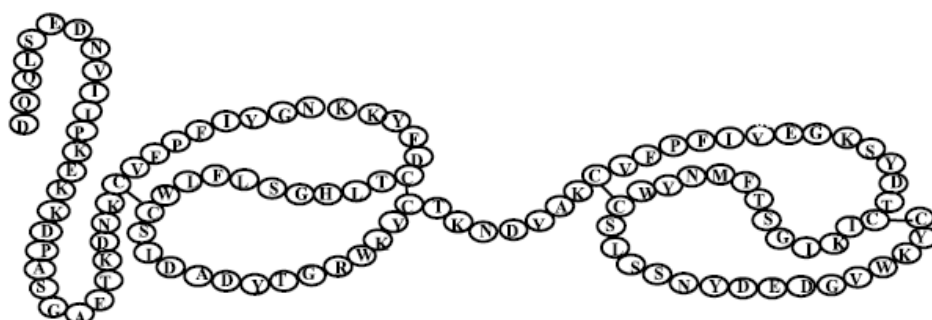
BSP-30-kDa protein

Fig. 1.11. Stuctures of the bovine seminal plasma (BSP) proteins. Taken from Manjunath & Thérien (2002)
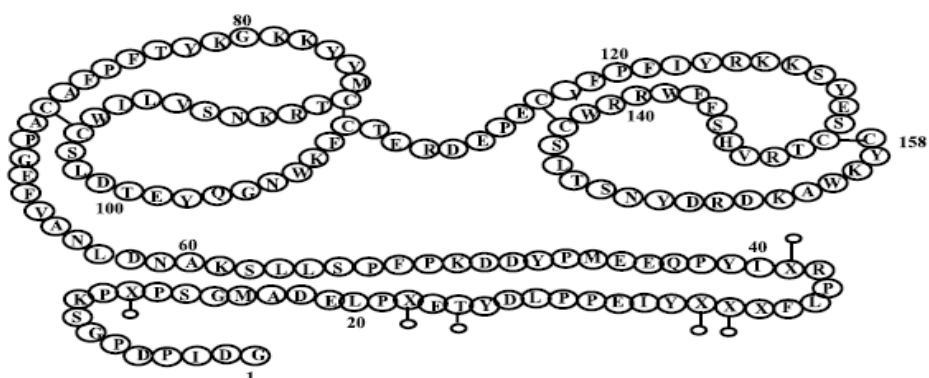
All these proteins are acidic with pI in the range: 3.6-5.2. BSP-A3 is homologous to PDC-109, with ca. 70% sequence identity; both are also homologous to collagen-binding domain of bovine fibronectin (type II sequence) [Seidah et al., 1987]. All BSP proteins are single-chain polypeptides and display a mosaic architecture, which consists of *N*-terminal distinctly *O*-glycosylated polypetide extensions of variable length, followed by two tandemly repeating fibronectin type II (FnII) domains [Calvete et al., 1996a]. Each domain consists of 38-41 amino acids with two disulfide bridges. BSP-A1, BSP-A2 and BSP-30 kDa proteins are glycosylated, while BSP-A3 is not [Manjunath et al., 1987b].

BSP-A1/BSP-A2 and BSP-A3 bind specifically to choline phospholipids [Desnoyer & Manjunath, 1992, 1993] that comprise over 70% of total bovine sperm plasma membrane phospholipids [Watson, 1981]. In contrast, BSP-30 kDa protein displays a much broader binding specificity. It preferentially binds to choline phospholipids but also interacts with phosphatidylethanolamine, phosphatidylserine, phosphotidylinositol, phosphatidic acid and cardiolipin [Desnoyer & Manjunath, 1992]. In addition to their heparin and lipid-binding activities, the BSP proteins interact with a variety of ligands including fibrinogen, apolipoprotein A1, apolipoprotein A1/high density lipoprotein complex, different collagens (types I, II, IV, V), and calmodulin [Thérien et al., 1995]. This suggests that these proteins are multifunctional.

1.7.2. PDC-109: structure and function

PDC-109 [Protein containing *N*-terminal asparatic acid (D) and *C*-terminal cysteine (C) with 109 amino acids], is the major protein of bovine seminal plasma. It is a 13 kDa protein and is present at a concentration of 15-20 mg/ml in the seminal plasma [Schiet et al., 1988]. The single polypeptide chain is composed of an *N*-terminal

23-residue stretch followed by two tandemly repeating fibronectin type II (FnII) domains [Esch et al., 1983].   Upon ejaculation, around 9.5 million PDC-109 molecules bind to spermatozoon [Calvete et al., 1994]. The interaction of PDC-109 with spermatozoa is mediated by its interaction with specific phospholipids, particularly with zwitterionic phosphatidylcholine (PC) [Desnoyers & Manjunath, 1992]. This binding results in the extraction of lipids, mainly phosphatidylcholine and cholesterol from the sperm membrane (referred to as *cholesterol efflux*), which is an important step in sperm capacitation before sperm undergo acrosome reaction [Thérien et al., 1998; Moraeu et al., 1998].   A decrease in the molar ratio of cholesterol to phospholipids in the sperm membrane is one of the events that take part in sperm capacitation [Yanagamachi, 1994].

PDC-109 specifically binds with the choline phospholipids [Desnoyers & Manjunath, 1992], with high density lipoprotein [Manjunath et al., 1988; Manjunath et al., 1989], heparin [Chandonnet et al., 1990], collagen, fibrinogen, apoA1, apoA1/ high density lipoproteins and low density lipoprotein [Majunath et al., 2002]. Each Fn-II domain contains a choline phospholipid binding site and both the binding sites are necessary to induce cholesterol efflux, which modulates sperm capacitation [Manjunath & Thérien, 2002]. Single crystal X-ray diffraction studies of PDC-109/phosphorylcholine complex show that the two choline phospholipid binding sites are on the same face of the protein molecule and binding is mediated by a cation-π interaction between the quaternary ammonium group of the choline moiety and the indole ring of a core tryptophan residue and hydrogen bonding between the phosphate group and exposed tyrosine residues of the protein [Wah et al., 2002].

Spin label electron spin resonance studies reveal that PDC-109 exhibit highest selectivity for the choline phospholipids. The selectivity for different lipids

is in the following order: phosphatidylcholine $\approx$ sphingomyelin $\geq$ phosphatidic acid $>$ phosphatidylglycerol $\approx$ phosphatidylserine $\approx$ androstanol $>$ phosphatidylethanolamine $\geq$ *N*-acyl phosphatidylethanolamine $>>$ cholestane [Ramakrishnan et al., 2001]. Presence of cholesterol in the membrane modulates the interaction of PDC-109 with lipid membranes [Swamy et al., 2002]. Surface plasmon resonance studies indicate that binding of PDC-109 to different phospholipid membranes containing 20% (wt/wt) cholesterol occurs by a single step mechanism. The association constants for different phospholipids are in the order: DMPC > DMPG > DMPA > DMPE [Thomas et al., 2003]. These results are consistent with those obtained from the earlier ESR studies, mentioned above. The high specificity of PDC-109 for the choline phospholipids has been shown to be due to a faster association rate constant and slower dissociation rate constant as compared to phospholipids bearing other head groups [Thomas et al., 2003].

1.7.3. Role of PDC-109 in sperm capacitation

BSP proteins potentiate sperm capacitation induced by heparin and high density lipoproteins. BSP proteins play a crucial role in membrane lipid modification events that occur during sperm capacitation induced by heparin and high density lipoproteins which are components of follicular and oviductal fluids [Manjunath & Thérien, 2002]. Upon ejaculation BSP proteins bind to choline phospholipids [Desnoyers & Manjunath, 1992]. The binding results in the removal of cholesterol accompanied by phospholipid efflux (referred to as *cholesterol effux*) which induces reorganization of the membrane lipids. A decrease in the molar ratio of cholesterol to phospholipids in the sperm membrane is one of the events that take part in sperm capacitation [Yanagamachi, 1994]. Furthermore, the binding of BSP proteins to sperm stabilizes the membrane by reducing the free movement of phospholipids. In female genital tract, sperm bound BSP proteins interacts with

high density lipiproteins, which stimulate the "*second cholesterol efflux*" from sperm membrane. This results in a further decrease in the cholesterol/phospholipid ratio which promotes further reorganization of the membrane and triggers the acrosome reaction by some signal transduction pathways [Manjunath, & Thérien, 2002].

1.8. Main objectives of the present study

Capacitation is a multi-step process which enables the sperm to undergo acrosome reaction followed by fertilization of ovum. Spermatozoa released from testis are morphologically mature but do not possess the fertilizing ability, but acquire it during their transit in the female reproductive tract by a process called capacitation. Chang (1951) and Austin (1952) proposed a role for seminal plasma proteins in sperm capacitation but the molecular and physiological basis of capacitation are still poorly understood. Mammalian seminal plasma contains specific acidic proteins that influence the fertilizing ability of spermatozoa. In bovine seminal plasma, PDC-109 is the major heparin binding protein among the four acidic BSP proteins, and at ejaculation PDC-109 binds to sperm plasma membrane, resulting in the removal of cholesterol accompanied by phospholipid efflux which is an important step in sperm capacitation before fertilization can take place. By studying the interaction between sperm surface and seminal plasma molecules, the molecular events involved in capacitation and fertilization can be understood. The binding sites of BSP proteins on spermatozoa are identified as phospholipids that contain phosphatidylcholine head group [Desnoyers & Manjunath, 1992]. Biochemical and biophysical studies on the interaction of BSP proteins and sperm membrane lipids may shed light on the mechanism involved in sperm capacitation.

BSP proteins potentiate epididymal sperm capacitaton induced by high-density lipoproteins (HDL) and heparin which are components of follicular and oviductal fluids. HDL acts as an exctracellular acceptor for the cholesterol of sperm cells [Davis et al., 1980; Ehrenwald et al., 1990]. Sperm bound BSP proteins interact with HDL, which could stimulate the cholesterol efflux from sperm. Bovine epididymal sperm undergo the Lyso-PC induced acrosome reaction (AR) only in the presence of BSP proteins and BSP proteins cannot promote the acrosome reaction in the absence of heparin [Thérien et al., 1995]. Also binding of BSP proteins leads to an immobilization of lipids on sperm membrane resulting in changes in mobility of membrane lipids i.e., membrane fluidity, which is one of the events that occur in sperm capacitation.

BSP proteins bind to a wide variety of molecules like phospholipids, heparin, fibrinogen, apolipoprotein A1, apolipoprotein A1/high density lipoprotein complex, collagen, and calmodulin. In view of the above, it is important to study the interactions of BSP proteins with sperm surface molecules, especially lipids in order to understand the biophysical mechanisms involved in the sperm capacitation. Such studies will be useful to resolve the causes of infertility and to aid in developing improved methods of sperm cryopreservation.

The aim of the studies reported in this thesis is to investigate the interaction of PDC-109 and domain B of PDC-109 (PDC-109/B) with model membranes containing phosphatidylcholine and various ligands such as heparin, *O*-acylcholines such as *O*-lauroylcholine and *O*-myristoylcholine, and hydrophobic ligands like 8-anilino-1-naphthlene-sulfonic acid (ANS), 2-(p-toluidino) naphthalene-6-sulfonic acid (TNS), 4,4'-dianilino-1,1'-binaphthyl-5,5'-disulphonic acid (bis-ANS). The main objectives of present study are:

❖ To investigate the effect of binding of PDC-109 to phosphatidylcholine membranes on the phase structure of the lipid by ^{31}P-NMR studies, and to study the effect of PDC-109 on erythrocyte membrane.

❖ To investigate the thermodynamic parameters characterizing the interaction of PDC-109 with heparin using isothermal titration calorimetry (ITC), fluorescence spectroscopy and circular dichroism (CD).

❖ To study the thermodynamic forces involved in the interaction of PDC-109 with *O*-acylcholine using isothermal titration calorimetry, fluorescence spectroscopy and CD spectroscopy.

❖ To investigate the thermodynamic forces governing the binding of PDC-109 and its domain B to hydrophobic ligands like ANS, TNS and bis-ANS by fluorescence spectroscopy and CD spectroscopy.

❖ To study the exposure and accessibility of tryptophan residues in the native and membrane bound state of PDC-109 domain B using different quenchers like acrylamide, succinimide, cesium ion and iodide by fluorescence quenching and time-resolved fluorescence experiments.

Chapter 2

Modulation of the structure of model membranes by PDC-109. A ^{31}P-NMR Study

2.1. Summary

The effect of binding of PDC-109 to dimyristoylphosphatidylcholine (DMPC) and dipalmitoylphosphatidylglycerol (DPPG) multilamellar membranes at various temperatures (10–50°C) and protein/lipid ratios was investigated by ^{31}P-NMR spectroscopy. In addition, the effect of cholesterol on the changes induced by the binding of PDC-109 to PC membranes was studied. It was observed that binding of PDC-109 to both DMPC and DPPGC induced the formation of an isotropic signal in the ^{31}P-NMR spectrum of the lipid dispersion, and the fraction of the isotropic signal increased with increasing protein/lipid ratio and temperature, suggesting that protein binding results in a disruption of the multilamellar vesicles leading to the formation of small unilamellar vesicles or micelles. Incorporation of cholesterol in the DMPC multilamellar vesicles afforded a partial stabilization of the lamellar structure. However, relative intensity of the isotropic signal is less in the case of DPPG at the same lipid/protein ratio as compared to DMPC, which is in good agreement with the earlier ESR and SPR results suggesting a significantly higher affinity of PDC-109 for phosphatidylcholine over phosphatidylglycerol. In addition to the above ^{31}P-NMR experiments, the effect of PDC-109 on the human erythrocyte membrane was studied using UV-Vis-spectroscopy. It was observed that addition of PDC-109 to human erythrocytes resulted in membrane disruption and release of hemoglobin into the solution, which increased with increase in the concentration of the protein and incubation time.

2.2. Introduction

From the overview given in Chapter 1 it is clear that PDC-109 and other BSP proteins bind to lipid molecules isolated from sperm plasma membranes, especially phospholipids containing the choline moiety in the head group [Desnoyers & Manjunath, 1992]. Such binding of PDC-109 to spermatozoa leads to the removal of choline phospholipids and cholesterol from the sperm plasma membrane (referred to as *cholesterol efflux*). A decrease in the molar ratio of cholesterol to phospholipids in the sperm membrane is an important step in sperm capacitation before undergoing the acrosome reaction [Thérien et al., 1998; Moreau et al., 1998]. In the light of these observations it was considered important to investigate the interaction of PDC-109 with lipid membranes, particularly membranes containing choline phospholipids such as phosphatidylcholine and sphingomyelin. Previous spin label electron spin resonance studies from this laboratory revealed that PDC-109 exhibits highest selectivity for the choline phospholipids, but also interacts with other phospholipids and sterols. The selectivity for different lipids is in the following order: phosphatidylcholine $\approx$ sphingomyelin $\geq$ phosphatidic acid (pH 6.0) > phosphatidylglycerol $\approx$ phosphatidylserine $\approx$ androstanol > phosphatidylethanolamine $\geq$ *N*-acyl phosphatidylethanolamine >> cholestane [Ramakrishnan et al., 2001]. Additional ESR studies have shown that cholesterol modulates the interaction of PDC-109 with lipid membranes, but does not directly interact with PDC-109 [Swamy et al., 2002; Müller et al., 2002]. Surface plasmon resonance studies indicate that binding of PDC-109 to different phospholipid membranes containing 20% (wt/wt) cholesterol occurs by a single step mechanism and that the association constants for different phospholipids are in the order: DMPC > DMPG > DMPA > DMPE.

PDC-109 affects the structure of lipid and biological membranes in that the mobility of spin-labeled analogues of PC is decreased in the membrane of epididymal spermatozoa. PDC-109 mainly interacts with phospholipids bearing a phosphotidylcholine head group [Desnoyers & Manjunath, 1992]. Phospholipids other than PC are also affected by PDC-109 where sc-SL-PE incorporated into a PC-containing membrane is partially immobilized in the presence of PDC-109. However, the extent of immobilization of PE analogues was significantly lower compare to that obtained with PC [Greube et al., 2001]. Permeability assays confirmed that PDC-109 induces disruption of the lipid vesicles, whereas the presence of cholesterol inhibited the process in a concentration-dependent manner. PDC-109 binding to dimyristoylphosphatidylcholine membranes at high protein/lipid ratio resulted in a complete abrogation of the gel-to-liquid phase transition [Gasset et al., 2000; Ramakrishnan et al., 2001].

Several observations suggest that PDC-109 may affect the structures of the lipid membranes to which it binds. Experiments by Manjunath and coworkers have shown that binding of PDC-109 to spermatozoa and cultured cells results in an efflux of choline phospholipids and cholesterol with the efflux particles having a size of ca. 80 nm [Thérien et al., 1998; Moreau et al., 1998; Moreau & Manjunath, 1999]. Binding of PDC-109 to DMPC multilamellar membranes resulted in a partial solubilization of the vesicles as could be observed from a decrease in the sample turbidity, with the mass of the particles obtained being about 1.3×10^6 daltons, which is consistent with a particle diameter of 80 nm [Ramakrishnan et al., 2001]. Presence of cholesterol appears to stabilize the membrane structure against PDC-109 induced disruption [Gasset et al., 2000; Thomas et al., 2003].

In the work reported in this chapter, ^{31}P-NMR spectroscopic studies have been carried out on multilamellar dispersions made up of DMPC, DPPG, DMPE as

well as DMPC membranes containing 40 mol% cholesterol with the objective of investigating the effect of PDC-109 binding on the structure of the lipid membranes. Studies have also been conducted with Lyso-PC micelles. For each lipid system, the effect of protein/lipid ratio and temperature have been investigated. The results obtained indicate that binding of PDC-109 induces the formation of an isotropic signal in the ^{31}P-NMR spectrum (which for the diacyl lipids alone is anisotropic with axial symmetry and negative chemical shift anisotropy that is characteristic of a lamellar bilayer structure). The intensity of this isotropic signal increases with increasing protein/lipid ratio and increasing temperature. Presence of cholesterol stabilizes the bilayer structure.

2.3. Materials and Methods

2.3.1. Materials

Choline chloride (Ca^{2+} salt), tris (hydroxymethyl)-aminomethane (Tris base), acrylamide, bis-acrylamide and TEMED were obtained from Sigma (St.Louis, MO, USA). Sephadex G-50 (superfine) and DEAE Sephadex A-25 were purchased from Pharmacia (Uppsala, Sweden). DMPC, DPPG, DMPE, Lyso-PC (from egg yolk) and cholesterol were products of Avanti Polar Lipids (Alabaster, AL, USA). Sodium chloride, dichloromethane, EDTA and sodium azide were obtained from local suppliers and were of the highest purity available.

2.3.2. Samples of bovine semen and extraction of BSP proteins

Freshly ejaculated semen from healthy Ongole bulls was kindly provided by the Department of Animal Reproduction, Acharya N. G. Ranga University of Agricultural Sciences, Hyderabad, and Lam Farm, Department of Animal Breeding

of the same university at Guntur, Andhra Pradesh, India. The samples were stored on ice for a maximum of 9 hours (until they were brought to the laboratory) and then centrifuged at 3000 rpm in a refrigerated centrifuge to separate sperm cells and seminal plasma. Total proteins from the seminal plasma were precipitated by cold ethanol and dissolved in double distilled water and lyophilized. The lyophilized protein fraction was delipidated by extraction with a mixture of n-butanol/di-isopropylether (40/60; v/v), as described by Desnoyers and Manjunath [1993].

2.3.3. Purification of PDC-109

PDC-109 was purified using protocols standardized in this laboratory [Anbazhagan, 2005; Anbazhagan & Swamy, 2005]. In this method delipidated BSP protein fraction obtained according to the procedure of Desnoyers and Manjunath [1993] was used instead of the bovine seminal plasma used by Calvete et al. [1996]. The delipidated BSP protein fraction was dissolved in 50 mM Tris buffer, 0.15 M NaCl, 5 mM EDTA, pH 7.4 (TBS-I) and subjected to gel filtration on a column of Sephadex G-50 (superfine, 2.5 × 170cm), pre-equilibrated with TBS-I. The major peak containing PDC-109 was collected, dialyzed against 25 mM Tris, 1.0 M NaCl, pH 6.4 (TBS-II) and loaded onto a column of DEAE Sephadex A-25, pre-equilibrated with the same buffer. After washing the column with TBS-II until no protein was found in the washings, the bound protein was eluted with 100 mM choline chloride in the same buffer. The eluted protein was dialyzed extensively against TBS-I to remove choline chloride, concentrated by lyophilization, and then dialyzed again against the same buffer and stored at 4°C. Purity of PDC-109 was assessed by SDS-PAGE on 12% acrylamide gels where the protein moved as two closely spaced bands of Mr~13 kDa, corresponding to the glycosylated and unglycosylated forms [Calvete et al., 1996].

2.3.4. Effect of PDC-109 on human erythrocyte membrane

The effect of PDC-109 binding on the integrity of human erythrocyte plasma membranes was investigated by monitoring the release of hemoglobin by its absorption according to the following procedure. To 200 μl of 4% RBC suspension in TBS-I buffer in glass test tubes, different quantities of PDC-109 (10 μg to 500 μg) were added and the volume was made up to 1.0 ml. The mixture was then incubated for 1 hour at room temperature. In another experiment, 300 μg of PDC-109 was added to 200 μl of 4% RBC suspension in different glass test tubes and incubated for different time intervals (15 min to 300 min). In both experiments, after incubation, the samples were centrifuged at 3000 rpm for 5 minutes and the supernatant was collected and the absorbance of the sample at 415 nm was recorded on a Shimadzu UV-3101PC UV-Vis-NIR double-beam spectrophotometer using 1.0 cm path-length cells.

## 2.3.5. ^{31}P-NMR spectroscopy

Samples for NMR spectroscopy were prepared by dissolving the lipid (DMPC, DPPG, DMPE, Lyso-PC) or a mixture of DMPC and cholesterol in dichloromethane in glass tubes to give the desired final composition. The mixture was dried under a stream of nitrogen gas followed by vacuum desiccation for a minimum of 3 hours. The lipid film obtained was hydrated with TBS-I (for lipid samples) or with an appropriate volume of a solution of PDC-109 in TBS-I (for lipid/protein recombinants) to give the final lipid-protein ratio. Lipid dispersions thus obtained were warmed to ~ 30°C in a water bath and were mildly vortexed and then subjected to eight freeze-thaw cycles in order to get a homogenous suspension. The lipid suspension (or lipid/protein complex) thus obtained was transferred to a 5 mm NMR tube and centrifuged. Excess supernatant was removed and the sample

was subjected to NMR spectroscopy. ^{31}P-NMR spectra were recorded at variable temperatures (10-50°C) on a Bruker Avance 400 NMR spectrometer using the zgpg30 pulse program provided by Bruker with ^{1}H decoupling with a decoupling power of 14db. The $\pi/2$ pulse width used was 9.5 μs for ^{31}P and the recycle delay was 1 sec. About 2048 to 4096 scans were accumulated for each spectrum and the free induction decay was processed using a line broadening of 100 Hz in order to improve signal/noise ratio. Temperature was regulated by a thermostatted air-flow system. The spectral width was set to 400 ppm.

2.4. Results

2.4.1. Effect of PDC-109 on human erythrocyte membrane

Effect of binding of PDC-109 to the human erythrocyte membranes was carried out using UV-Vis-spectroscopy. Addition of PDC-109 to 4% erythrocyte solution resulted in the breakdown of erythrocyte membrane and release hemoglobin in to the solution. The content of hemoglobin increased with increase in concentration of protein and reached saturation when the concentration of PDC-109 was ≥ 300 μg/ml (Fig. 2.1). In the light of this, the kinetics of release of hemoglobin from erythrocyte suspension was studied at 300 μg/ml concentration of PDC-109. In these studies it was observed that release of hemoglobin into the solution increased with increasing incubation time and reached a saturation point at ca. 210 min (Fig. 2.2).
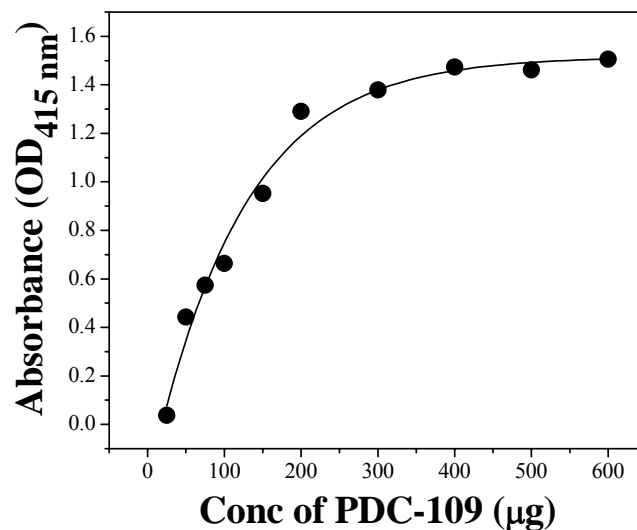
**Fig. 2.1:** Effect of PDC-109 on human erythrocyte membranes at different concentrations.
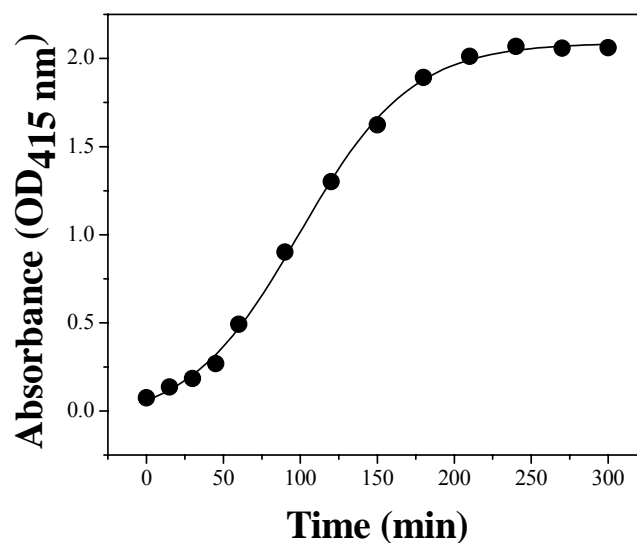
Fig. 2.2: Effect of PDC-109 on human erythrocyte membranes at different time intervals.

2.4.2. ^{31}P-NMR studies

In this study, the effect of PDC-109 on the phase structure of multilamellar vesicles of dimyristoylphosphotidylcholine (DMPC), DMPC with 40 mol% cholesterol and

dipalmitoylphosphatidylglycerol (DPPG) has been investigated by ^{31}P-NMR spectroscopy. ^{31}P-NMR spectra of DMPC, DMPC with 40 mol% cholesterol and DPPG are shown in Fig. 2.3. From this figure is seen that the ^{31}P-NMR spectra of all the above three samples are characteristic of lamellar (bilayer) membranes at both 20°C and 30°C. The spectra obtained at 20°C are broad, axially anisotropic with a high-field peak and low-field shoulder which are typical for lamellar gel phase with chemical shift anisotropy (CSA) values of -49.5, -51.5, and -69.1, respectively (Fig. 2.3). The spectra recorded at 30°C are also qualitatively similar, but are somewhat sharper with lower CSA values, which is consistent with the liquid crystalline phase exhibited by DMPC at this temperature. Although the spectrum of DPPG recorded at 30°C is somewhat sharper than that recorded at 20°C, the corresponding CSA value (62.8 ppm) indicates that the spectrum corresponds to gel phase. This is consistent with the gel-liquid crystalline phase transition temperature of DPPG at 41.5°C [Harlos & Eibl, 1980].
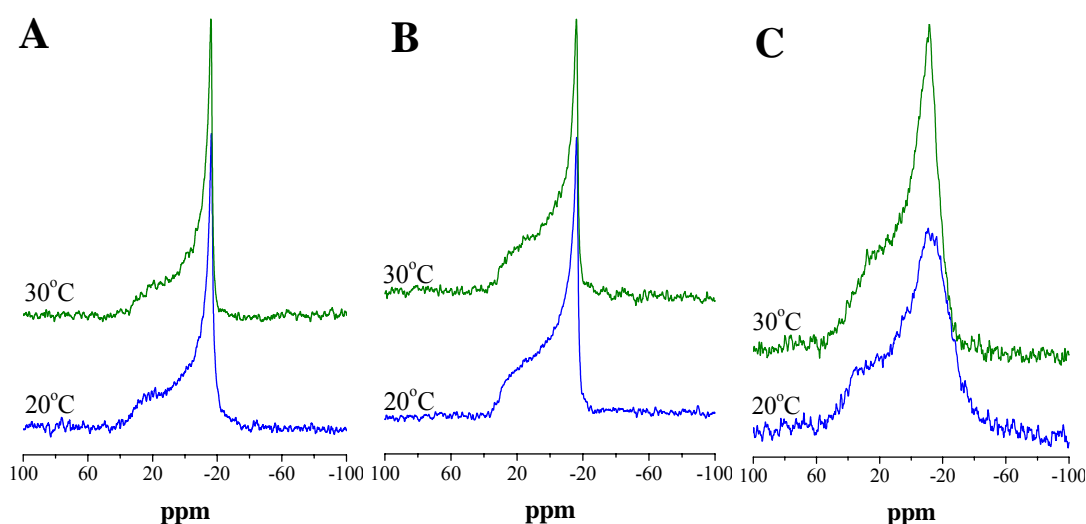
Fig. 2.3: ^{31}P-NMR spectra of (A) DMPC, (B) DMPC with 40 mol% cholesterol, (C) DPPG.

^{31}P-NMR spectra of DMPC/PDC-109 mixture at the ratio of 1:0.25 (wt/wt) and DMPC with 40 mol% cholesterol/PDC-109 in the ratio of 1:0.25 are shown in Fig. 2.4. For both systems, spectra were recorded at different temperatures between 10°C and 50°C. Binding of PDC-109 to DMPC membrane induced the formation of an isotropic signal in the ^{31}P-NMR spectrum, which can be seen superimposed on the lamellar spectrum of DMPC. The fraction of the isotropic signal appears to increase with increase in temperature (Fig. 2.4A). Binding of PDC-109 binding to DMPC membranes containing 40 mol% cholesterol also resulted in the formation of an isotropic signal, but the intensity is less compared to pure DMPC membranes (Fig. 2.4B).
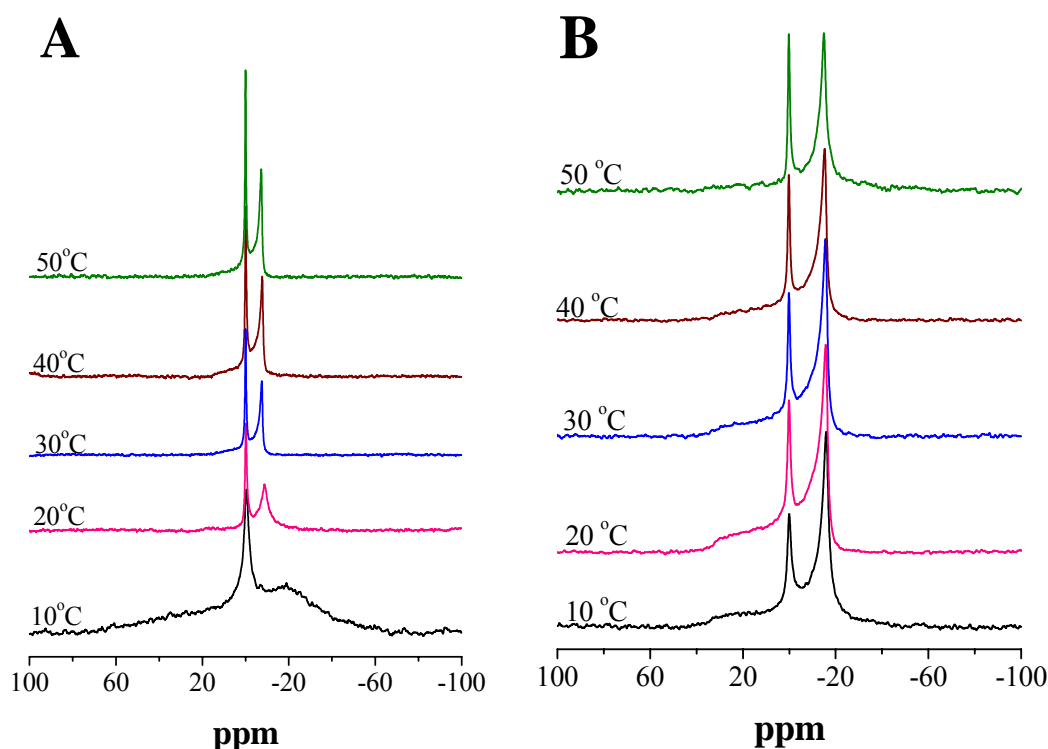
Fig. 2.4: ^{31}P-NMR spectra of (A) DMPC in presence of PDC-109 [L/P = ratio 1:0.25 (wt/wt)], (B) DMPC with 40 mol% cholesterol in presence of PDC-109 [L/P ratio = 1: 0.25 (wt/wt)].

Further ^{31}P-NMR studies were carried out at different lipid-protein ratios (1:0.25, 1:0.5, 1:1, 1:1.5, and 1:2; wt/wt) for both DMPC vesicles and DMPC with 40 mol% cholesterol. In all cases it was observed that binding of PDC-109 induced
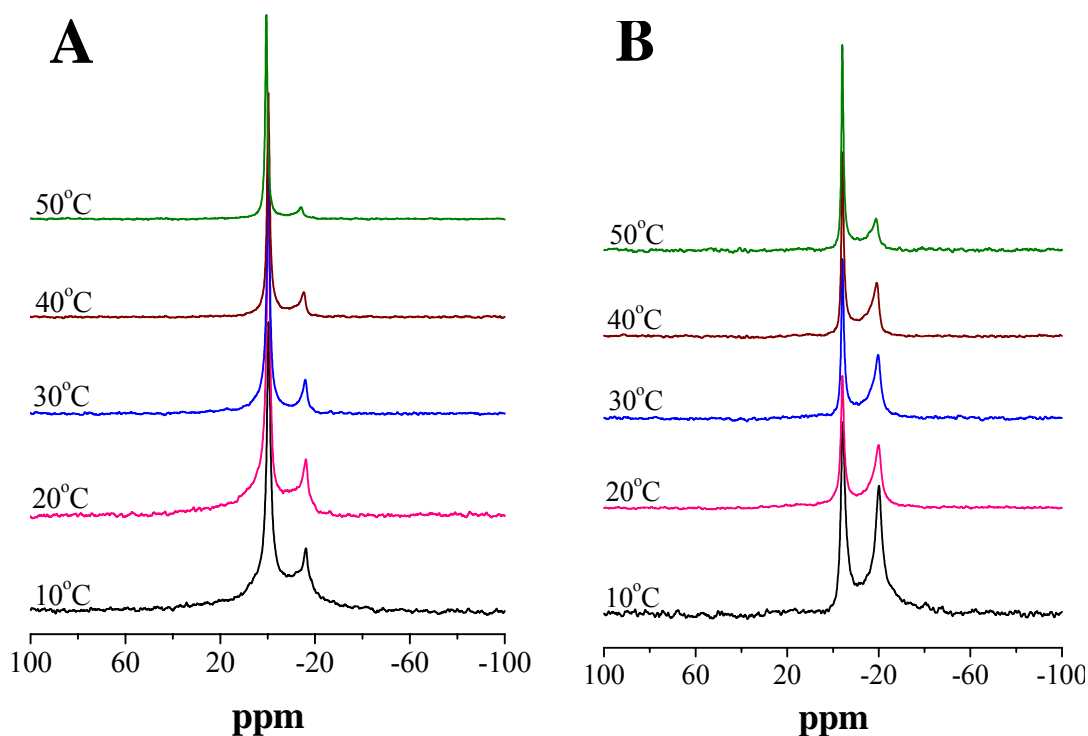
Fig. 2.5: ^{31}P-NMR spectra of (A) DMPC in presence of PDC-109 [L/P = ratio 1:1 (wt/wt)], (B) DMPC with 40 mol% cholesterol in presence of PDC-109 [L/P ratio = 1: 1 (wt/wt)].

the formation of an isotropic signal, the relative intensity of which increased with increasing concentration of protein as well as with increase in temperature from 10°C to 50°C. For pure DMPC vesicles, binding of PDC-109 at a lipid protein ratio of 1:1.5 (wt/wt) strongly disrupted the multilamellar vesicles (MLVs), resulting in a total abrogation of the anisotropic spectral pattern corresponding to the lamellar structure with only isotropic signal being seen in the ^{31}P-NMR spectrum of the sample even at the low temperature of 10°C. The isotropic signal became gradually sharper as the temperature was increased up to 50°C. In the case of DMPC MLVs

containing 40 mol% cholesterol, even at higher lipid-protein ratios (upto 1:2; wt/wt), the ^{31}P-NMR spectra contained a lamellar pattern along with isotropic signal at all temperatures, except the spectrum recorded at 50°C for the sample at the lipid-protein ratio of 1:2 (wt/wt). These results suggest that presence of cholesterol at 40 mol% in the DMPC vesicles partially stabilized the membrane against the action of PDC-109 (Figs. 2.4-2.7).

Fig. 2.6: ^{31}P-NMR spectra of (A) DMPC in presence of PDC-109 [L/P = ratio 1:1.5 (wt/wt)], (B) DMPC with 40 mol% cholesterol in presence of PDC-109 [L/P ratio = 1: 1.5 (wt/wt)].

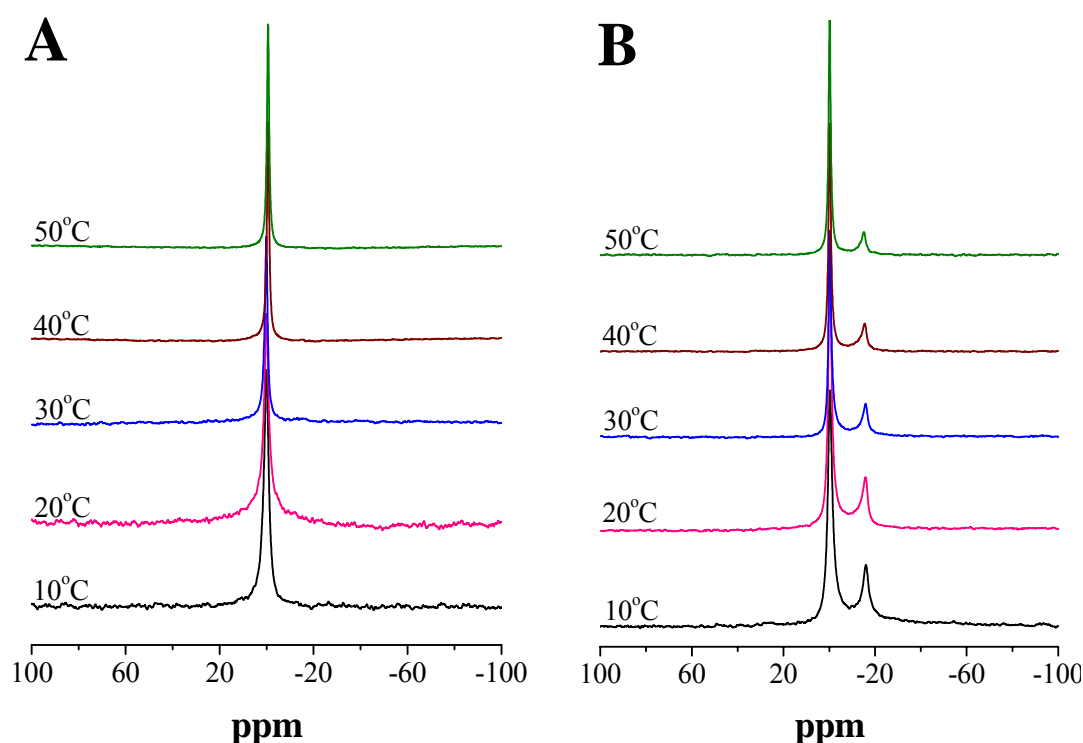In order to get quantitative information on the temperature dependence of the relative distribution of the lamellar and isotropic signals, the spectral signals were integrated and the fractions of the lamellar and isotropic components for samples with different lipid/protein ratios have been plotted as a function of temperature (Fig. 2.8). With membranes made up of only DMPC

at 1:0.25 (w/w) lipid/protein ratio, it is seen that the fraction of isotropic component increases from about 0.13 at 10°C to 0.24 at 50°C, i.e., it nearly doubles. The isotropic component increases with increasing protein/lipid ratio also, with the corresponding fractions being 0.18 and 0.23 for the samples with lipid/protein (w/w) ratios of 1:0.5 and 1:1, respectively. At 50°C, these values increase to 0.31 and 0.43, respectively. At lipid/protein ratios of 1:1.5 (w/w) or higher only isotropic signal is seen.
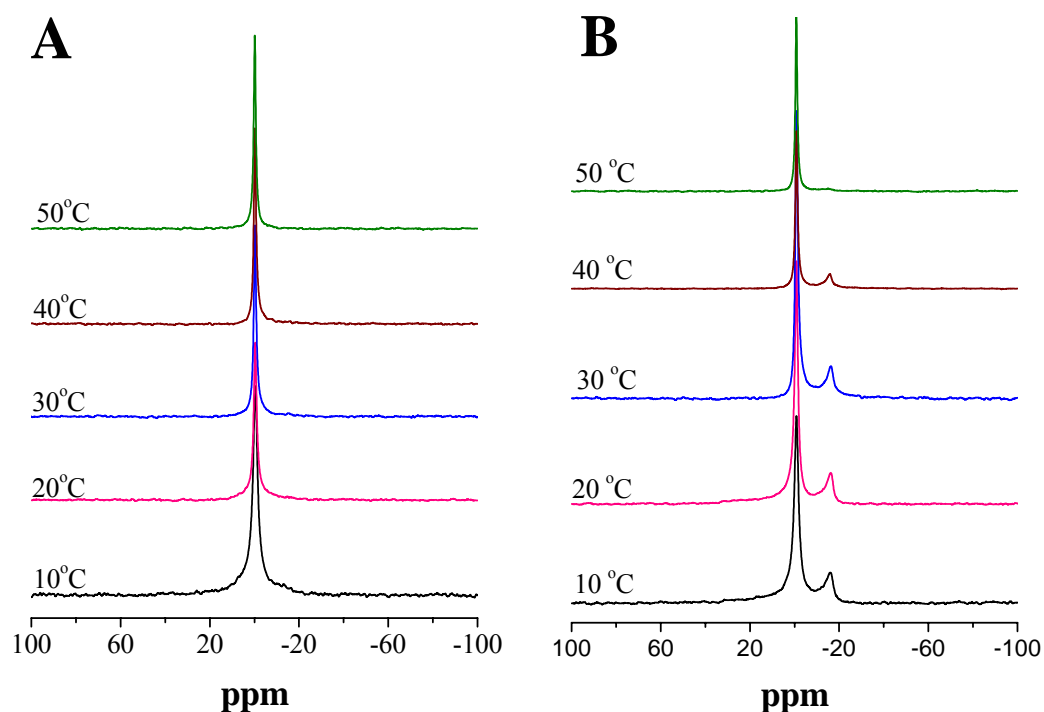
Fig. 2.7: ³¹P-NMR spectra of (A) DMPC in presence of PDC-109 [L/P = ratio 1:2(wt/wt)], (B) DMPC with 40 mol% cholesterol in presence of PDC-109 [L/P ratio = 1: 2 (wt/wt)].

Data presented in Fig. 2.8B clearly shows that in the samples containing 40 mol% cholesterol, the fraction of the isotropic signal is considerably less at all lipid/protein ratios. At a lipid/protein (w/w) ratio of 1:0.25, the fraction of the isotropic signal is only 0.077 at 10°C, which increases to 0.13 at 50°C. As

the lipid/protein ratio is increased the fraction of the isotropic component also increases with values of 0.26 and 0.34 being observed at 10°C for samples with lipid/protein (w/w) ratios of 1:1 and 1:2. These values increase further to 0.35 and 0.46, respectively, at 50°C.
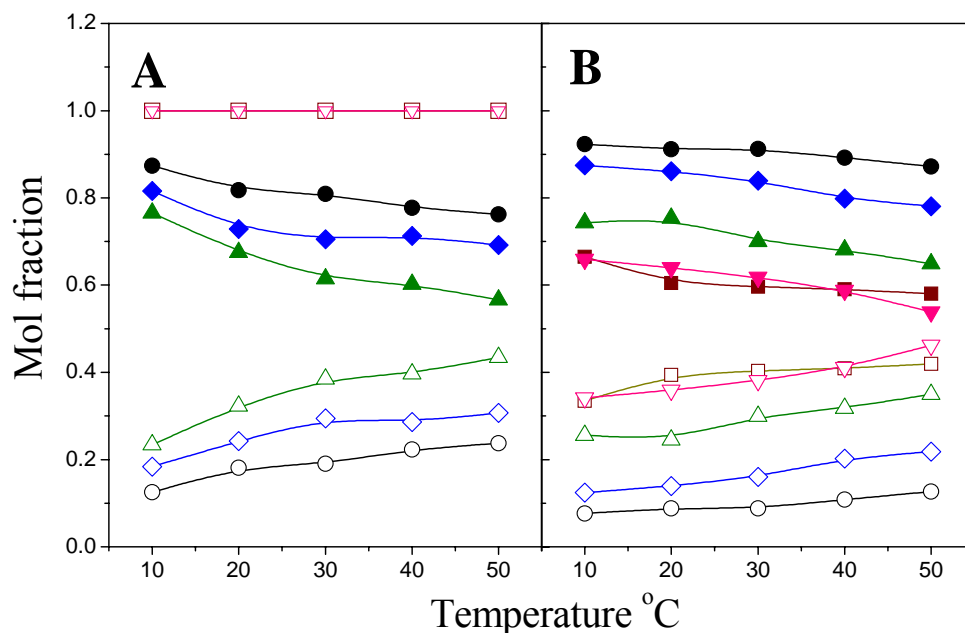
Fig. 2.8: Variation in the fraction of the lamellar and isotropic signals in the ^{31}P-NMR spectra of DMPC/PDC-109 mixtures in the absence (A) and presence (B) of cholesterol. The lipid/protein (w/w) ratios for different samples are: (●,○) 1:0.25; (♦,◊) 1:0.5; (▲,△) 1:1; (▼,▽) 1:1.5; (■,□) 1:2. Closed symbols correspond to lamellar signal and open symbols correspond to isotropic signal.

The ^{31}P-NMR spectrum of pure DPPG is characteristic of lamellar phase (Fig. 2.3C). Addition of PDC-109 to DPPG at the lipid/protein ratio of 1:0.5 resulted in only minor changes in the lamellar structure at 10°C, with a very small isotropic peak sitting on the lamellar pattern, but as the temperature increased from 10°C to 50°C the isotropic signal intensity increased and the spectral intensity corresponding to lamellar phase decreased (Fig. 2.9A). Addition of PDC-109 to DPPG at a lipid/protein ratio of 1:1 (wt/wt), induced the formation of a somewhat

larger isotropic signal at 10°C whose intensity increased with increase in temperature at the expense of the lamellar signal and at 40°C, the anisotropic signal corresponding to the lamellar phase completely disappeared (Fig. 2.9B). Integration of the spectral components show that the isotropic signal which was only 1.5% of the total intensity at 10°C for the sample with a lipid/protein (w/w) ratio of 1:0.5, increases to about 36% at 50°C. For the 1:1 (w/w) sample, the isotropic component increases from about 8% at 10°C to 11% at 30°C. Further increase in temperature to 40°C leads to a complete conversion of the lamellar signal to isotropic. These results suggest that PDC-109 binding to DPPG MLVs also causes their disintegration, leading to the formation of smaller lipid/protein aggregates with high curvature. Although at low temperatures, the fraction of the isotropic signal is relatively smaller for DPPG/PDC-109 recombinants as compared to DMPC/PDC-109 mixtures of the same lipid/protein ratio, the DPPG samples
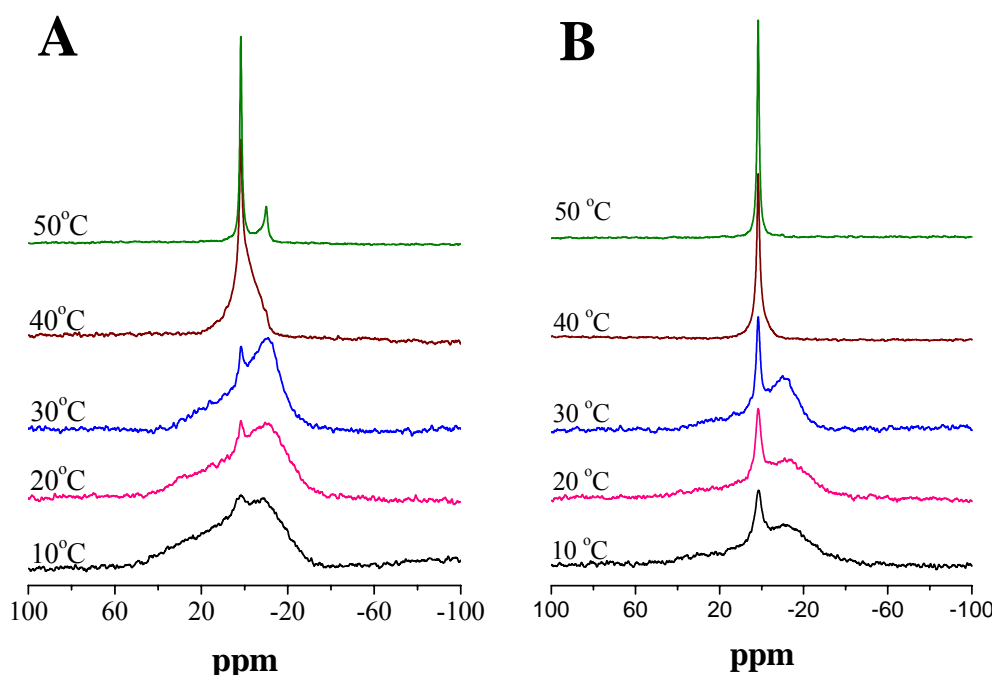
Fig. 2.9: ^{31}P-NMR spectra of (A) DPPG in presence of PDC-109 [L/P = ratio 1:0.5 (wt/wt)], (B) DPPG in presence of PDC-109 [L/P ratio = 1: 1 (wt/wt)].
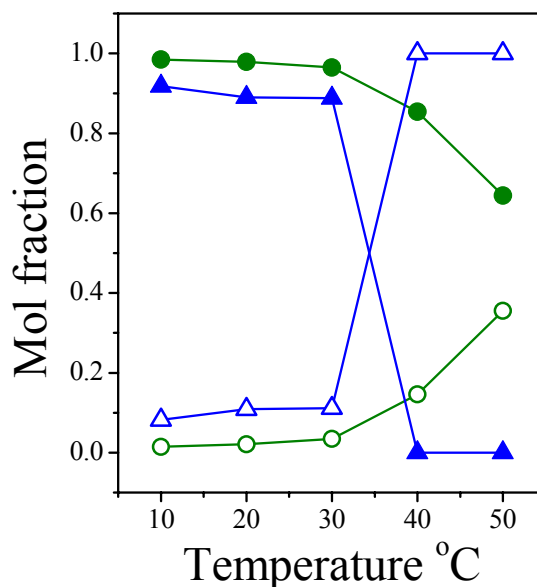
Fig. 2.10: Variation in the fraction of the lamellar and isotropic signals in the ^{31}P-NMR spectra of DPPG/PDC-109 mixtures. The lipid/protein (w/w) ratios for different samples are: (●,○) 1:0.5; (▲,△) 1:1. Closed symbols correspond to lamellar signal and open symbols correspond to isotropic signal.

exhibited significant increase in the isotropic fraction at higher temperatures. Although we do not have any specific explanation for this sharp increase in the fraction of the isotropic signal, these results are generally consistent with the results of the earlier spin-label ESR and surface plasmon resonance (SPR) studies which indicated that besides choline phospholipids PDC-109 also interacts with other phospholipids, especially phosphatidylglycerol and phosphatidylserine. Furthermore, consistent with the results obtained from ESR and SPR studies, addition of PDC-109 at 1:1 (wt/wt) ratio to dimyristoylphosphatidylethanolamine (DMPE) did not have any effect on the ^{31}P-NMR spectrum of the lipid (not shown).

^{31}P-NMR spectra for Lyso-PC alone and Lyso-PC in presence of PDC-109 at the lipid protein ratio of 1:1 recorded at various temperatures in the range of 10-

50°C are presented in Fig. 2.11. Lyso-PC gave a single isotropic resonance at all temperatures investigated, which is consistent with the micellar structure that this lipid is known to form in aqueous medium. Addition of PDC-109 at a lipid/protein ratio of 1:1 (wt/wt) did not result in any detectable change in the structure of the ^{31}P-NMR spectra, indicating that even after the binding of PDC-109, Lyso-PC remains most likely in the micellar state.
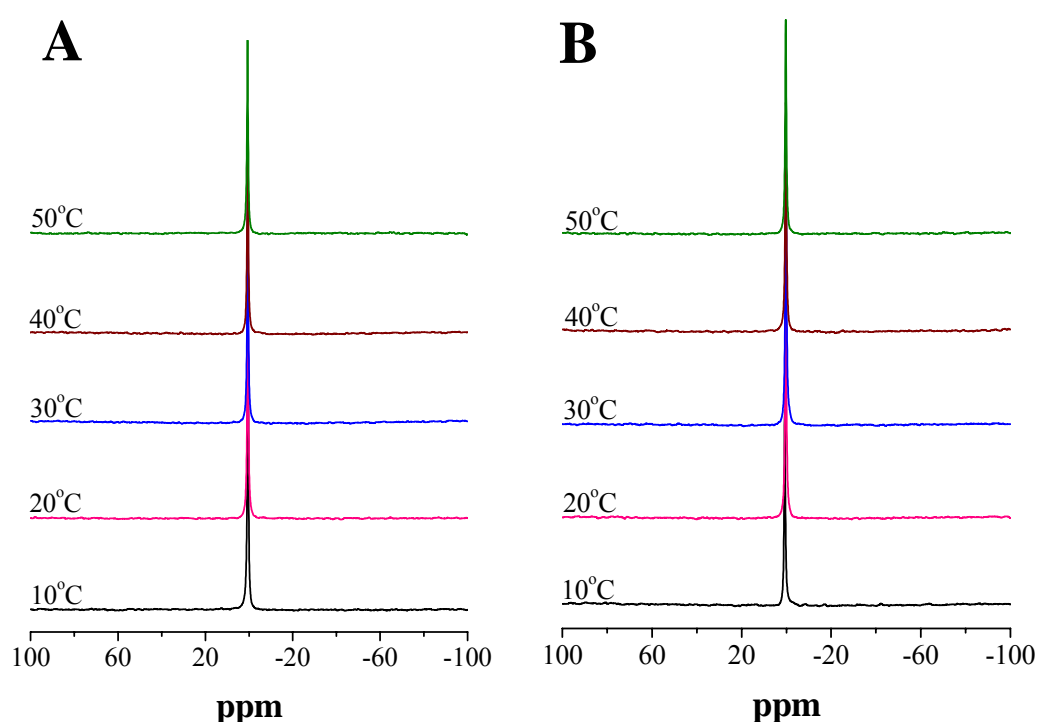
Fig. 2.11: ^{31}P-NMR spectra of (A) Lyso-PC (B) Lyso-PC in presence of PDC-109 [L/P ratio = 1: 1 (wt/wt)].

Chemical shift anisotropy (CSA) has been measured for the lamellar component in the ^{31}P-NMR spectra of DMPC alone and in the presence of different concentrations of PDC-109 as well as for the ^{31}P-NMR spectra of DMPC having 40 mol% cholesterol and in the presence of different concentrations of PDC-109. Furthermore CSA values have been determined for DPPG in the presence of PDC-

109 at different concentrations. In all cases it was observed that CSA values decreases as the temperature increases and also decreased with increasing concentration of PDC-109. The CSA values are shown in Table 2.1, 2.2 and 2.3.

Table 2.1: ^{31}P-NMR chemical shift anisotropy (CSA) values for DMPC/PDC-109 mixtures at different lipid/protein (L/P) ratios and temperatures.

Temp.(°C)	Chemical shift anisotropy (CSA)		
	1:0.25 (L/P)	**1:0.5** (L/P)	**1:1** (L/P)
10	-76.12	-71.36	-53.91
20	-54.78	-48.84	-47.28
30	-40.97	-41.27	-43.67
40	-38.49	-32.81	-36.96
50	-36.76	-32.26	-28.97

Table 2.2: ^{31}P-NMR chemical shift anisotropy (CSA) values for DMPC with 40mol% cholesterol /PDC-109 mixtures at different lipid/protein (L/P) ratios and temperatures.

Temp.(°C)	Chemical shift anisotropy (CSA)				
	1:0.25 (L/P)	**1:0.5** (L/P)	**1:1** (L/P)	**1:1.5** (L/P)	**1:2** (L/P)
10	-53.8	-49.01	-50.92	-40.79	-41.14
20	-47.1	-46.31	-47.02	-36.43	-40.16
30	-43.6	-13.59	-39.03	-29.92	-35.07
40	-38.7	-40.61	-34.11	-29.49	-28.89
50	-37.5	-37.94	-25.49	-27.66	-

Table 3.3: ^{31}P-NMR chemical shift anisotropy (CSA) values for DPPG/PDC-109 mixtures at different lipid/protein (L/P) ratios and temperatures.

Temp.(°C)	Chemical shift anisotropy (CSA)	
	1:0.5 (L/P)	**1:1** (L/P)
10	-52.43	-51.15
20	-48.41	-50.53
30	-47.22	-47.61
40	-22.42	-
50	-20.25	-

2.5. Discussion

Hemolytic studies suggest that PDC-109 binds to the surface of erythrocyte membrane and causes the breakdown of the membrane similar to the action of PDC-109 on sperm plasma membrane. The interaction of PDC-109 to erythrocyte membrane and disruption of the membrane was supported by the release of hemoglobin from the cell into the solution. The action of PDC-109 on erythrocytes indicates the binding of PDC-109 to choline containing phospholipids on the surface of erythrocyte membrane.

Upon ejaculation BSP proteins bind to choline containing phospholipids present on spermatozoa membrane. Earlier studies have shown that binding of PDC-109 to DOPC multilamellar vesicles (MLVs) leads to vesicle fragmentation, contents leakage and the formation of smaller lipid/protein particles ranging from 10 to 40 nm [Gasset et al., 2000]. The efflux particles are similar in size as compared to the efflux particles obtained from incubation of bovine epididymal sperm with PDC-109 and other BSP proteins [Thérien et al., 1998]. But the phase structure of particles formed is not known. In the present study we have investigated the effect of PDC-109 on the phase structure of aqueous dispersions of DMPC, DMPC dispersions containing 40 mol% cholesterol and DPPG as well as Lyso-PC by ^{31}P-NMR spectroscopy.

In ^{31}P-NMR studies, the formation of isotropic signal is consistent with the disruption of the DMPC MLVs and the formation of smaller aggregates. The isotropic signal further indicates the absence of hexagonal structures and suggests that the aggregates are structures with high curvature. Micelles, SUVs and cubic phases can yield an isotropic structure. Among these three types of aggregates, cubic structures are known to be highly viscous and visual inspection of the

samples upon incubation with PDC-109 at different lipid/protein ratios indicated that the samples do not exhibit high viscosity. Therefore the formation of cubic phases upon binding of PDC-109 to the different lipid systems investigated here can be excluded. However, the current NMR data cannot distinguish between SUVs and micelles.

Addition of cholesterol at 40 mol% led to a partial stabilization of the lamellar phase in that the fraction of the isotropic signal was less in the presence of cholesterol for the same PDC-109/DMPC ratio. These results are consistent with the observations of Gasset et al. [2000], who reported that presence of cholesterol inhibited the disruption of DOPC vesicles induced by PDC-109 in a dose dependent manner. In the presence of PDC-109 there was no change in the ^{31}P-NMR spectrum (bilayer) of DMPE, indicating that very weak (negligible) binding of PDC-109 to DMPE. This is consistent with the results of Tannert et al. [2007] which show that PDC-109 disturbed membranes containing PC and SM, and perturbation was diminished in PE- containing membranes. The above results are consistent with the weaker affinity exhibited by PDC-109 towards phosphatidylethanolamine and phosphatidylglycerol as compared to phosphatidylcholine [Thomas et al., 2003].

Chapter 3

Isothermal titration calorimetric studies on the interaction of PDC-109 with heparin

3.1. Summary

The energetics of interaction of PDC-109 with heparin has been investigated by isothermal titration calorimetric (ITC) studies. Titration of PDC-109 with heparin resulted in large endothermic peaks, indicating that the binding process is associated with positive enthalpy change. From the ITC measurements, the association constant (K_a), stoichiometry (n) and the thermodynamic parameters, change in enthalpy (ΔH^o), change in entropy (ΔS^o) and change in free energy (ΔG^o) for the binding of heparin at 20°C were obtained as 1.45×10^5 M^{-1}, 0.09, 17.0 kcal.mol^{-1}, 82.1 cal.mol^{-1}.K^{-1} and -6.93 kcal.mol^{-1}, respectively. These values indicate that the binding of PDC-109 to heparin is governed by a positive entropic contribution, which more than compensates the positive enthalpy value that contributes negatively towards the binding process. ITC experiments carried out at different temperatures (between 14 and 30°C), indicate that while K_a, ΔH^o and ΔS^o increased with temperature, the stoichiometry (n) increased up to 25°C but decreased at 30°C. Changes in fluorescence properties of PDC-109 induced by heparin were investigated with native PDC-109 and in presence of 20 mM phosphorylcholine (PrC). In addition, binding of chondroitin-6-sulfate to PDC-109 was also studied using fluorescence spectroscopy. The conformational changes in the structure of PDC-109 due to the binding of heparin in the native state and in presence of 20 mM PrC have been studied by CD spectroscopy.

3.2. Introduction

In mammals fertilization takes place when the spermatozoa from the male interacts with the egg in the female uterus and fuses with it. However, various studies show that sperm cells do not possess the ability to fertilize the egg at the time of ejaculation, but acquire it during their transit through the female genital tract by a process termed capacitation [Shivaji et al., 1990; Yanagamachi, 1994]. Despite its identification over 50 years ago [Yanagamachi, 1994; Chang, 1951; Austin, 1952], the detailed steps involved in capacitation are not yet clearly understood, although ultrastructural and biochemical studies have indicated that spermatozoa undergoing capacitation exhibit a membrane-remodelling process, which involves a decrease in the cholesterol/phospholipid ratio leading possibly to membrane fluidity changes as well as modification of the chemical composition and topographical distribution of the integral and peripherally bound membrane proteins [Yanagamachi, 1994; Harrison, 1996; Visconti et al., 1998].

Studies on different species have shown that the seminal plasma contains proteinaceous factors that play important roles in priming the sperm cells for fertilization [see Chapter 1]. In the bull (*Boa taurus*), the seminal plasma contains a group of four closely related acidic proteins – called BSP-A1, BSP-A2, BSP-A3 and BSP-30-kDa – that bind to sperm plasma membranes upon ejaculation by specific interaction with the phospholipids [Manjunath et al., 1987a; Desnoyers & Manjunath, 1992]. Together these proteins are referred to as bovine seminal plasma proteins (BSP proteins). BSP-A1 and BSP-A2 are identical in their amino acid sequence and differ only in the degree of glycosylation and their mixture, referred to as PDC-109, is the major protein of the bovine seminal plasma and is present at a concentration of 15-25 mg/ml [Scheit et al., 1988]. Its 109-residue polypeptide consists of a 23-residue *N-*

terminal stretch that is rich in acidic amino acids, followed by two tandemly repeating fibronectin type-II (FnII) domains [Esch et al., 1983; Baker, 1985; seidah et al., 1987]. The 3-dimensional structure of PDC-109, determined by single-crystal X-ray diffraction studies has revealed that each FnII domain can bind a choline phospholipid on the sperm plasma membrane by its specific interaction with the phosphorylcholine head group [Wah et al., 2002]. This interaction of PDC-109 with the sperm cell membrane results in an efflux of cholesterol and choline phospholipids, a process referred to as *cholesterol efflux*, which appears to be important for capacitation which is a necessary event before fertilization can occur [Thérien et al., 1998; Moreau & Manjunath, 1999]. In view of this, the interaction of PDC-109 with phospholipid membranes was investigated by different approaches [Swamy, 2004]. Spin-label ESR studies indicated that upon binding to phosphatidylcholine (PC) and PC/cholesterol membranes, PDC-109 penetrates into the membrane interior and directly interacts with the lipid acyl chains [Ramakrishnan et al., 2001; Greube et al., 2001; Swamy et al., 2002]. Surface plasmon resonance (SPR) studies have demonstrated that the binding of PDC-109 to PC membranes is due to a combination of faster association and slower dissociation rate constants [Thomas et al., 2003]. Association constants and thermodynamic parameters associated with the binding of phosphorylcholine, Lyso-PC and diacyl PC indicate that although the phosphorylcholine moiety is obligatory for the recognition of this lipid by PDC-109, additional interactions with the glycerol backbone and acyl chain(s) stabilize the binding further [Thomas et al., 2003; Anbazhagan & Swamy, 2005].

Besides their interaction with the sperm plasma membrane, the BSP proteins also bind to heparin and this ability has been exploited in their purification by affinity chromatography [Manjunath et al., 1987]. Purified PDC-109 and other BSP proteins have been shown to potentiate heparin-induced acrosome reaction [Thérien et al., 1995]. Affinity chromatographic experiments have shown that while polydisperse

PDC-109 binds heparin, the monomeric form does not display heparin binding ability [Calvete et al., 1999]. In addition, proteolytic digestion and chemical modification studies on the native and heparin bound PDC-109 indicated that charged residues, specifically lysines and arginines are important for heparin binding. In view of this, it is important to investigate the interaction of PDC-109 and other BSP proteins with heparin. In the present study, the interaction of PDC-109 with heparin has been investigated by isothermal titration calorimetry as well as by fluorescence and CD spectroscopy. In addition, the binding of chondroitin-6-sulfate has been investigated by fluorescence spectroscopy. The results indicate that the binding of heparin to PDC-109 is driven by a strong entropic contribution with negative contribution from enthalpy and provide significant clues towards understanding the thermodynamic forces that govern the PDC-109/heparin interaction.

3.3. Materials and Methods

3.3.1. Materials

Choline chloride (Ca^{2+} salt), tris (hydroxymethyl)-aminomethane (Tris base), heparin, chondroitin-6-sulfate, acrylamide, phosphorylcholine, bis-acrylamide and TEMED were obtained from Sigma (St. Louis, MO, USA). Sephadex G-50 (Superfine) and DEAE Sephadex A-25 were from Pharmacia Biotech (Uppsala, Sweden). Sodium chloride, EDTA and sodium azide were obtained from local suppliers and were of the highest purity available.

3.3.2. Isothermal titration calorimetry (ITC)

Purified PDC-109 was dialyzed extensively against 50 mM Tris buffer (pH 7.4) containing 150 mM NaCl, 5 mM EDTA and 0.025 % sodium azide and diluted to a

final working concentration of 0.20 – 0.25 mM (of the protein). Heparin in powder form was weighed accurately and dissolved in the dialysis buffer to a final concentration of 1.0 – 1.2 mM. To minimise contribution to binding heat from dilution, the final dialysate obtained after the protein dialysis was used to prepare heparin solution. Calorimetric titrations were performed using these solutions in a high-sensitivity VP-ITC microcalorimeter (MicroCal LLC, Northampton, MA, USA). Experiments were carried out between 14°C and 30°C. Prior to use both heparin and protein solutions were degassed under vacuum to eliminate air bubbles. The data were acquired by the computer software developed by MicroCal. Typically, 20-40 aliquots (5 µl each) of the heparin solution were injected from the syringe into the cell of 1.445 ml filled with the protein solution. Successive additions were separated by 200 s intervals to allow the endothermic peak resulting from the reaction to return to the baseline. In order to ensure proper mixing after each injection, a constant stirring speed of 300 rpm was maintained during the experiment. Usually the first injection was found to be inaccurate; therefore a 1 or 2 µl injection was added first and the resultant point was deleted before the remaining data were analyzed. Raw ITC data were integrated using the MicroCal Origin software, background heats from ligand to buffer titrations were subtracted, and the corrected heats from the binding were obtained.

The total heat released or absorbed at the end of the ith injection, $Q(i)$, was then fitted by a nonlinear least squares method to the total ligand concentration, X_i, according to the equation [Wiseman et al., 1989]:

$$Q(i) = nP_t\Delta H_b V\{1 + X_i/nP_t + 1/nK_bP_t - [(1 + X_i/nP_t + 1/nK_bP_t)^2 - 4X_i/nP_t]^{1/2}\}/2 \qquad (1)$$

where n is the number of binding sites, P_t is the protein concentration, V is the cell volume, K_b is the binding constant and ΔH_b is the binding enthalpy. The heat released in the ith injection is then given by:

$$\Delta Q(i) = Q(i) + \mathrm{d}V_i/2V[Q(i) + Q(i\text{-}1)] - Q(i\text{-}1) \tag{2}$$

where $\mathrm{d}V_i$ is the volume of the titrant added to the solution [ITC data analysis in Origin®]. The thermodynamic parameters, $\Delta G^o{}_b$ and ΔS_b are calculated according to equations (3) and (4):

$$\Delta G^o{}_b = \text{-}RT\ln K_b \tag{3}$$

$$\Delta G^o{}_b = \Delta H_b - T\Delta S_b \tag{4}$$

where R is the molar gas constant. Heat capacity change (ΔCp^o) for the binding was also determined from enthalpy changes at different temperature.

3.3.3. Fluorescence spectroscopy

Steady state fluorescence measurements were performed using a Spex model Fluoromax-3 spectrofluorimeter at 25ºC, with both the excitation and emission band pass filters set at 3 nm. PDC-109 samples of $OD_{280nm} < 0.1$ in TBS-I buffer taken in $1 \times 1 \times 4.5$ cm fluorescence cuvettes were excited at 280 nm and emission spectra were recorded between 300 and 400 nm. Titrations were performed by adding small aliquots of 1 mM heparin or chondroitin-6-sulfate solution to PDC-109 solution in the spectrometer cuvette. All spectra were corrected for inner filter effect and contribution, if any, from the buffer used.

3.3.4. Circular dichroism spectroscopy (CD)

Circular dichroism (CD) spectra were recorded on a Jasco-J-810 spectropolarimeter at 25°C with a scan speed of 20 nm/min using 0.2cm path length quartz cell. Far-UV and near-UV spectra were recorded at PDC-109 concentration of about 0.12 mg/ml and 1.0 mg/ml, respectively. Data were collected with a response time of 2 s and a slit width of

1 nm. Each spectrum reported was the average of 20 consecutive scans from which the buffer scans, recorded under the same conditions, were subtracted. The observed ellipticities were converted to mean residual ellipticities (Θ) using a mean molecular mass/residue of 117 [Gasset et al., 2000].

3.4. Results

3.4.1. ITC studies on heparin binding to PDC-109

Thermodynamic parameters characterizing the interaction of PDC-109 with heparin were obtained from isothermal titration calorimetric studies. Fig. 3.1 shows an ITC profile for the binding of PDC-109 to heparin at 20°C. Injection of 5 μl aliquots of 1mM heparin (from the syringe) into 0.215 mM PDC-109 solution (in sample cell) resulted in large endothermic peaks, indicating that the binding process is associated with positive enthalpy change ($\Delta H^o > 0$) with a positive entropy change ($\Delta S^o > 0$). The magnitude of the endothermic peaks decreased with subsequent injections, showing saturation of the binding sites at high heparin concentration. The data could be fit satisfactory by nonlinear least squares method to '*one set of sites*' binding model using MicroCal Origin.

The association constant (K_a), stoichiometry (n) and the thermodynamic parameters, ΔH^o, ΔS^o and ΔG^o for the binding of heparin at 20°C have been obtained as 1.45×10^5 M^{-1}, 0.09, 17.0 kcal.mol^{-1}, 82.1 cal.mol^{-1}.K^{-1} and -6.93 kcal.mol^{-1}, respectively. These values as well as the corresponding values obtained at different temperatures, obtained from the ITC measurements are listed in Table 3.1. These values indicate that the binding of PDC-109 to heparin is governed by a positive entropic contribution, which more than compensates the positive enthalpy value that contributes negatively towards the binding process.

The data presented in Table 3.1 indicates that while binding constant (K_a), ΔH^o and ΔS^o increased with temperature, the stoichiometry (n) increases up to 25ºC but decreases slightly at 30ºC. The slope of the linear least square fit of the enthalpy (ΔH^o) as a function of $T\Delta S^o$ was obtained as 0.94 cal.mol^{-1}.K^{-1} for the binding of heparin to PDC-109 which suggests that the binding is entropy-driven. From the slope of the linear least squares fits of the enthalpy data, the ΔCp value was calculated as 339 cal.mol^{-1}.K^{-1} for the binding of heparin to PDC-109.
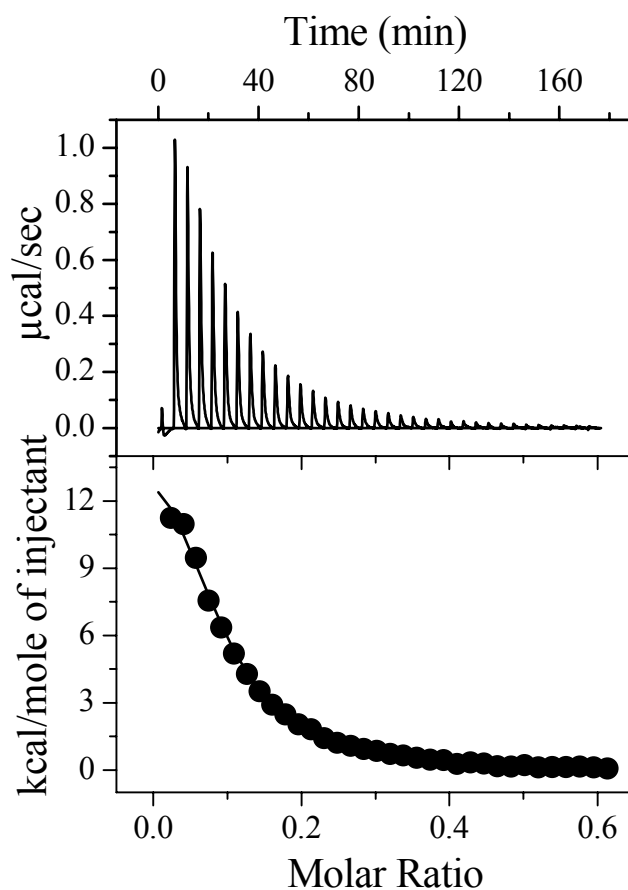
Fig. 3.1: ITC profile of heparin titration with PDC-109 at 20ºC. The upper panel shows the raw data for the titration 0.25 mM PDC-109 (in the ITC cell) with small aliquots of 1 mM heparin (in the syringe). The lower panel shows the integrated data obtained from the raw data shown in the upper panel, after subtracting the heat of dilution. The solid line in the bottom panel represents the best curve fit to the experimental data, using the '*one set of sites*' model from Microcal Origin.

Table 3.1: Thermodynamic parameters obtained for the binding of PDC-109 to heparin at various temperatures.

Temp.(^{o}C)	n	$K_a \times 10^{-4}$ (M^{-1})	ΔH° (kcal.mol^{-1})	ΔS° (cal.mol^{-1}.K^{-1})
14	0.061 ($\pm$0.012)	5.86($\pm$1.0)	13.99($\pm$3.2)	70.5
18	0.081($\pm$0.0028)	9.07($\pm$0.5)	16.58($\pm$0.7)	79.6
20	0.089($\pm$0.0025)	14.5($\pm$1.0)	17.13($\pm$0.6)	82.1
25	0.089($\pm$0.0023)	22.0($\pm$1.9)	17.29($\pm$0.6)	82.4
30	0.076($\pm$0.0012)	47.4($\pm$4.0)	33.93($\pm$0.7)	138.0

3.4.2. Effect of phosphorycholine (PrC) on heparin binding – ITC studies

In order to investigate how the binding of PrC to PDC-109 affects its interaction with heparin ITC experiments were conducted as follows. PDC-109 was incubated with 20 mM PrC (resultant concentration) and titrated with heparin by the addition of small aliquots from the syringe as described above. Barring the first injection (1μl) which is neglected (see above), all the subsequent injections gave very small and nearly identical heat changes that are in the range of the values observed for the dilution of the heparin sample into buffer. This data is consistent with the observation that PrC-bound PDC-109 is incapable of binding heparin [Calvete et al., 1996]. Fig. 3.2 shows ITC profile for heparin titration with PDC-109 in the presence of 20 mM PrC at 20ºC.
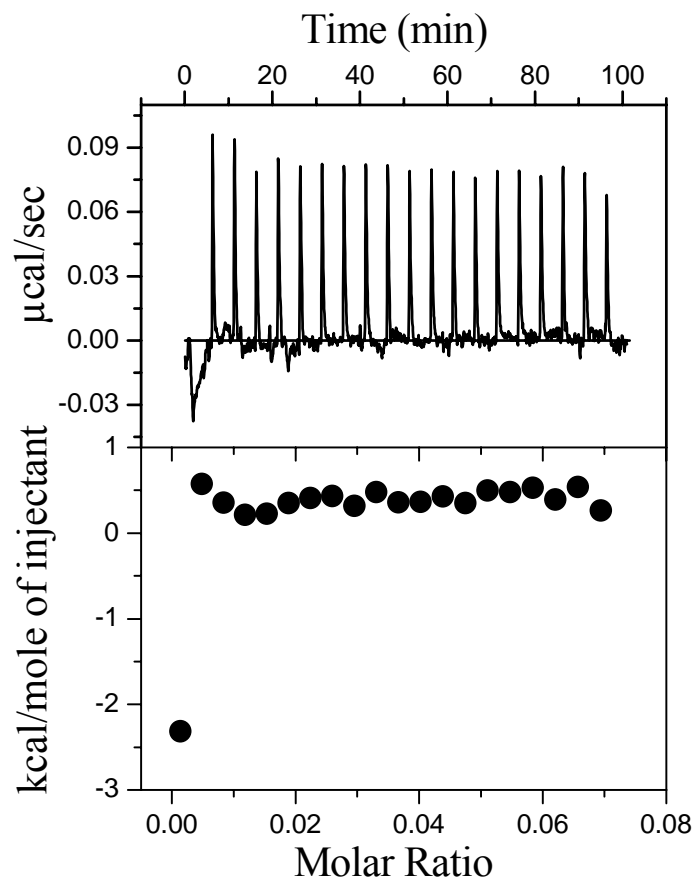
Fig. 3.2: ITC profile of heparin titration with PDC-109 containing 20 mM PrC at 20ºC. The upper panel shows the raw data for the titration of 0.25 mM PDC-109 containing 20 mM PrC (in the ITC cell) with 1 mM heparin (in the syringe). The lower panel shows the integrated data obtained from the raw data shown in the upper panel.

3.4.3. Fluorescence studies on the binding heparin to PDC-109

Fluorescence spectroscopic investigations on the binding of heparin to PDC-109 were performed at 25°C. The interaction of heparin with PDC-109 resulted in a gradual decrease in the fluorescence intensity of PDC-109 initially, whereas at higher concentrations of heparin, the intensity changes were significantly smaller, displaying saturation behaviour. The spectra obtained for the titration of heparin with PDC-109 are

given in Fig. 3.3A. A plot of the change in fluorescence intensity (ΔF) *vs* the concentration of added heparin yielded the binding curve for the interaction of PDC-109 with heparin (Fig.3.3B).
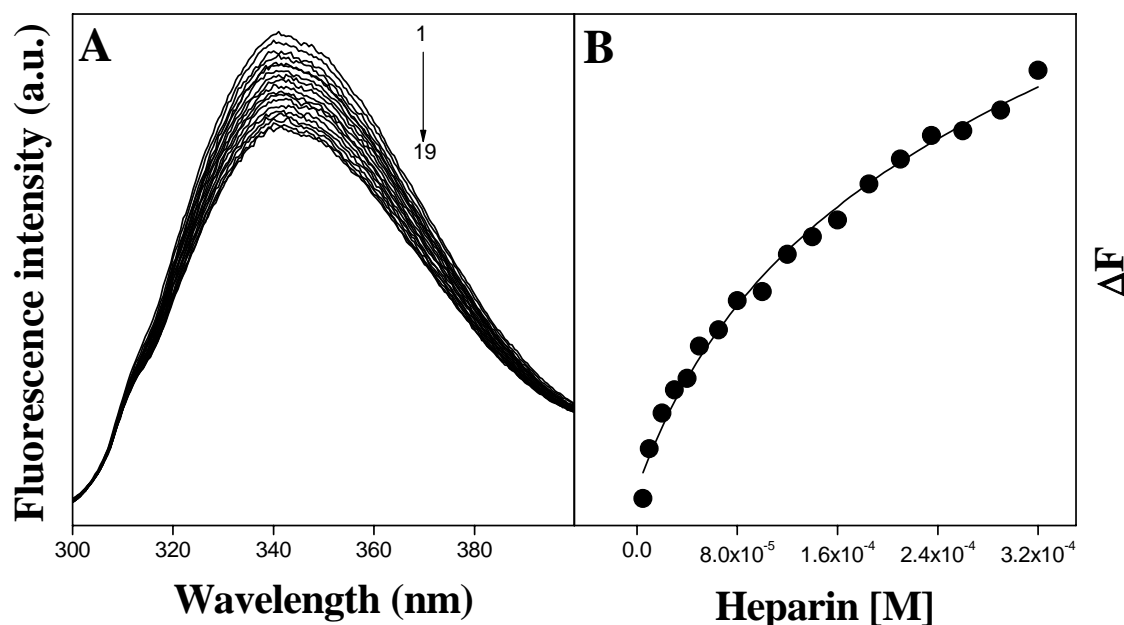
Fig. 3.3: **(A)** Fluorescence emission spectra for the interaction of PDC-109 with heparin at 25°C. Spectrum 1 corresponds to PDC-109 alone and spectra 2-19 corresponds to spectra of PDC-109 in presence of increasing concentrations of heparin. **(B)** Binding curve for the interaction of PDC-109 with heparin. The change in fluorescence intensity (ΔF) was plotted as a function of the concentration of heparin added. The solid line corresponds to a hyperbolic fit of the experimental data.

3.4.4. Effect of phoshorylcholine on heparin binding– Fluorescence spectroscopy

The effect of PrC on the interaction of PDC-109 with heparin was also studied using fluorescence spectroscopy. To a 0.1 OD solution of PDC-109 in the fluorescence cuvette, PrC was added in small aliquots from a 50 mM stock solution, and the fluorescence spectra were recorded after each addition. It was observed that the fluorescence intensity increased gradually during the titration and reached saturation when about 80 µl of PrC solution was added (Fig. 3.4). The increase in fluorescence

intensity with the addition of 50 mM PrC was calculated to be 18.9%. After the addition of 100 μl of PrC to PDC-109, small aliquots of 0.5 mM heparin were added. Addition of heparin resulted in a decrease in the fluorescence intensity, but the changes observed were very small and saturation was attained after the addition 35 μl of heparin; the corresponding decrease in fluorescence intensity was calculated to be 2.3%.
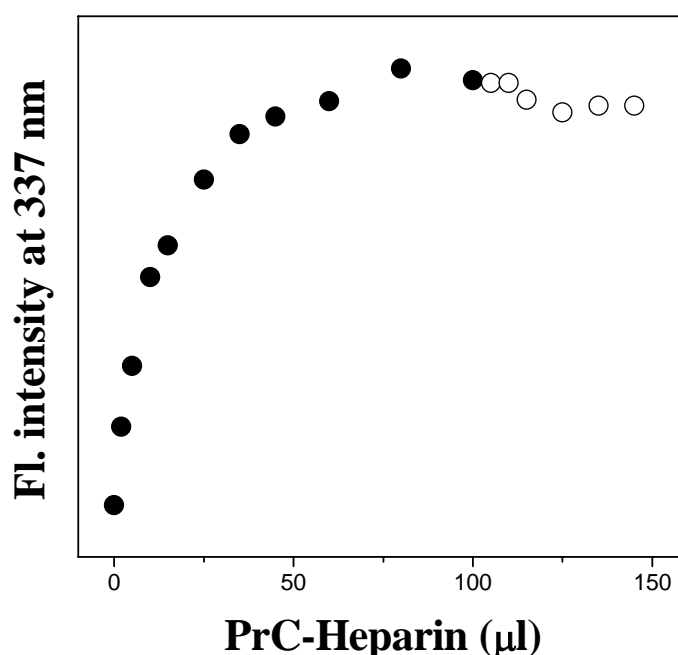
Fig. 3.4: Titration of PDC-109 with PrC followed by heparin. To PDC-109, PrC was added from a 50 mM stock solution in small aliquots (●), followed by addition of small aliquots of 0.5 mM heparin (○).

In another experiment, small aliquots of 0.5 mM heparin was added to PDC-109, which resulted in a gradual decrease in the fluorescence intensity of the protein. The decrease in the fluorescence intensity for the interaction of heparin with PDC-109 was calculated to be 10.86%. After successive addition of heparin (up to 100 μl) to PDC-109, 50 mM PrC was added in small aliquots which resulted in the increase of fluorescence intensity of PDC-109 and reached saturation after 45 μl addition of PrC, and the increase in intensity was calculated to be 17.22% (Fig. 3.5).
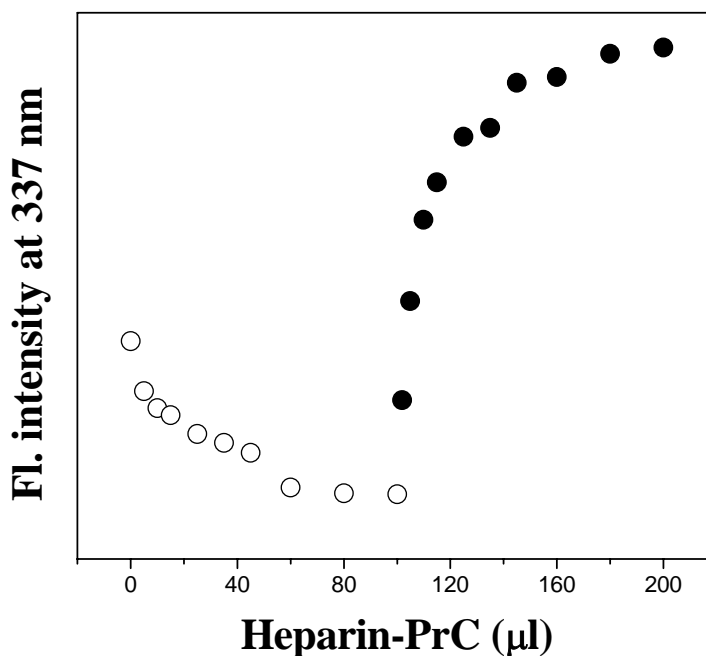
Fig. 3.5: Titration of PDC-109 with heparin followed by PrC. To PDC-109, heparin was added from a 0.5 mM stock solution in small aliquots (O), followed by addition of small aliquots of 50 mM PrC (●).

3.4.5. Interaction of PDC-109 with Chondroitin-6-sulfate

Chondroitin-6-sulfate (also called chondrotin sulfate C) is a sulfated glycosaminoglycan composed of a chain of alternating sugars such as *N*-acetylgalactosamine and glucuronic acid. Initial attempts to study the interaction of chondroitin-6-sulfate (CS) with PDC-109 using ITC gave very small changes in the enthalpy. On the other hand, when PDC-109 was titrated with CS, considerable decrease was observed in the fluorescence intensity of PDC-109. Therefore, further investigations on the interaction of CS with PDC-109 were carried out by monitoring changes in the fluorescence emission intensity
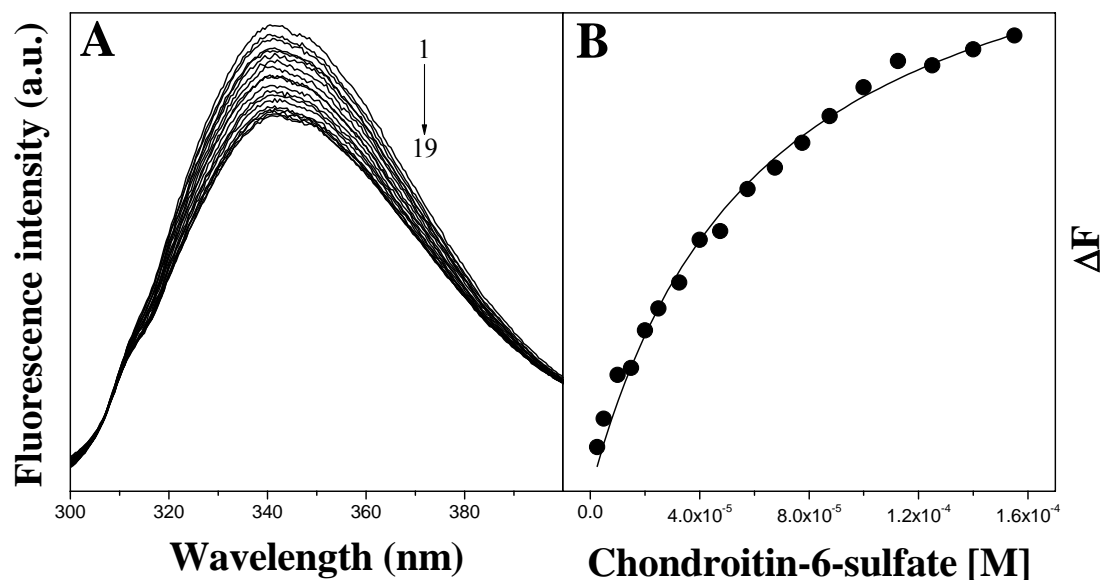
Fig. 3.6: **(A)** Fluorescence emission spectra for the interaction of PDC-109 with chondroitin-6-sulfate at 25°C. Spectrum 1 corresponds to the fluorescence emission spectrum of PDC-109 and spectra 2-19 corresponds to spectra of PDC-109 in presence of increasing concentration of 1 mM chondroitin-6-sulfate. **(B)** Binding curve for the interaction of PDC-109 with chondroitin-6-sulfate. The change in fluorescence intensity (ΔF) was plotted as a function of the concentration of chondroitin-6-sulfate added.
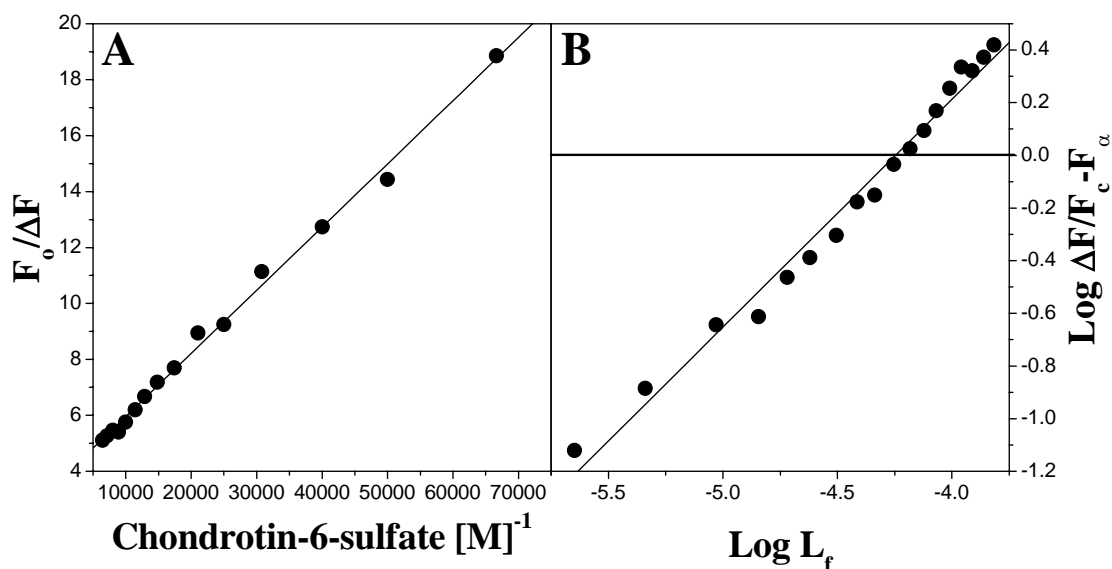
Fig. 3.7: **(A)** Plot of ($F_o/\Delta F$) *vs* ($1/[L]_t$) for the interaction of PDC-109 with chondroitin-6-sulfate. From the Y-intercept of this plot fluorescence intensity of the ligand at saturation binding was determined. **(B)** Chipman plot for the binding of chondroitin-6-sulfate to PDC-109. The abscissa of the plot yields pK_a, from which the association constant, K_a was determined.

of the protein when titrated with CS. Fluorescence emission spectra of PDC-109 in the absence and in the presence of different concentrations of CS are shown in Fig. 3.6A. The changes in the fluorescence intensity of PDC-109 decreased with the subsequent addition of 1 mM chondroitin-6-sulfate initially and reached saturation at higher concentrations of added ligand. The binding curve for the interaction of PDC-109 with chondroitin-6-sulfate is shown in Fig. 3.6B. The association constant involved in the interaction of PDC-109 with chondroitin-6-sulfate was calculated from the fluorescence data by Chipman analysis. A plot of $(F_o/\Delta F)$ *vs* $(1/[L]_t)$ where F_o is the fluorescence intensity of PDC-109 alone, ΔF is $(F_o\text{-}F_c)$ and F_c is the fluorescence intensity of PDC-109/B with added ligand at concentration $[L]$ was obtained. From the intercept of the plot the fluorescence intensity of the sample at infinite concentration, F_∞ was calculated. K_a value was calculated from the plot of $\log \{\Delta F/(F_c\text{-}F_\infty)\}$ versus $\log [L]_f$ according to equation 1.

$$\text{Log} [\Delta F/(F_c\text{-}F_\infty)] = \log K_a + \log [L]_f \qquad (1)$$

Where, F_c is the fluorescence intensity of the sample at any point during the titration. $[L]_f$ is the free ligand concentration and is given by

$$[L]_f = \{[L]_t - ([P]_t \times (\Delta F/\Delta F_\infty)\} \qquad (2)$$

$[P]_t$ is the total protein concentration. K_a value estimated from the fluorescence data for the binding of chondroitin-6-sulfate to PDC-109/B was 1.58×10^4 M^{-1} at 25°C.

3.4.6. CD spectroscopy

The far and near-UV CD spectra for the interaction of PDC-109 alone and in presence of heparin and PrC are shown in Fig. 3.8. The far-UV CD spectrum of PDC-109 was

characterized by a broad positive asymmetric band with maximum at 223 nm and a minor shoulder at 214 nm. These results are consistent with previous results [Gasset et al., 1997; Anbazhagan & Swamy 2005]. In the presence of 1 mM heparin the intensity of the far-UV CD spectrum of PDC-109 decreased considerably with band maximum observed at 222.2 nm. In the presence of 20 mM PrC, the intensity increased and the band peak shifted to 224 nm. In presence of 20 mM PrC and 1 mM heparin the intensity of the PDC-109 spectrum increased but it is lower than the intensity of PDC-109 in presence of 20 mM PrC (Fig. 3.8A).
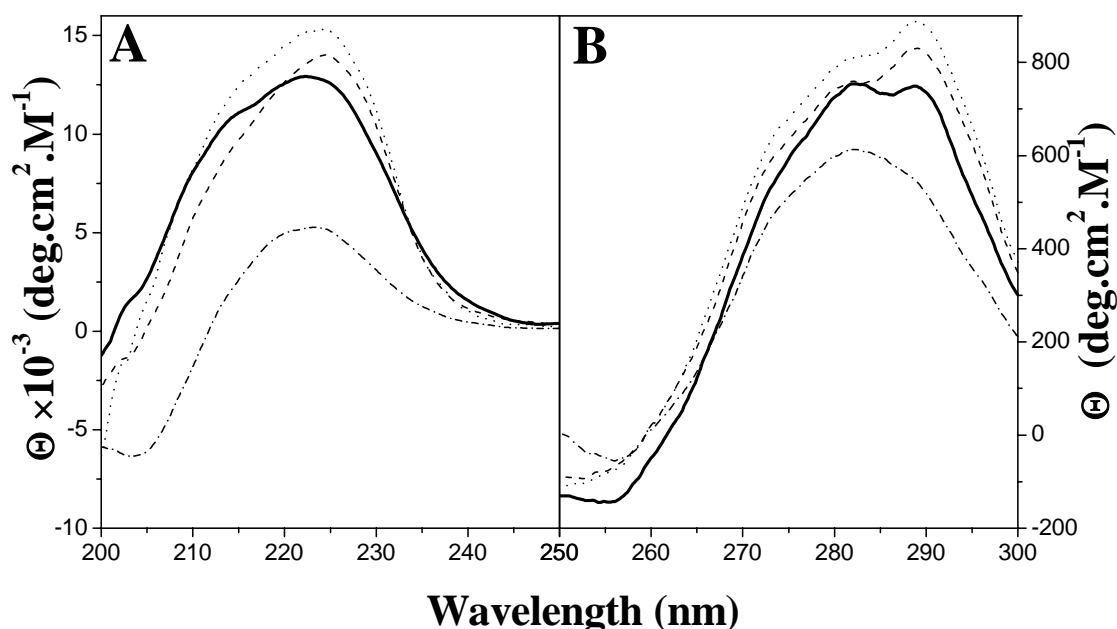
Fig. 3.8: Far and Near-UV CD spectra of PDC-109. **(A)** Far-UV CD spectra of PDC-109 in TBS-I buffer, pH 7.4, **(B)** Near-UV CD spectra of PDC-109 in TBS-I buffer, pH 7.4. PDC-109 in native condition (thick line), in the presence of 1 mM heparin (dash dot), in presence of 20 mM PrC (dot) and in the presence of 20 mM PrC and 1mM heparin (dash).

The near-UV CD spectrum of PDC-109 contains two overlapping positive bands with maxima at 282 nm and 289 nm (Fig. 3.8B). In the presence of 20 mM PrC, the intensity of PDC-109 spectrum increased and there was no change in the band positions. Both these observations are in agreement with the previous reports [Gasset et

al., 1997; Anbazhagan & Swamy, 2000]. In the presence of 1 mM heparin the two bands merge, yielding a single maximum centered at 282 nm, with a concomitant decrease in the intensity of the signal. In presence of 1 mM heparin and 20 mM PrC also there is no change in the band positions and the spectral intensity increased compared to PDC-109 alone but the change in intensity was less compared to near-UV CD spectrum of PDC-109 in presence of 20 mM PrC. In both cases, i.e., PDC-109 in presence of PrC and in presence of PrC and heparin, the peak at 289 nm became more intense compared to PDC-109 alone.

3.5. Discussion

Isothermal titration calorimetry (ITC) is a sensitive and powerful method for investigating the interaction between two species. It yields a number of thermodynamic parameters such as association constant, stoichiometry, enthalpy, entropy and free energy associated with the binding and thus provides critical information about the nature of interaction in single experiment. The positive values of change in enthalpy and change in entropy for the binding of heparin to PDC-109 indicate that binding of heparin to PDC-109 is driven by entropic factors rather than enthalpy. Although the binding event should reflect an increase in order, resulting in a decrease in the entropy, the positive value of ΔS^o obtained here for the binding of PDC-109 to heparin indicates an increase in entropy suggesting that the entropy of the system increases upon binding. This may be explained as resulting from the release of ordered water molecules that may be associated with the protein or the ligand or both from the interacting surfaces. The slope of the fit of the plot of ΔH^o *vs* $T\Delta S^o$ is 0.94, which suggests that the binding is entropy-driven (Fig. 3.9).

From fluorescence spectroscopic studies it was observed that addition of heparin to PDC-109 resulted in a decrease of the fluorescence intensity of PDC-109. Similarly,
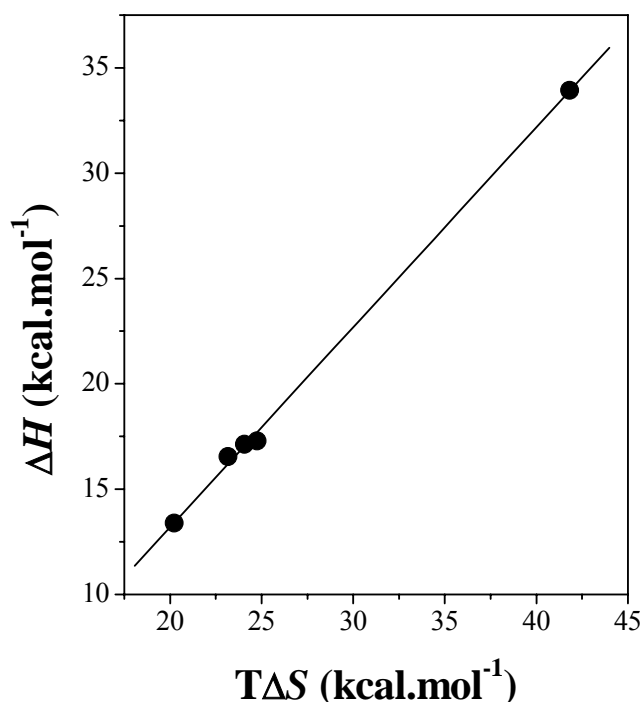
Fig. 3.9. Enthalpy-entropy compensation plot for the interaction of PDC-109 with heparin. The straight line corresponds to a linear least squares fit.

addition of chondroitin-6-sulfate to PDC-109 also resulted in a decrease in the fluorescence intensity of the protein. This is in contrast to the increase in fluorescence intensity when PrC or choline phospholipids are added to PDC-109. This suggests that heparin binding occurs at a site that is distinctly different from the site where PrC and choline phospholipids bind on the protein surface. These results are fully in agreement with the results of proteolytic digestion and chemical modification studies on PDC-109 which suggested that the side chains of lysines and arginines are critical for the binding of heparin to PDC-109 (the binding of PrC and choline phospholipids require tyrosine and tryptophan residues) [Calvete et al., 1999]. When heparin was added to PDC-109

containing PrC, weak binding to PDC-109 was observed. In ITC experiments addition of heparin to PDC-109 preincubated with 20 mM PrC resulted in negligible changes in the enthalpy, suggesting very weak binding of heparin to PDC-109. On the other hand, when PrC was added to PDC-109 containing heparin, a significant increase was observed in the fluorescence intensity of the protein, suggesting binding of PrC to PDC-109. These results support that PDC-109 binds strongly to choline containing phospholipids than the other ligands. In this case PrC replaced heparin from the binding site from the PDC-109 – heparin complex.

Previous CD spectroscopic studies have shown that binding of PrC and Lyso-PC leads to significant changes in the secondary and tertiary structure of PDC-109 [Gasset et al., 1997; Anbazhagan & Swamy 2005]. CD spectroscopic studies reported in this chapter clearly indicate that binding of heparin to PDC-109 resulted conformational changes in both secondary and tertiary structure.

Chapter 4

Isothermal titration calorimetric studies on the interaction of PDC-109 with *O*-acylcholines

4.1. Summary

Thermodynamic parameters characterizing the interaction of *O*-lauroylcholine (OLC) and *O*-myristoylcholine (OMC) with PDC-109 have been determined by isothermal titration calorimetric studies. Titration of OLC or OMC with PDC-109 resulted in exothermic peaks, the magnitude of which decreased with subsequent injections, showing saturation of the binding sites at high protein concentration and indicating that the binding process is associated with negative enthalpy change ($\Delta H^o < 0$). Association constant (K_a), Stoichiometry (n), and thermodynamic parameters, ΔH^o, ΔS^o and ΔG^o for the binding of OLC to PDC-109 have been obtained at different temperatures (25 - 40°C), with the values obtained at 25°C being 5.08×10^5 M^{-1}, 0.47, -4.46 kcal.mol^{-1}, 11.13 cal.mol^{-1}.K^{-1} and -7.78 kcal.mol^{-1}, respectively. Values of thermodynamic parameters obtained at different temperatures indicate that the binding of PDC-109 to *O*-lauroylcholine is governed by a negative enthalpy contribution. Also interaction of *O*-lauroylcholine with PDC-109 was studied using fluorescence spectroscopy. The association constant, K_a, for the interaction of PDC-109 with *O*-lauroylcholine from fluorescence studies at 25°C was estimated to be 5.46×10^4 M^{-1}, which is somewhat lower than the K_a value determined by ITC. Circular dichroism spectroscopic studies indicate that interaction of *O*-lauroylcholine with PDC-109 induced changes in the secondary and tertiary structure of PDC-109.

4.2. Introduction

PDC-109 (BSP-A1/-A2), BSP-A3 and BSP-30kDa constitute the major protein fraction of bovine seminal plasma (about 65 % of total proteins) [Manjunath & Thérien, 2002]. At ejaculation, PDC-109 binds to sperm surface mainly through a specific interaction with phospholipids containing choline head group. The high specificity of PDC-109 towards choline phospholipids was established in several studies [Desnoyers & Manjunath, 1992, 1993; Ramakrishnan et al., 2001]. The high specificity is due to a faster association rate constant and a slower dissociation rate constant for choline phospholipids than other phospholipids containing different head groups [Thomas et al., 2003]. Earlier studies have shown that both PrC and Lyso-PC bind to PDC-109 and that the binding affinity for the interaction of PDC-109 with Lyso-PC is higher than the affinity of PrC [Desnoyers & Manjunath, 1992, 1993; Müller et al., 2002]. A thermodynamic analysis of the binding of PrC and Lyso-PC to PDC-109 has shown that PDC-109 binding to Lyso-PC binds 250 fold stronger than its binding to PrC [Anbazhagan & Swamy, 2005]. This suggests that, in spite of the obligatory requirement of the choline head group in phospholipids, addition of the glycerol backbone and acyl chains enhance the strength of binding of PDC-109 for choline containing phospholipids.

Isothermal titration calorimetric studies carried out in this laboratory earlier have shown that Lyso-PC exhibits two types of binding sites for PDC-109, one set of high affinity sites and another set of low affinity sites [Anbazhagan, 2005]. This is most likely due to the coexistence of Lyso-PC micelles and the monomer. It was not possible to carry out experiments at low concentration where Lyso-PC would be in the monomeric form because of the very low CMC of this lipid. Therefore, we have synthesized *O*-acylcholines, viz., *O*-lauroylcholine and *O*-myristoylcholine, in which

the acyl chain is directly connected to the choline group without the phosphate and glycerol units. The interaction of OLC and OMC with PDC-109 was investigated at various temperatures by ITC under conditions where the OACs exist in the monomer form. As expected the binding data could be fitted to '*one set of sites*' model and the thermodynamic parameters indicate that the binding is predominantly enthalpically driven with some additional stabilization contributed by entropic factors at low temperatures. Structural changes in PDC-109 resulting from the binding to *O*-lauroylcholine were studied by circular dichroism (CD) spectroscopy.

4.3. Materials and methods

4.3.1. Materials

Choline chloride (Ca $^{2+}$ salt), tris (hydroxymethyl)-aminomethane (Tris base), acrylamide, phosphoryl choline, bis acrylamide and TEMED were obtained from Sigma (St.Louis, MO, USA). Sephadex G-50 (Superfine) and DEAE Sephadex A-25 were from Pharmacia Biotech (Uppsala, Sweden). *O*-lauroylcholine and *O*-myristoylcholine were synthesized by condensing *N*, *N*-dimethylethanolamine with lauric acid or myristic acid, followed by quaternization of the product with methyl iodide. The *O*-acylcholines obtained were characterized by FTIR and ^{1}H-NMR spectroscopy and were found to be pure by thin layer chromatography. Sodium chloride, EDTA and sodium azide were obtained from local suppliers and were of the highest purity available.

4.3.2. Isothermal titration calorimetry (ITC)

A MicroCal high sensitivity VP-ITC instrument (Northampton, MA, USA) was used to study the interaction of PDC 109 with *O*-acylcholines such as *O*-lauroylcholine and *O*-myristoylcholine. Experiments were carried out at different temperatures between 20

and 40°C. Both lipid and protein solutions were degassed under vacuum prior to use. A 360 μM solution of PDC-109 was taken in the syringe and injected in 12 μl aliquots into the ITC cell filled with 1.443 ml of 50 μM O-lauroylcholine. Injections were made at 5 minute intervals and a constant stirring speed of 300 rpm was maintained during the experiment in order to ensure proper mixing after each injection.   To minimise contribution to binding heat from dilution, the final dialysate obtained after the protein dialysis was used to prepare lipid solution (TBS-I, pH 7.4). The Control experiments were performed by titrating PDC-109 into TBS-I and the resulting heats were subtracted from measured heats from O-acylcholine-PDC-109 binding. The binding data were analysed using the Origin software provided by MicroCal. The equilibrium association constants (K_a), the enthalpy of binding (ΔH^o), the entropy change (ΔS^o) and the stoichiometry (n), were obtained from the curve fitting of the experimental data to '*one set of sites*' model in MicroCal origin. The values of K_a and ΔH^o obtained from curve fitting were used to calculate the standard free energy change (ΔG^o) and the standard entropy change (ΔS^o) for the binding using the equation:

$$\Delta G^o = -RT\ln K_a = \Delta H^o - T\Delta S^o$$

where R is the molar gas constant. Heat capacity change (ΔCp^o) for the binding was also determined from the enthalpy changes determined at different temperatures.

4.3.3. Fluorescence spectroscopy

Steady state fluorescence measurements were performed using a Spex model Fluoromax-3 spectrofluorimeter at 25ºC. The excitation and emission band pass filters were set at 3 nm. PDC-109 in TBS-I (pH 7.4) buffer with $OD_{280nm} < 0.1$ was excited at 280 nm and emission spectra were recorded between 300 and 400 nm. Titrations were

performed by adding small aliquots of 1 mM solution of *O*-lauroylcholine to PDC-109 in TBS-I buffer taken in a $1 \times 1 \times 4.5$ cm quartz fluorescence cuvette.

4.3.4. Circular dichroism spectroscopy (CD)

Circular dichroism (CD) spectra were recorded on a Jasco-J-810 spectropolarimeter thermostatted with water bath at 25°C with a scan speed of 20 nm/min using 0.2 cm path length quartz cell. Far-UV measurements were carried out in the 200-250 nm range and near-UV CD measurements were carried out in the 250-300 nm range. The protein concentration used in far-UV and near-UV measurements was 0.1 mg/ml and 1.0 mg/ml, respectively. Data were collected with a response time of 2 s and a slit width of 1 nm. Each spectrum reported was the average of 20 consecutive scans for which the buffer scans, recorded under the same conditions, were subtracted. The observed ellipticities were converted to mean residual ellipticities (Θ) using a mean molecular mass/residue of 117 [Gasset et al., 2000].

4.4. Results

4.4.1. Isothermal titration calorimetry

In the present study the interaction of PDC-109 with *O*-lauroylcholine and *O*-myristoylcholine, two synthetic derivatives of choline, has been investigated by isothermal titration calorimetry and the thermodynamic parameters characterising the binding have been determined. Fig. 4.1 shows a representative ITC profile for the binding of OLC to PDC-109 at 25°C. Qualitatively similar profiles were obtained for this interaction at other temperatures as well as for the interaction of OMC and PDC-109 at different temperatures. Injection of 12 μl aliquots of 360 μM PDC-109 (from syringe) into 50 μM solution of *O*-lauroylcholine (in sample cell) resulted in exothermic

peaks, indicating that the binding process is associated with negative enthalpy change ($\Delta H^o < 0$).   The magnitude of the exothermic peaks decreased with subsequent injections, showing saturation of the binding sites at high protein concentration.   The data could be fit satisfactory by nonlinear least squares method to '*one set of sites*' binding model from MicroCal Origin.   Data obtained at other temperatures for the binding of OLC to PDC-109 as well as for the interaction of OMC with PDC-109 at various temperatures could also be fitted satisfactorily to the '*one set of sites*' model in a similar fashion.
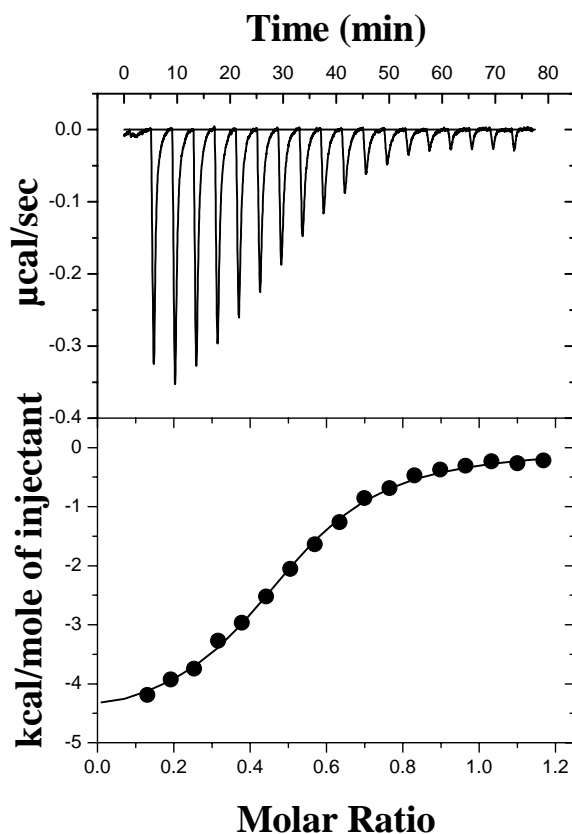
Fig. 4.1: ITC profile of PDC-109 titration with *O*-lauroylcholine at 25ºC. The upper panel shows the raw data for the titration of 50 μM *O*-lauroylcholine with 360 μM of PDC-109. The lower panel shows the integrated data obtained from the raw data shown in the upper panel, after subtracting the dilution experiments. The solid line in the bottom panels represents the best curve fit to the experimental data, using the '*one set of sites*' model from MicroCal Origin.

Values of stoichiometry (n), the equilibrium association constant (K_a) and thermodynamic parameters, ΔH^o and ΔS^o for the binding of OLC and OMC to PDC-109 at different temperatures were obtained from the above analysis and listed in Table 4.1 and Table 4.2, respectively. The association constant (K_a), stoichiometry (n) and the thermodynamic parameters, ΔH^o and ΔS^o for the binding of OLC at 25ºC are 5.08×10^5 M^{-1}, 0.47, -4.46 kcal.mol^{-1}, 11.13 cal.mol^{-1}.K^{-1} and -7.78 kcal.mol^{-1}, respectively. These values indicate that the binding of PDC-109 to *O*-lauroylcholine is governed by a negative enthalpy contribution. The entropic contribution is positive, which augments the favourable enthalpy and makes the binding stronger.

Table 4.1: Temperature dependence of the thermodynamic parameters associated with the binding of PDC-109 to *O*-lauroylcholine. The values listed are average of duplicate experiments.

Temp. (ºC)	n	$K_a \times 10^{-5}$ (M^{-1})	ΔH° (kcal.mol^{-1})	ΔS° (cal.mol^{-1}.K^{-1})
25	0.47(±0.02)	5.08(±0.69)	-4.46(±0.27)	11.13(±1.17)
30	0.42(±0.04)	3.76(±1.00)	-7.74(±0.44)	-0.09(±0.09)
35	0.49(±0.04)	2.60(±0.12)	-10.19(±0.01)	-8.31(±0.075)
40	0.45(±0.08)	1.25(±0.125)	-16.27(±1.1)	-28.65(±3.75)

Table 4.2: Thermodynamic parameters obtained for the interaction of PDC-109 with *O*-myristoylcholine. The values obtained are average of duplicate experiments.

| Temp. (ºC)	n	$K_a \times 10^{-5}$ (M^{-1})	ΔH° (kcal.mol^{-1})	ΔS° (cal.mol^{-1}.K^{-1})
30	0.29(±0.01)	19.9(±10)	-7.01(±0.48)	5.69
35	0.30(±0.04)	8.88(±2.05)	-11.4(±0.30)	-9.97(±1.4)
40	0.36(±0.001)	4.3(±0.39)	-16.6(±0.35)	-27.4

The data presented in Table 4.1 show that the enthalpy of binding decreases with increase in temperature, i.e., the magnitude of $\Delta H°$ increases while retaining the negative sign. This would be expected to result in an increase of the association constants with temperature. However, the K_a values decrease with increase in temperature, due to a larger negative change in the entropy of binding. The stoichiometry of binding (n) ranges between 0.42 and 0.49, which is consistent with each protein molecule binding two molecules of OLC.

At 30°C the K_a value obtained for the binding of OMC to PDC-109 is 19.9×10^5 M^{-1}, which is considerably larger than the value of 3.76×10^5 M^{-1}, obtained for the OLC/PDC-109 interaction. This is clearly due to the larger positive entropy of binding observed with OMC (5.69 cal.mol^{-1}.K^{-1}) as compared to that observed with OLC (-0.09 cal.mol^{-1}.K^{-1}). It appears that the interaction of the longer acyl chain in OMC with the protein exhibits a larger hydrophobic component which leads to larger entropy of binding.

4.4.2. Fluorescence studies on the interaction of PDC-109 to *O*-lauroylcholine

The binding of *O*-lauroylcholine to PDC-109 was studied using fluorescence spectroscopy at 25°C. The fluorescence emission spectra obtained for the titration of OLC with PDC-109 are shown in Fig. 4.2A. Spectrum 1 corresponds to PDC-109 alone and spectra 2 to 20 correspond to PDC-109 in presence of increasing concentrations of OLC. The binding of *O*-lauroylcholine to PDC-109 resulted in gradual decrease in the fluorescence intensity of PDC-109. The emission maximum for PDC-109 was observed at 340.5 nm, which upon addition of OLC exhibits a blue shift to 333 nm. A plot of ΔF *vs* concentration of added OLC gives the binding curve for the PDC-109/OLC interaction. A typical binding curve thus obtained is given in Fig. 4.2B. This

binding curve shows that the change in the fluorescence intensity of protein decreases with increased ligand concentration, displaying saturation behaviour.
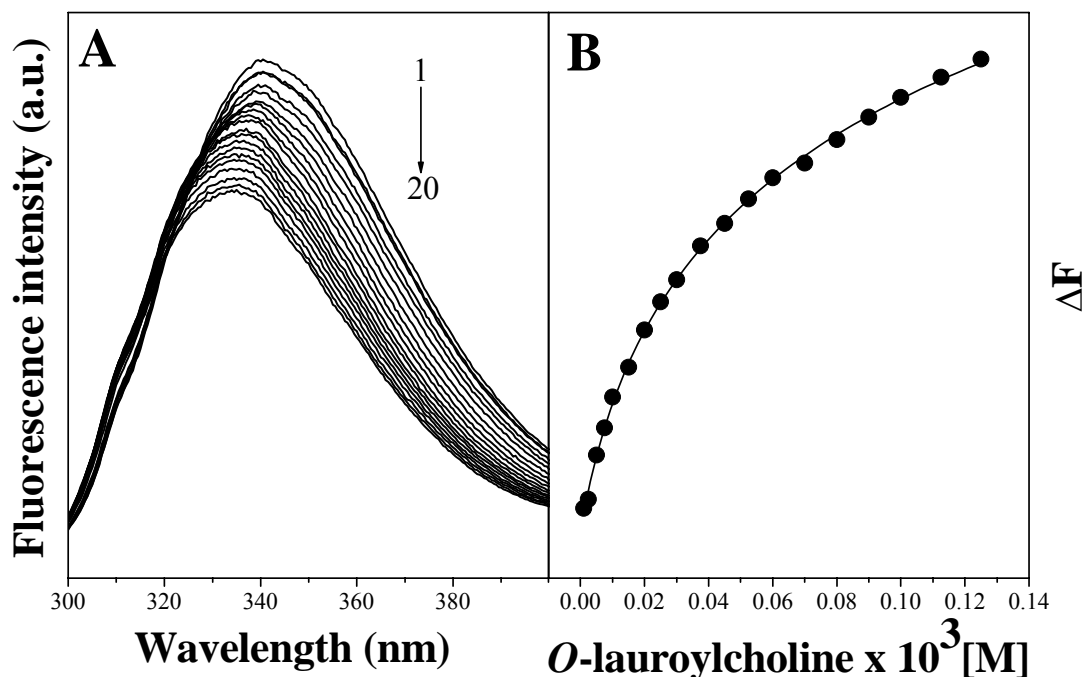
Fig. 4.2. (A) Fluorescence emission spectra of PDC-109 in the absence and presence of *O*-lauroylcholine at 25°C. Spectrum 1 corresponds to native PDC-109 and 2-20 corresponds to spectra of PDC-109 in presence of increasing concentrations of *O*-lauroylcholine. (B) Binding curve for the titration of PDC-109 with *O*-lauroylcholine at 25°C. The change in fluorescence intensity (ΔF) was plotted as a function of the concentration of *O*-lauroylcholine added.

A plot of ($F_o/\Delta F$) *vs* ($1/[L]_t$), where F_o refers to the fluorescence intensity of protein in the absence of any ligand and $[L]_t$ is the total ligand (OLC) concentration, yielded a straight line (Fig. 4.3A). From the ordinate intercept of the plot, the fluorescence intensity of the protein at infinite concentration of *O*-lauroylcholine (F_∞) was obtained. The maximal change in fluorescence intensity (ΔF_∞) corresponding to the complete saturation was calculated using the expression, $\Delta F_\infty = F_o - F_\infty$. Now, the p$K_a$ for the PDC-109/OLC interaction was obtained from the abscissa intercept of a plot of $[L]_f$ *vs* log $[\Delta F/(F_c - F_\infty)]$ according to the relationship,

$$\text{Log } [\Delta F/(F_c\text{-}F_\infty)] = \log K_a + \log [L]_f \qquad (1)$$

Where, F_c is the fluorescence intensity of the sample at any point during the titration and $[L]_f$ is the free ligand concentration and is given by:

$$[L]_f = \{[L]_t - ([P]_t \times (\Delta F/\Delta F_\infty)\} \qquad (2)$$

where $[P]_t$ is the total protein concentration. A plot of $\log[\Delta F/(F_c\text{-}F_\infty] \ vs \ [L]_f$ is shown in Fig. 4.3B. From the abscissa of the plot which gives pK_a, the association constant, K_a, at 25°C was estimated to be $5.46 \times 10^4 \ M^{-1}$.
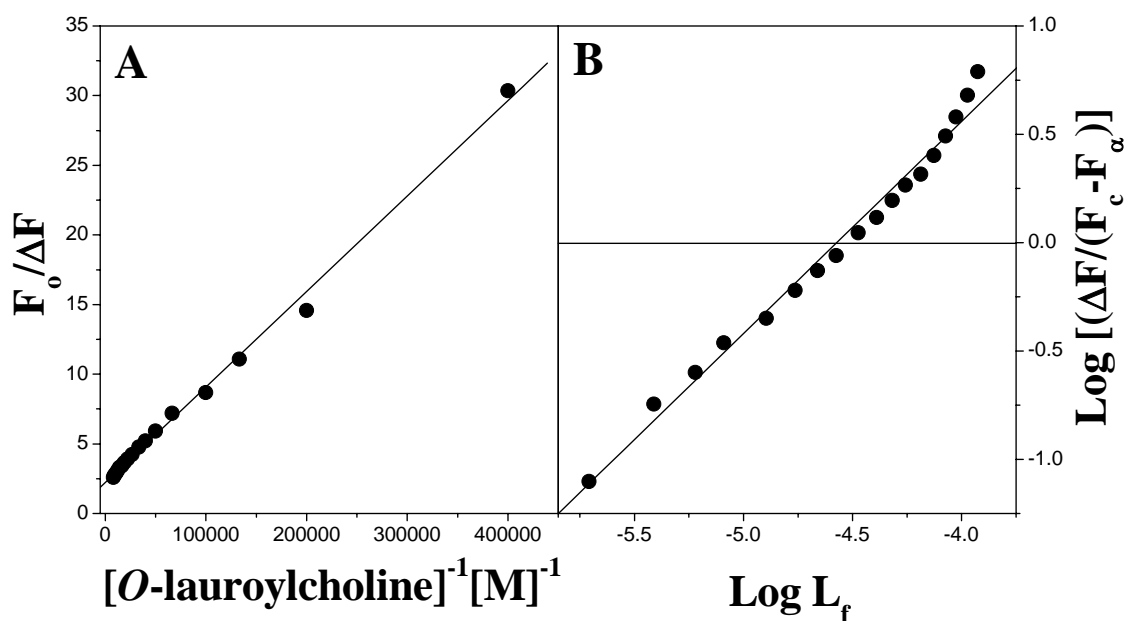
Fig. 4.3. (A) Plot of $(F_o/\Delta F)$ *vs* $(1/[L]_t)$. From the Y-intercept of this plot fluorescence intensity of the ligand at saturation binding was determined. (B) Chipman plot for the binding of PDC-109 to *O*-lauroylcholine. The abscissa of the plot yields pK_a, from which the association constant, K_a was determined.

4.4.3. CD spectroscopy

The far-UV and near-UV circular dichroic (CD) spectra of PDC-109 alone and in the presence of *O*-lauroylcholine are shown in Fig. 4.4A and Fig. 4.4B, respectively. The far-UV CD spectrum of PDC-109 (Thick line, Fig. 4.4A) is characterised by a broad positive band with a maximum at 222.2 nm and a shoulder at 211.8 nm which is consistent with previous reports [Gasset et al., 1997; Anbazhagan & Swamy, 2005].
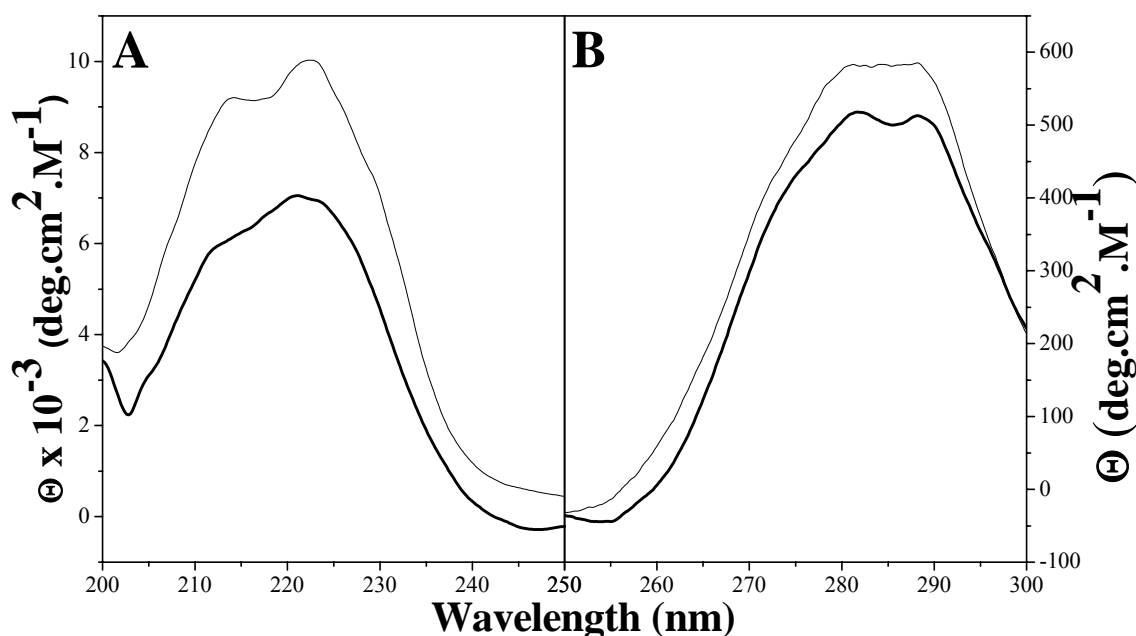
Fig. 4.4. Far and Near-ultraviolet CD spectra of PDC-109 in presence and absence of *O*-lauroylcholine. **(A)** Far-ultraviolet CD spectra of PDC-109 **(B)** Near-ultraviolet CD spectra of PDC-109. In both cases, PDC-109 in native condition (thick line), in the presence of 1 mM *O*-lauroylcholine (thin line).

Binding to OLC resulted in a considerable increase in the intensity of PDC-109 band and there was no significant change in the position of broad band maximum which is observed at 222.4 nm, whereas the shoulder has moved closed to major band with maximum at 213.8 nm (Fig. 4.4A). The near-UV CD spectrum of PDC-109 was

characterized by positive band with discrete maxima at 281.8 nm and 288.4 nm. Binding of OLC leads to an increase in the intensity in the band with the two maxima merging some what, leading to a relatively flat region at the top of the band.

4.5. Discussion

From the literature survey presented in Chapter 1 it is evident that PDC-109 specifically recognises the choline moiety in the head group of choline phospholipids. Therefore, it is of considerable interest to investigate its interaction with synthetic, choline containing molecules. Such studies can lead to the development of new synthetic molecules with high affinity to PDC-109. In preliminary work done in this direction, the interaction of two *O*-acyl derivatives of choline, namely *O*-lauroylcholine and *O*-myristoylcholine with PDC-109 was investigated by isothermal titration calorimetry, fluorescence spectroscopy and CD spectroscopy and the results obtained are discussed here.

Isothermal titration calorimetry is a powerful technique for investigating the interaction between different compounds. In addition to association constants that characterize the binding process, ITC also yields thermodynamic parameters that are associated with it and thus provides critical information about the nature of the interaction. Although the binding of OLC to PDC-109 is favoured by both enthalpy and entropy at 25°C, at higher temperatures the entropic factors do not favour binding. Thus the $\Delta S°$ value which is positive at 25°C becomes negative at 30°C, although very small in magnitude (-0.09 cal.mol^{-1}.K^{-1}). As the temperature is increased further, the magnitude of the (negative) entropy of binding increases further. These values outweigh the larger (negative) values of enthalpy of binding, which results in a decrease in the association constants.
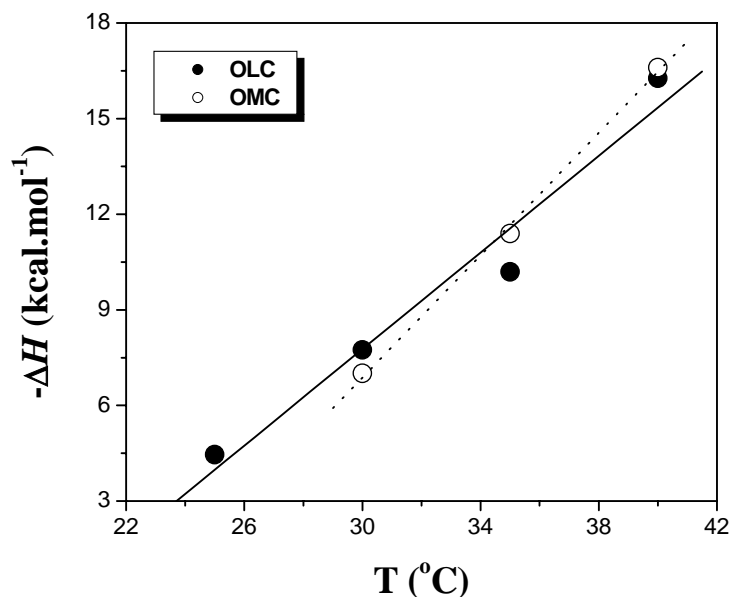
Fig. 4.5. Plot of ΔH^o versus T for the binding of *O*-lauroylcholine (●) and *O*-myristoylcholine (○) to PDC-109. From the slope of the linear least squares fits, the ΔC_p values were obtained.

From the temperature dependence of the enthalpy of binding for the interaction of OLC and OMC with PDC-109, we have obtained the change in heat capacity (ΔC_p) of the binding process (Fig. 4.5). The ΔC_p values obtained are -258 cal.mol^{-1}.K^{-1} and -233 cal.mol^{-1}.K^{-1}, for OLC and OMC, respectively. Negative values of ΔC_p have been reported earlier for the binding of chitobiose (-347 J.mol^{-1}.K^{-1}) and chitotriose (-498 J.mol^{-1}.K^{-1}) to lysozyme [Srinivas et al., 1999; García-Hernández et al., 2003] and for the association of mono- and disaccharides with the *Momordica charantia* lectin [Sultan & Swamy, 2005]. In these two studies, the decrease in ΔC_p has been attributed to the dehydration of polar groups that accompanies the binding process. If no protonation/deprotonation takes place during the binding process, the ΔC_p values can be attributed to hydration and dehydration of apolar and polar groups [Gómez et al., 1995]. Conformational changes induced by the binding reaction may also be responsible for a change in the heat capacity upon binding [Baxa et al., 2001]. Because the CD spectra

shown in Fig. 4.4 indicate changes in the secondary structure of PDC-109 upon binding of OLC, at least part of the changes in heat capacity associated with the binding could be due to conformational changes in the protein. Additionally, dehydration of the binding site resulting from the binding of OLC/OMC could also be responsible for the negative heat capacity changes observed as fluorescence spectroscopic studies have suggested that water molecules are most likely removed from the choline binding site upon binding of PrC and choline phospholipids [Anbazhagan et al., 2008].
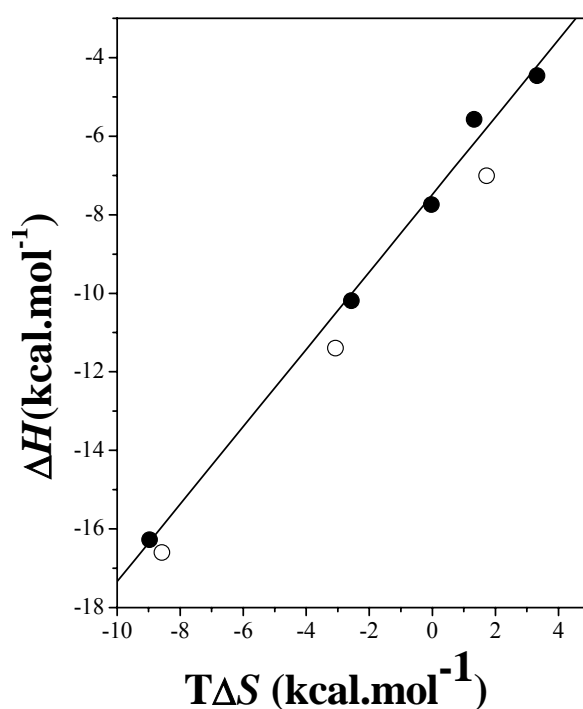
Fig. 4.6. Enthalpy-entropy compensation plot for the interaction of PDC-109 with *O*-acylcholines. The straight line corresponds to a linear least squares fit. (●) *O*-lauroylcholine, (○) *O*-myristoylcholine.

The thermodynamic data presented in Tables 4.1 and 4.2 show that the increase in (negative) enthalpy of binding is compensated by a corresponding (negative) change in entropy. This is clearly seen in the enthalpy-entropy compensation plot of ΔH *vs* $T\Delta S$ for the interaction of PDC-109 with *O*-lauroylcholine and *O*-myristoylcholine at

different temperatures (Fig. 4.6). This plot shows that the enthalpy and entropy of binding for the binding of OLC and OMC are very closely compensated with a slope of 0.985. An exact compensation of enthalpy by entropy would be expected to yield a slope of 1.0 [Eads et al., 1998].

The CD spectra presented in Fig. 4.4 show that binding of *O*-lauroylcholine results in an increase in the intensity of the spectral bands of PDC-109 in the near UV and far UV region, which is similar to the changes observed upon binding of phosphorylcholine or Lyso-PC with previous results [Gasset et al., 1997; Anbazhagan & Swamy, 2005]. These changes could be due to the changes in the secondary and tertiary structure of the protein, as PDC-109 which exist as a polydisperse aggregate in solution dissociates into dimeric form upon ligand binding [Gasset et al., 1997].

The K_a value of $5.08 \pm 0.69 \times 10^5$ M^{-1} for the binding of OLC to PDC-109 at 25°C is significantly higher than the K_a value estimated at the same temperature for the low affinity site ($1.19 \pm 0.09 \times 10^5$ M^{-1}) but somewhat lower than that for the high affinity site ($7.01 \pm 0.15 \times 10^5$ M^{-1}) for the Lyso-PC/PDC-109 interaction [Anbazhagan, 2005]. It should be possible to increase the binding affinity further by modifying the structure of the ligands suitably. The 3-dimensional structure(s) of complex(es) of single chain, choline-containing amphiphiles such as OLC or Lyso-PC would greatly help in designing suitable structures for such studies.

Chapter 5

Fluorescence and CD spectroscopic studies on the interaction of hydrophobic ligands to PDC-109 and its domain B

5.1. Summary

Binding of hydrophobic ligands, 8-anilino-1-naphthlene-sulfonic acid (ANS), 2-(*p*-toluidino) naphthalene-6-sulfonic acid (TNS), and 4,4'-dianilino-1,1'-binaphthyl-5,5'-disulphonic acid (bis-ANS) to the major bovine seminal plasma protein, PDC-109 and to domain B of PDC-109 (PDC-109/B) has been investigated by fluorescence and CD spectroscopy. Binding of ANS, TNS and bis-ANS to PDC-109 resulted in a decrease in the fluorescence intensity of protein and these changes were analysed to obtain the association constants for the binding process. At 25°C, the association constants, K_a, were determined to be 5.76×10^4 M^{-1}, 2.21×10^4 M^{-1} and 2.11×10^5 M^{-1} for ANS, TNS and bis-ANS respectively. Similar results were observed with PDC-109/B and the association constants for the binding of hydrophobic ligands, ANS, TNS and bis-ANS to domain B of PDC-109 were calculated to be 5.78×10^4 M^{-1}, 3.93×10^4 M^{-1} and 51.0×10^4 M^{-1} respectively. CD spectroscopic studies indicate that hydrophobic ligand binding lead to significant changes in the secondary and tertiary structures of PDC-109 and domain B.

5.2. Introduction

From the Introduction it is clear that PDC-109, the major protein of bovine seminal plasma plays an important role in the sperm fertilization by a process called capacitation which involves the removal of cholesterol and phospholipids from the sperm membrane. PDC-109 binds specifically to choline phospholipids that comprise over 70% of total phospholipids of bovine sperm plasma membrane [Desnoyers & Manjunath, 1992]. PDC-109 is a multifunctional protein as it binds to a variety of ligands in addition to heparin and lipid-binding which include different collagens (types, I, II, IV, V), fibrinogen, apolipoprotein A1, apolipoprotein A1/high-density lipoprotein complexes, high density lipoproteins, low density lipoproteins and calmodulin [Thérien et al., 1995].

PDC-109 contains two type II domains, homologous to those of fibronectin. Type II domains are found in many proteins such as in BSP-A3 [Esch et al., 1983; Seidah et al., 1987]; in blood coagulation factor XII [McMullen & Fujikawa, 1985]; in insulin-like growth factor II receptor/cation-independent mannose-6-phosphate receptor [Morgan et al., 1987; Lobel et al., 1988]; and in 72-kDa and 92-kDa type IV collagenases [Collier et al., 1988; Wilhelm et al., 1989]. The ubiquitous occurrence of this module type and its presence in the proteins with diverse functions make this domain an interesting object for structural and functional studies. Domain B of PDC-109 binds to gelatine-Sepharose 4B and the affinity was found to increase with increasing solvent ionic strength, suggesting that hydrophobic interactions play a major role in the binding. The presence of hydrophobic binding site was also supported by the observation that the domain B has an affinity for the neopentyl groups of alkyl-Superose [Bányai et al., 1990].

Naphthalene dyes have proven to be very useful as molecular probes in characterizing conformational changes in proteins. 8-anilino-1-naphthalene sulfonic acid is a much utilized fluorescent "hydrophobic probe" for examining the nonpolar character of the proteins and membranes. ANS is commonly used to investigate hydrophobic regions on the surface of proteins [Banerjee & Kishore, 2006]. ANS is considered to bind to hydrophobic surfaces of the protein, primarily through its nonpolar anilinonaphthalene group. However, titration calorimetric studies have demonstrated that ANS binding to a number of proteins occurs through electrostatic forces, in which ion pairs are formed between the sulfonate groups of ANS and cationic groups on the protein [Matulis & Lovrien, 1998].

Previous CD spectroscopic studies have shown that phosphorylcholine (PrC) and Lyso-PC binding leads to notable changes in the secondary and tertiary structure of PDC-109 [Gasset et al., 1997; Anbazhagan & Swamy, 2005]. In order to investigate effect of hydrophobic ligand binding on the structure of PDC-109 and PDC-109/B and to compare the effect of these ligands on the structure of PDC-109 and second type II domain under similar conditions, we have carried out CD spectroscopic studies. The binding of hydrophobic ligands to PDC-109 and PDC-109/B was investigated at 25°C by monitoring the changes in the fluorescence intensity of protein upon titration with the ligand in order to determine the association constant of the binding.

5.3. Materials and Methods

5.3.1. Materials

Choline chloride (Ca^{2+} salt), tris (hydroxymethyl)-aminomethane (Tris base), 8-anilino-1-naphthlene-sulfonic acid (ANS), 2-(p-toluidino) naphthalene-6-sulfonic acid (TNS), 4,4'-dianilino-1,1'-binaphthyl-5,5'-disulphonic acid (bis-ANS), citraconic anhydride,

trypsin, acrylamide, phosphorylcholine (PrC), bis-acrylamide and TEMED were obtained from Sigma Chemical Co. (St. Louis, MO). Sephadex G-50 (Superfine) and DEAE Sephadex A-25 were from Pharmacia Biotech (Uppsala, Sweden). Sodium chloride, EDTA, sodium azide and all other reagents were obtained from local suppliers and were of the highest purity available.

5.3.2. Fluorescence spectroscopy

Steady state fluorescence measurements were performed using a Spex model Fluoromax-3 spectrofluorimeter at 25ºC. The excitation and emission band pass filters were set at 3 nm. PDC-109 in TBS-I (pH 7.4) buffer with $OD_{280nm} < 0.1$ was excited at 280 nm and emission spectra recorded between 300 and 400 nm. Fluorescence titrations were performed by adding small aliquots of 1 mM ANS, TNS, or 0.5 mM bis-ANS solution to 2 ml of PDC-109 or PDC-109/B solution in cuvette. All the binding data reported here corresponds to the average values obtained from two independent titrations. Fluorescence data were corrected for dilution effects as well as for inner filter effect as described in Chapter 3.

5.3.3. Circular dichroism spectroscopy (CD)

Circular dichroism (CD) spectra were recorded on a Jasco-J-810 spectropolarimeter equipped with a thermostatted water bath. All measurements were carried out at 25°C with a scan speed of 20 nm/min using a 0.2 cm path length quartz cell. Far-UV measurements were carried out in the 200-250 nm range and near-UV CD measurements were carried out in the 250-300 nm range. Far-UV and near-UV CD spectra were recorded at PDC-109 concentrations of about 0.1 mg/ml and 1.0 mg/ml, respectively. For measurements with PDC-109/B the protein concentration was 0.18 mg/ml and 1.01 mg/ml, respectively, in the Far-UV and near-UV CD. Data were

collected with a response time of 2 s and a slit width of 1 nm. Each spectrum reported was the average of 20 consecutive scans for which the buffer scans, recorded under the same conditions, were subtracted. The observed ellipticities were converted to mean residual ellipticities (Θ) using a mean molecular mass/residue of 117 for PDC-109 [Esch et al., 1983].

5.4. Results and Discussion

The binding of three hydrophobic ligands, namely ANS, TNS, and bis-ANS to PDC-109 and domain B of PDC-109 (PDC-109/B) was studied using fluorescence spectroscopy at 25°C. Fluorescence emission spectra of PDC-109 in the absence and in the presence of different concentrations of ANS are shown in Fig. 5.1A. The binding of ANS to PDC-109 resulted in a significant decrease in the fluorescence intensity of PDC-109 initially, whereas at higher concentrations of the added ligand, the changes in
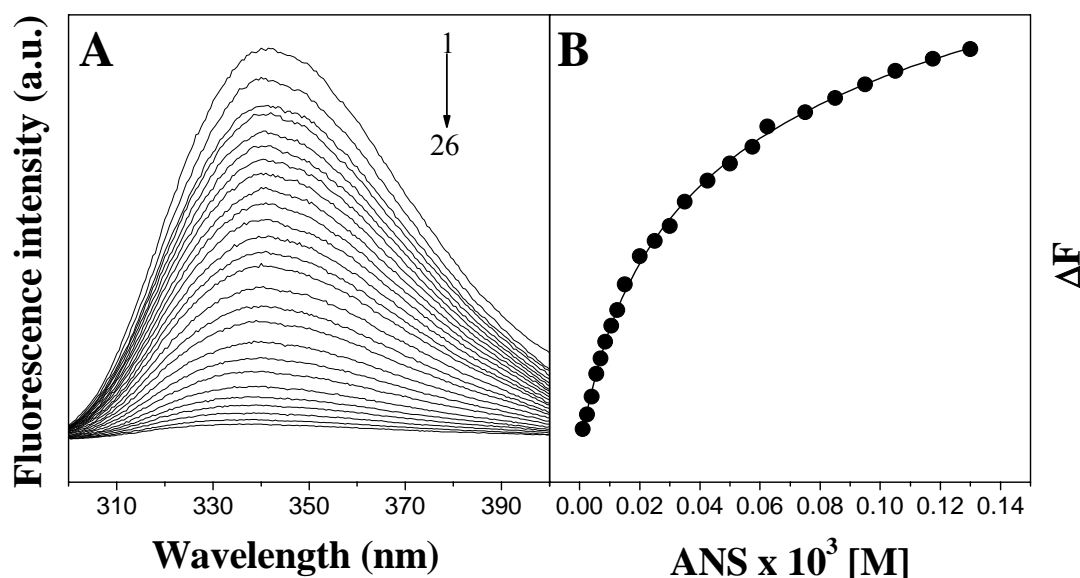
Fig. 5.1. (A) Fluorescence emission spectra of PDC-109 in the absence and presence of ANS. Spectrum 1 corresponds to native PDC-109 and spectra 2-26 correspond to spectra of PDC-109 in the presence of increasing concentrations of ANS. **(B)** Binding curve for the binding of PDC-109 to ANS at 25°C. The change in fluorescence intensity (ΔF) was plotted as a function of the concentration of ANS added.

the fluorescence intensity become gradually smaller, showing saturation behaviour. The fluorescence titration data for the binding of ANS to PDC-109 were analyzed in the following manner.   A plot of ΔF (= F_o-F_c) as a function of the added ligand concentration gave the binding curve (Fig. 5.1B).   The binding curve shows that the change in fluorescence intensity decreases with increase in ligand concentration, displaying saturation behaviour.

A plot of ($F_o/\Delta F$) *vs* ($1/[L]_t$), where F_o refers to the fluorescence intensity of protein in the absence of ANS, and $[L]_t$, is the total ligand concentration, yielded a straight line for interaction of PDC-109 with ANS (Fig. 5.2A).   From the ordinate intercept of the plot, the fluorescence intensity of the protein was found to be totally quenched at infinite concentration of ANS (i.e., $F_\infty = 0$).   The maximal change in fluorescence intensity ($\Delta F_\infty = F_o - F_\infty$) corresponding to complete saturation is therefore equal to F_0.   The pKa for the PDC-109 - ANS interaction was obtained from the abscissa of a plot of $[L]_f$ *vs* log $[\Delta F/(F_c-F_\infty)]$ according to the equation given below [Chipman et al., 1967]:

$$\text{Log } [\Delta F/(F_c\text{-}F_\infty)] = \log K_a + \log [L]_f \qquad\qquad (1)$$

Where, F_c is the fluorescence intensity of the sample at any point during the titration. $[L]_f$ is the free ligand concentration and is given by

$$[L]_f = \{[L]_t - [P]_t \times (\Delta F/\Delta F_\infty)\} \qquad\qquad (2)$$

where $[P]_t$ is the total protein concentration. A plot of log$[\Delta F/(F_c\text{-}F_\infty)]$ *vs* $[L]_f$ (which we shall refer to as a Chipman plot) is shown in Fig. 5.2B. From the abscissa intercept of the plot which gives pK_a, the association constant, K_a, at 25°C was estimated as 5.76 $\times 10^4$ M^{-1} for ANS binding to PDC-109.
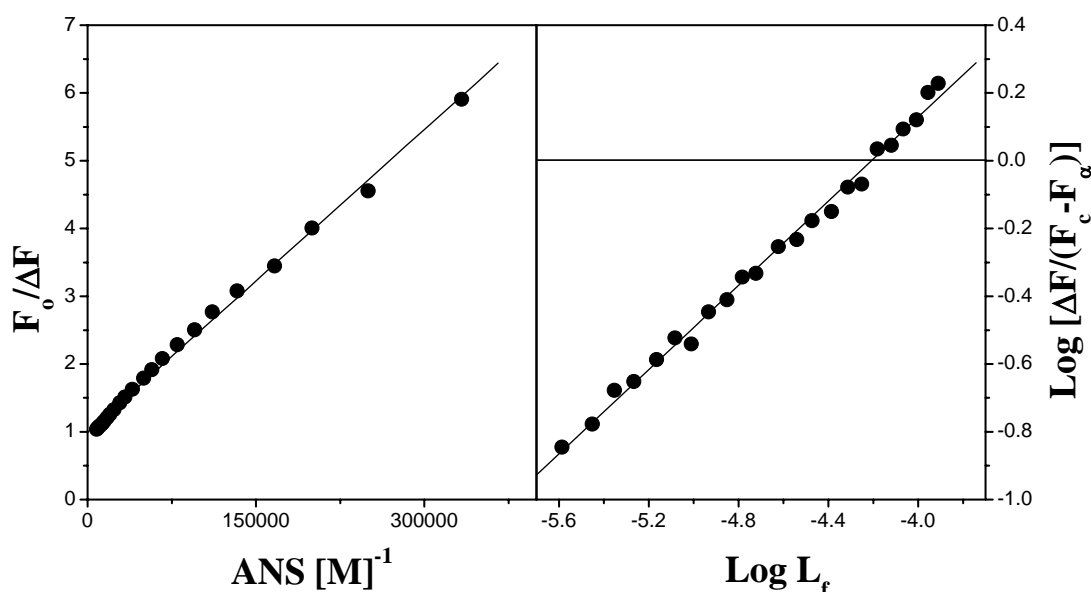
Fig. 5.2. (A) Plot of $(F_o/\Delta F)$ *vs* $(1/[L]_t)$ for the binding of PDC-109 to ANS at 25°C. From the Y-intercept of this plot fluorescence intensity of the ligand at saturation binding was determined. **(B)** Chipman plot for the binding of PDC-109 to ANS. The abscissa of the plot yields pK_a, from which the association constant, K_a was determined.

The fluorescence spectra of PDC-109 corresponding to the titration with bis-ANS and the corresponding binding curve are given in Fig. 5.3A and Fig. 5.3B, respectively. Plots of $(F_o/\Delta F)$ *vs* $(1/[L]_t)$ and Chipman plot corresponding to the binding of bis-ANS to PDC-109 are given in Fig. 5.4A and Fig. 5.4B, respectively. For bis-ANS also the fluorescence intensity of PDC-109 was found to be totally quenched at saturation binding, whereas for TNS at saturation binding the fluorescence emission intensity of the protein was found to be quenched by 83% (spectra not shown). The titration data obtained with TNS and bis-ANS were also analysed in a similar manner and the association constants for the interaction of these two fluorescent probes with PDC-109 were determined. The K_a values obtained from this analysis for the interaction of bis-ANS and TNS with PDC-109 are 2.11×10^5 M^{-1} and 2.21×10^4 M^{-1}, respectively. From the K_a values obtained for ANS, TNS, and bis-ANS it is clear that the interaction of
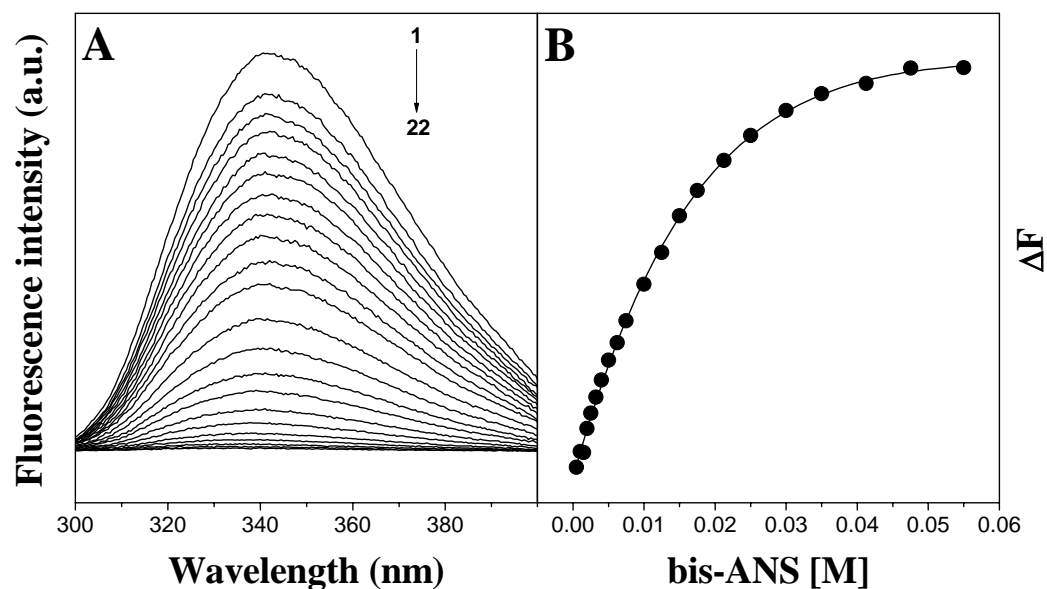
Fig. 5.3. (A) Fluorescence emission spectra of PDC-109 in the absence and presence of bis-ANS. Spectrum 1 corresponds to native PDC-109 and spectra 2-22 correspond to spectra of PDC-109 in the presence of increasing concentrations of bis-ANS. **(B)** Binding curve for the binding of PDC-109 to bis-ANS at 25°C.
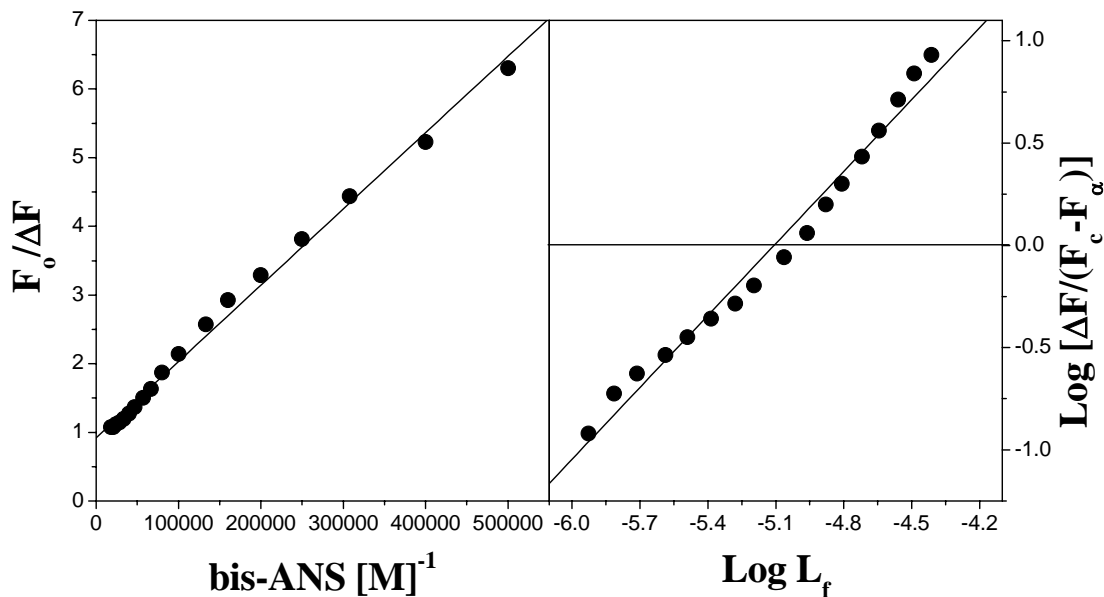

F**ig. 5.4. (A)** Plot of $(F_o/\Delta F)$ *vs* $(1/[L]_t)$ for the binding of PDC-109 to bis-ANS at 25°C. From the Y-intercept of this plot fluorescence intensity of the ligand at saturation binding was determined. **(B)** Chipman plot for the binding of PDC-109 to bis-ANS. The abscissa of the plot yields pK_a, from which the association constant, K_a was determined.

bis-ANS with PDC-109 is characterized by a stronger affinity with the K_a value for bis-ANS being 3.66 and 9.54 times higher than ANS and TNS, respectively. All these K_a values are listed in Table 5.1.

Table 5.1: Association constants, K_a, obtained from fluorescence titrations for the interaction of different hydrophobic ligands with PDC-109 and domain B of PDC-109.

Protein	Ligand	$K_a \times 10^{-4}$ (M^{-1})
PDC-109		
	ANS	5.76
	TNS	2.21
	bis-ANS	21.1
PDC-109/B		
	ANS	5.78
	TNS	3.93
	bis-ANS	51.0

5.4.1. Fluorescence studies on binding of hydrophobic ligands to PDC-109/B

Emission spectra of domain B of PDC-109 in the absence and presence of different concentrations of ANS are shown in Fig. 5.5A. The spectra are characterized by an emission maximum at 345 nm and the fluorescence intensity decreases with increasing concentrations of the ligand. However, there was no shift in the emission maximum in presence of ANS or the other hydrophobic ligands investigated here, namely TNS or bis-ANS (spectra not shown).

A plot of ΔF *versus* concentration of ligand added gives the binding curve for the interaction of PDC-109/B with ANS (Fig. 5.5B). A plot of ($F_o/\Delta F$) *vs* ($1/[L]_t$) where F_o is the fluorescence intensity of PDC-109 alone, ΔF ($=F_o-F$) is the change in

fluorescence at any point during the titration and F is the fluorescence intensity of PDC-109/B with added ligand at concentration [L]. From the intercept of the plot the fluorescence intensity of the sample at infinite concentration of the ligand, F_∞ was determined and it was found that the fluorescence intensity of PDC-109/B is quenched by 82% at saturation binding.
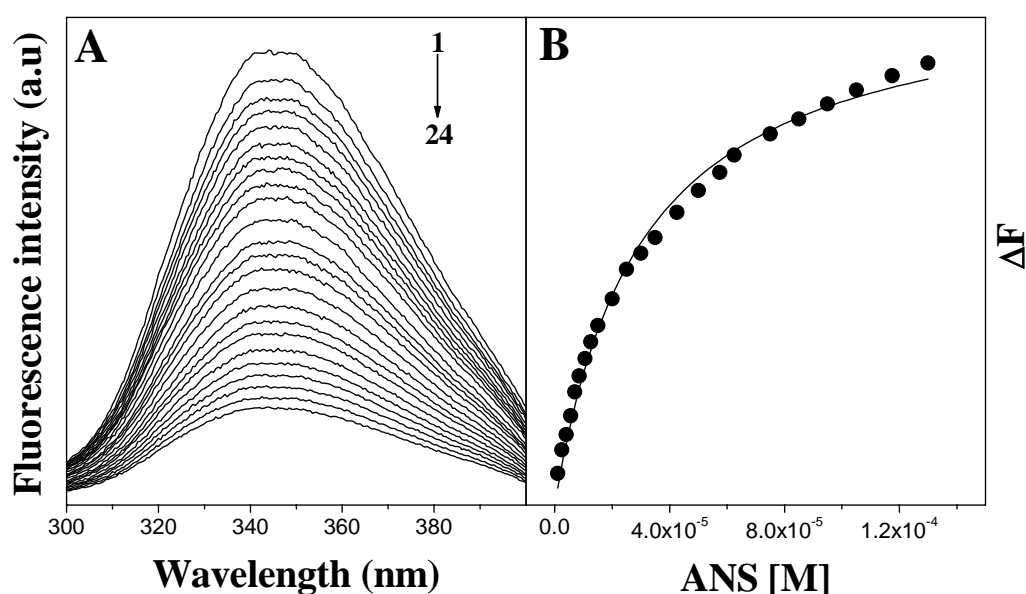
Fig. 5.5. (A) Fluorescence emission spectra of PDC-109/B in the absence and presence of ANS at 25°C. Spectrum 1 corresponds to native PDC-109 and 2-24 corresponds to spectra of PDC-109/B in presence of increasing concentrations of ANS. **(B)** Binding curve for the titration of PDC-109/B with ANS at 25°C.

The K_a value for ANS-PDC-109/B association was calculated from the plot of log $\{\Delta F/(F_c - F_\infty)\}$ versus log $[L]_f$ according to equation 1 as 5.78×10^4 M^{-1}(Fig. 5.6). Addition of TNS and bis-ANS to PDC-109 also resulted in a decrease in the fluorescence intensity of the protein and the maximum quenching at infinite concentration of these two ligands was estimated to be 65% and 100%, respectively (data not shown). The association constant obtained for the interaction of TNS and bis-

ANS with PDC-109/B by the Chipman analysis is 3.93×10^4 M^{-1} and 5.1×10^5 M^{-1} respectively (Fig. 5.6B). These values show that the binding of bis-ANS is about 8.8 and 13 fold stronger than ANS and TNS, respectively.
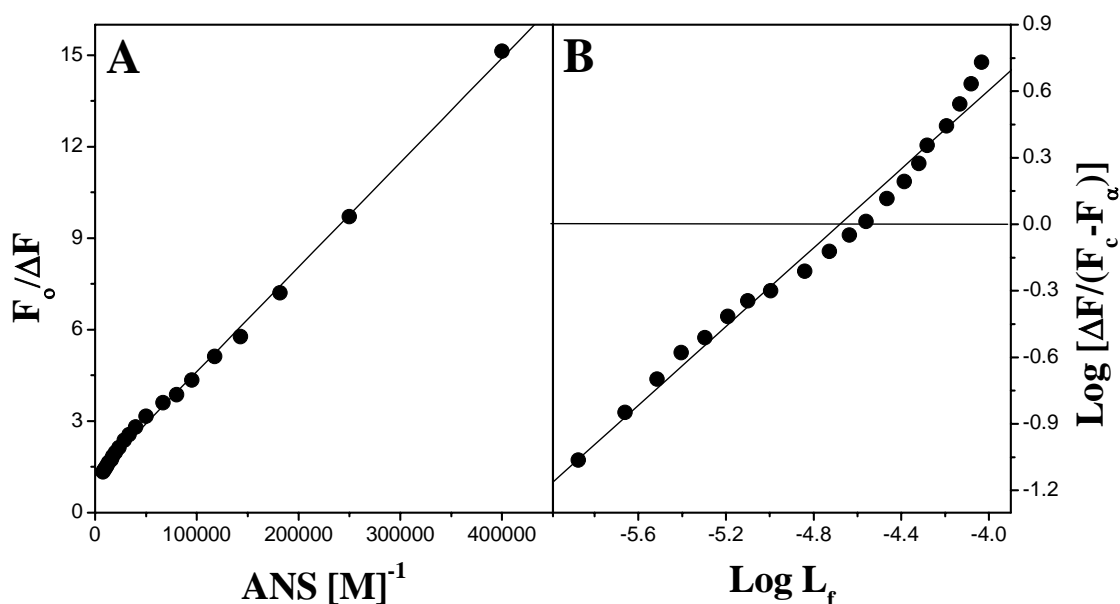
Fig. 5.6. **(A)** Plot of $(F_o/\Delta F)$ *vs* $(1/[L]_t)$ for the binding of PDC-109/B to ANS at 25°C. From the Y-intercept of this plot fluorescence intensity of the ligand at saturation binding was determined. **(B)** Chipman plot for the binding of PDC-109/B to ANS. The abscissa of the plot yields pK_a, from which the association constant, K_a was determined.

5.4.2. Effect of hydrophobic ligand binding - CD spectroscopic analysis

The far-UV and near-UV Circular dichroic (CD) spectra of PDC-109 alone and in the presence of ANS and TNS are shown in Figure 5.7A and Figure 5.7B, respectively. Consistent with the previous reports, the far UV CD spectrum (thick line, Fig. 5.7A) of the native protein is characterised by a broad positive, asymmetric band with a maximum at 223.4 nm and a shoulder at about 213.2 nm, which appears to be due to the high content of aromatic amino acids and disulfide bonds in the protein [Gasset et al., 1997]. These spectral features have been identified in the fibronectin type II domains of

gelatinase A and have been ascribed to the native conformation [Bányai et al., 1996]. PDC-109 contains eight tyrosines, five tryptophans, six phenylalanine residues and four intramolecular disulfide bonds [Esch et al., 1983]. Analysis of the far-UV CD spectra to obtain secondary structure composition was not possible due to the lack of appropriate protein reference data set [Esch et al., 1983; Gasset et al., 1997]. Binding of ANS or TNS to PDC-109 resulted in a reduction in the overall intensity in the CD spectrum of native PDC-109. The band at 223.4 nm was blue shifted to 220.2 nm and 222.6 nm upon binding of PDC-109 to ANS and TNS, respectively, whereas the shoulder at 213.2 nm experiences a slight red shift to 213.4 nm and 214.8 nm, respectively.
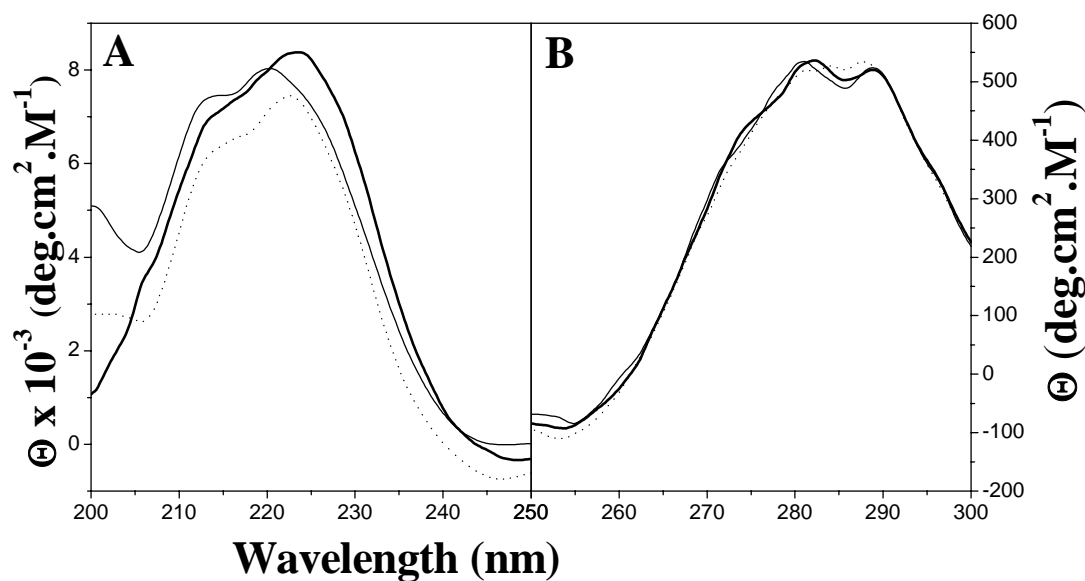
Fig. 5.7. Far and Near-ultraviolet CD spectra of PDC-109. (**A**) Far-ultraviolet CD spectra of PDC-109 in TBS-I buffer, pH 7.4, (**B**) Near-ultraviolet CD spectra of PDC-109 in TBS-I buffer, pH 7.4. PDC-109 in native condition (thick line), in the presence of 1 mM ANS (thin line), and in the presence of 1 mM TNS (dotted line).

The near-UV CD spectrum of PDC-109 has shown a major positive band with two discrete maxima at 282 nm and 289 nm which is consistent with the previous

studies by Gasset et al. [1997]. There was not much change in the intensity of the near-UV CD spectrum of PDC-109 upon interaction with ANS or TNS. In the presence of ANS also two closely spaced and overlapping bands are seen; however, these bands are slightly blue shifted and occur at 280.8 nm and 288.8 nm, whereas in case of TNS, peak position of PDC-109 at 289 nm is shifted to 287.8 nm and there was no change in the position of 282 nm peak.

5.4.3. CD spectroscopic studies on domain B of PDC-109

The far-UV and near-UV Circular dichroic (CD) spectra of domain B of PDC-109 alone and in the presence of ANS and TNS are shown in Figure 5.8A and Figure 5.8.B, respectively. The far-UV CD spectrum of PDC-109/B has shown band maximum at 224.8 nm and minimum at 203.2 nm, which is consistent with the previous results which indicated that proteins containing single Type II modules are characterized by a maximum at 224 nm [Bányai et al., 1996]. The maxima at 224 nm are characteristic of the ordered native structure of the type II modules. Binding of PDC-109/B to ANS and TNS resulted in a net increase in the intensity of PDC-109/B spectrum and the effect was more in case of TNS. There was no change in the band position of 224.8 nm upon binding of ANS to PDC-109/B, but there was slight shift in the minimum from 203.2 nm to 204.4 nm. Interaction of PDC-109/B to TNS resulted in a blue shift from band maximum from 224.8 nm to 222.2 nm and red shift of band minimum from 203.2 nm to 205.2 nm.

The near-UV CD spectrum of PDC-109/B has shown a major positive band with two discrete maxima at 281.6 nm and 290 nm with a pattern that is similar to native PDC-109, but the peaks are not as sharp as in case of PDC-109. There was an increase in the intensity of the spectrum of PDC-109/B upon interaction with ANS or TNS. In the presence of ANS or TNS also two closely spaced bands are seen. There was a slight

change in the band positions from 281.6 nm to 281.8 nm and there was no shift in band at 290 nm in case of ANS binding to PDC-109/B, whereas in presence of TNS the band position has slightly blue shifted from 281.6 nm to 281.2 nm and from 290 nm to 289 nm.
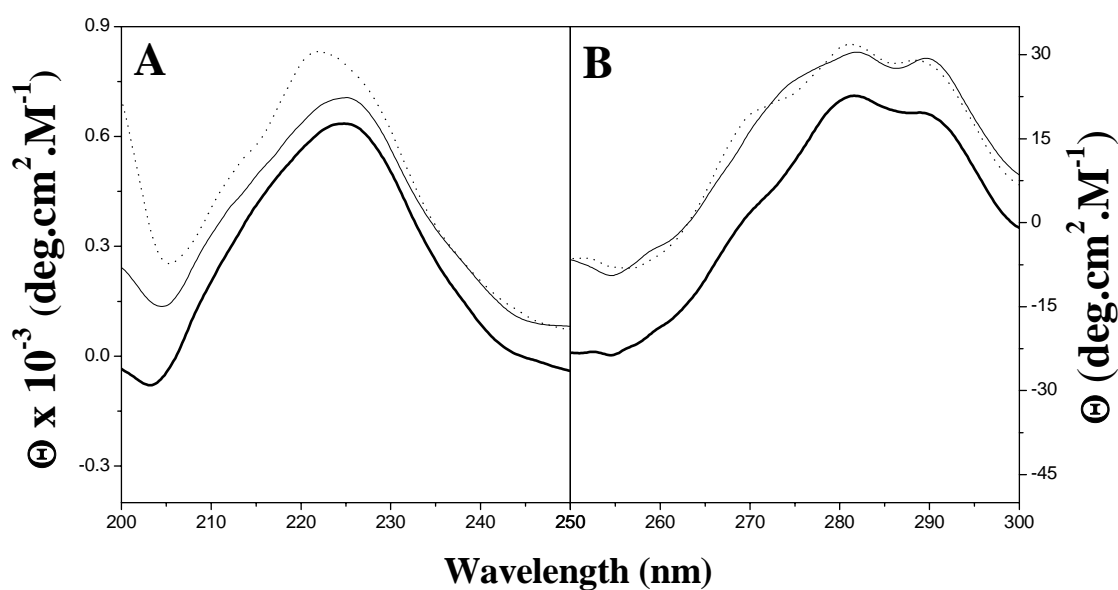
Fig. 5.8. Far and Near-ultraviolet CD spectra of domain B of PDC-109. (A) Far-ultraviolet CD spectra of PDC-109/B in TBS-I buffer, pH 7.4, **(B)** Near-ultraviolet CD spectra of PDC-109/B in TBS-I buffer, pH 7.4. PDC-109 in native condition (thick line), in the presence of 1 mM ANS (thin line), in the presence of 1 mM TNS (dotted line).

Previous CD spectroscopic studies have shown that PrC and Lyso-PC binding to PDC-109 leads to significant changes in the secondary and tertiary structure of PDC-109 [Gasset et al., 1997; Anbazhagan & Swamy, 2005]. X-ray studies have revealed that binding of PrC leads to conformational changes in the polypeptide backbone of PDC-109 [Wah et al., 2000]. In the present study also, changes have been observed in the far and near-UV CD spectra upon binding of ANS and TNS, reflecting changes in the secondary and tertiary structure of the protein.

The present study shows that interaction of ANS and TNS with PDC-109/B increased the intensity of the CD spectra. These changes suggest a modification of the environment of aromatic side chains and disulfide bonds of the protein, which may be a result of direct interaction of ligand with chromophores, or polypeptide backbone rearrangement. Binding of PrC to PDC-109 also resulted in considerable increase in the near-UV and far-UV CD spectra of the protein [Gasset et al., 1997].

Studies on single type II domain of PDC-109 and other proteins may significantly help further studies on the molecular mechanisms of their interaction with ligands and thus contribute in understanding the biological activity of various proteins containing homologous type II modules.

Chapter 6

Fluorescence spectroscopic investigations on the interaction of PDC-109/B with phospholipid membranes

6.1. Summary

The microenvironment and accessibility of the tryptophan residues in domain B of PDC-109 (PDC-109/B) in the native state and upon ligand binding have been investigated by fluorescence quenching, time resolved fluorescence and red-edge excitation shift (REES) studies. The extent of quenching of the intrinsic fluorescence of PDC-109/B by acrylamide, succinimide, iodide ion and cesium ion at a quencher concentration of 0.5 M was 88.4%, 83.9%, 62.1% and 46.2%, respectively. Binding of PrC, Lyso-PC and DMPC to domain B resulted in a progressive decrease in the degree of quenching, suggesting that, in addition to the choline head group, presence of acyl chains stabilize the binding resulting in a tightening of the protein structure, leading to decreased accessibility of the tryptophan residues to the different quenchers. A red-edge excitation shift (REES) of 3.5 nm was observed with native PDC-109/B, suggesting that the microenvironment surrounding the Trp residues in this protein has a reduced mobility and that the reorientation of the solvent water molecules around them is significantly restricted. Changes observed in REES values for PDC-109/B in the presence of Lyso-PC and DMPC were smaller as compared to the corresponding changes in the case of intact PDC-109. This suggested that PDC-109/B is probably unable to induce cholesterol efflux because it does not penetrate deep into the hydrophobic interior of the membrane.

6.2. Introduction

PDC-109 is the major protein of bovine seminal plasma which binds to choline phospholipids present on sperm plasma membrane. The binding results in the efflux of cholesterol and phospholipids from the sperm membrane which is a crucial step in sperm capacitation. In view of this, it is important to understand the interaction of this protein with choline containing membranes in order to know the molecular events that takes place in sperm capacitation. Spin label electron spin resonance studies reveal that PDC-109 exhibit highest selectivity for the choline phospholipids than the phospholipids containing other head group. Upon binding to PC membranes, PDC-109 penetrates into the hydrophobic core of the membrane, indicating the direct interaction of segments of the protein with lipid acyl chains [Ramakrishnan et al., 2001]. Surface plasmon resonance studies indicate that binding of PDC-109 to different phospholipid membranes containing 20% (wt/wt) cholesterol occurs by a single step mechanism. The high specificity of PDC-109 for the choline phospholipids has been shown to be due to a faster association rate constant and a slower dissociation rate constant as compared to phospholipids bearing other head groups [Thomas et al., 2003]. PDC-109 affects the membrane structure of lipid vesicles and biological membranes in that the mobility of spin-labelled phospholipids was reduced in the presence of the protein. The immobilizing effect of PDC-109 was not restricted to analogues of phosphotidylcholine (PC) but was also detected with spin-labeled phosphatidylethanolamine (PE), however, the extent of immobilization was significantly lower for the PE compared with PC, supporting the lipid head group specificity of the protein. PDC-109 induced an immobilization of about 50% of spin-labeled analogues molecules, indicating an influence mainly those molecules incorporated into the outer membrane leaflet [Greube et al., 2001]. PDC-109 extracts

phospholipids with a phosphorylcholine head group mainly from the outer leaflet of human erythrocytes, bovine epididymal sperm cell membranes [Tannert et al., 2007].

Although the above biophysical studies yielded much valuable information on the interaction of PDC-109 with membranes, molecular events of the interaction are not very clear. Additional studies are required to understand the structural and functional aspects of the protein. Fluorescence spectroscopy has proved to be a very successful technique to study the protein structure and conformations. The emission characteristics of aromatic amino acids, especially tryptophan residues in proteins have been widely used to obtain information about protein structure and conformational changes resulting from a variety of factors such as ligand/substrate binding, association/dissociation of subunits in oligomeric proteins, and unfolding [Grinvald & Steinberg, 1976; Lakowicz, 1999]. From our laboratory, systematic studies have been carried out on the intrinsic fluorescence of PDC-109 in the native state, upon binding to PrC, Lyso-PC micelles and DMPC SUVs, and upon denaturation. Also the accessibility and environment of the fluorescent Trp residues have been investigated by quenching studies using two neutral quenchers, acrylamide and succinimide and two ionic quenchers, iodide and cesium ion. These studies indicate that ligand (PrC, Lyso-PC micelles, DMPC SUVs) binding shields the Trp residues from different quenchers, with shielding ability in following order: PrC < Lyso-PC < DMPC, indicating that while PDC-109 binds to PC-containing membranes by specific recognition of the phosphorylcholine moiety, the acyl chains of the lipid also interact with the protein, resulting in a further tightening of the protein structure [Anbazagan et al., 2008].

PDC-109 is composed of an *N*-terminal 23-residue stretch followed by two tandemly repeating fibronectin type II (FnII) domains. Each FnII domain contains a

choline phospholipid binding site and both the binding sites are necessary to induce cholesterol efflux. PDC-109 contains five tryptophan residues at positions 47, 58, 90, 93 and 106 [Esch et al., 1983]. The second fibronectin type II domain of PDC-109 (PDC-109/B) contains 3 tryptophan residues, whose fluorescence properties can be monitored to investigate changes in its conformation and to study the effect of ligand binding.

In the present study, systematic studies have been carried out on the intrinsic fluorescence of PDC-109/B in the native state and in the presence of PrC, Lyso-PC micelles and DMPC SUVs. The environment and accessibility of Trp residues has been investigasted by fluorescence quenching studies employing two neutral quenchers, acrylamide and succinimide, an anionic quencher, iodide (I^{P-}) and a cationic quencher, cesium ion (Cs^{+}). Shift in the wavelength of maximum fluorescence emission toward higher wavelength, caused by a shift in the excitation wavelength towards the red edge of absorption band (commonly referred to as REES), has been investigated in order to obtain information on the environment and organization of the Trp residues in this protein in the native state, upon binding to PrC, Lyso-PC and DMPC, and upon denaturation. REES arises from slow rates of solvent relaxation (reorientation) around an excited state fluorophore which is a function of the motional restriction imposed on the solvent molecules in the immediate vicinity of the fluorophore [Chattopadhyay, 1999a]. REES can be used to study motional restriction experienced by membrane-bound molecules and serve as a powerful means to monitor organization and dynamics of probes and peptides bound to micelles or membranes [Chatopadhyay, 1999b].

6.3. Materials and Methods

6.3.1. Materials

Acrylamide, guanidine hydrochloride, β-mercaptoethanol, phosphorylcholine (PrC), choline chloride, succinimide, cesium chloride, trypsin, citraconic anhydride and Sephadex G-50 were purchased from Sigma (St. Louis, MO, USA). Potassium Iodide (KI) was purchased from Qualigens (Mumbai, India). Dimyristoylphosphatidylcholine (DMPC). dimyristoylphosphatidylglycerol (DMPG), dimyristolylphosphatidic acid (DMPA) and lysophosphatidylcholine (Lyso-PC) were from Avanti Polar lipids (Alabaster, AL, USA). PDC-109 was purified by a combination of gel filtration and affinity chromatography on DEAE Sephadex A-25 as described in Chapter 2. All other chemicals used were of analytical grade and were obtained from local suppliers.

6.3.2. Isolation of domain B of PDC-109

One hundred milligrams of PDC-109 was dialyzed against 0.25 M borate buffer pH 9.0 and was citraconylated with 250 µl of citraconic anhydride at 25ºC. The pH of the reaction mixture was maintained at 9.0 by adding small aliquots of 1 M NaOH as required. The reaction mixture was then dialyzed thoroughly against 0.1 M ammonium carbonate buffer, pH 8.0. The citraconylated protein was digested with 2 mg of trypsin for 15 min at 25ºC. The reaction was stopped by adding acetic acid (10% final concentration) and kept for incubation for 24 hours at 37ºC to decitraconylate the protein. The decitraconylated protein was subjected to gel filtration on Sephadex G-50 (fine) column pre-equilibrated with 10% acetic acid. Fractions were collected and absorbance was monitored at 280 nm. The elution

profile yielded a broad peak with a shoulder corresponding to ca. 10 kDa and a second sharper peak corresponding to 5 kDa, consistent with the report by Bányai et al. [1990]. This 5 kDa fragment corresponds to the second fibronectin type II domain of PDC-109 and is referred to as domain B (PDC-109/B) [Bányai et al., 1990; Constantine et al., 1992]. Purity of domain B was assessed by SDS-PAGE on 16% gels, where it moved as a single band.

6.3.3. Preparation of liposomes

Lipids dissolved in dichloromethane in a glass tube were dried under a gentle stream of nitrogen gas. After removing the traces of solvent by vacuum desiccation for over 3 h, the lipid was hydrated with TBS-I [pH 7.4] to give the desired lipid concentration. Small unilamellar vesicles (SUVs) were prepared by sonication of the lipid suspension for 30 min at room temperature.

6.3.4. Steady state fluorescence measurements

All steady state fluorescence measurements were performed using a Spex Fluoromax-3 spectrofluorimeter at 25°C, with both the excitation and emission band pass filters set at 3 nm. Experiments were carried out using solutions of PDC-109/B samples with OD$_{280nm}$ < 0.1 in TBS-I. Samples were excited at 295 nm to excite the indole side chains of Trp residues selectively and emission spectra were recorded between 310 and 400 nm. Quenching of the protein intrinsic fluorescence was done by adding small aliquots of the quenchers from 5 M stock (4 M in case of succinimide) solutions in TBS-I to the protein. Stock solution of KI contained 0.2 mM sodium thiosulfate to prevent the formation of triiodide. In Red-edge excitation shift (REES) experiments,

excitation wavelength was changed from 280 nm to 307 nm and the emission spectra were recorded between 320 and 400 nm.

To correct the fluorescence intensity values for the inner filter effect, the absorbance at excitation and the emission wavelength of an experimental solution were measured. Correction was made using the following equation [Lakowicz, 1999].

$$F_{corr} = F_{obs} \times \text{antilog} \left[\{OD_{ex} + OD_{em}\}/2 \right]$$

where F_{corr} is the corrected fluorescence intensity and F_{obs} is the observed intensity, OD_{ex} and OD_{em} is the absorbance of the solution at the excitation and emission wavelengths, respectively.

6.3.5. Fluorescence lifetime measurements

Fluorescence lifetime measurements were performed on an IBH-5000 single photon counting spectrofluorimeter equipped with a nanoLED excitation source and a cooled microchannel plate photomultiplier tube from Hamamatsu (Model R0839U-50). The time resolution of the spectrometer was ~50 ps. Samples of $OD_{280nm} < 0.1$ were exited at 281 nm and emission was monitored at 345 nm for native PDC-109/B and at 337 nm for PDC-109/B in the presence of Lyso-PC micelles or DMPC SUVs. All experiments were performed using excitation and emission slits with a nominal bandpass of 12 nm or less. Lamp profiles were measured at the excitation wavelength using Ludox (colloidal silica) as the scatterer. To optimize the signal/noise ratio, 5000 photon counts were collected in the peak channel. The resultant fluorescence decay curves were analyzed by a multiexponential iterative fitting program supplied by IBH.

6.4. Results

In previous studies it was shown that upon excitation at 280 nm, PDC-109 exhibits maximum emission intensity at 342 nm indicating tryptophan residues are the major contributors to the fluorescence. Binding of PC SUVs and Lyso-PC micelles resulted in a considerable blue shift of emission maximum with a significant increase in the fluorescence intensity. On the other hand addition of DMPE and DMPA to PDC-109 resulted in very minor changes in the emission λ_{max} and intensity, whereas addition of DMPG led to a moderate blue shift in the emission λ_{max} and an increase in the emission intensity [Müller et al., 1998; Anbazhagan et al., 2008]. In this study, similar experiments were conducted with PDC-109/B in order to compare the results obtained with the whole protein with those obtained with the domain B.
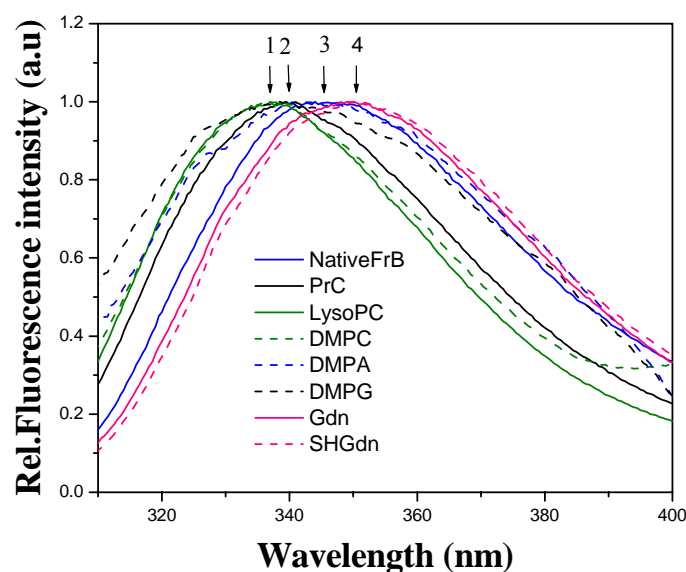
Fig. 6.1. Fluorescence emission spectra of domain B of PDC-109 obtained under different conditions. The samples investigated are indicated in the figure. Arrows marked with numbers indicate λ_{max} as indicated: 1) PDC-109/B + DMPC 2) PDC-109/B + PrC 3) Native PDC-109/B 4) PDC-109/B upon denaturation with 6 M Gdn. HCl.

The fluorescence spectra of PDC-109/B in the native state and in the presence of PrC, Lyso-PC, DMPC, DMPA and DMPG, and upon denaturation with 6 M Gdn.HCl in the absence and presence of 10 mM β-mercaptoethanol are shown in Fig. 6.1. The fluorescence emission maximum of PDC-109/B is seen at 345 nm, which is blue shifted to 339.5 nm with about 27% increase in the fluorescence intensity in the presence of 20 mM PrC. In the presence of 0.15 mM Lyso-PC emission maximum shifted to 337 nm with about 43% increase in the intensity, whereas upon binding to 0.15 mM DMPC vesicles the λ_{max} shifted to 337 nm, accompanied by 47% increase in the intensity (Fig. 6.2). In presence of DMPA and DMPG the emission maxima shifted to 343.5 nm and 339.5 nm, respectively. Upon denaturation with 6 M Gdn.HCl the emission maximum was red shifted to 349.5 nm and to 350.5 nm in presence of 6 M Gdn.HCl and 10 mM β-mercaptoethanol (Fig. 6.1).
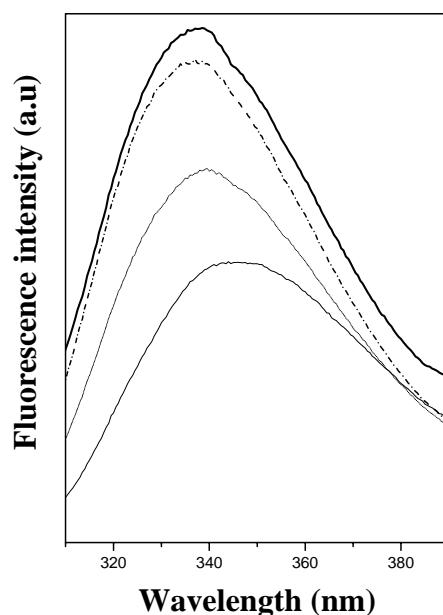
Fig. 6.2. Fluorescence emission spectra of PDC-109/B obtained under different conditions. Native PDC-109/B (thin line); in the presence of 20 mM PrC (dotted line); in the presence of 0.15 mM Lyso-PC (dashed line) and in the presence of 0.15 mM DMPC (thick line).

6.4.1. Quenching studies of PDC-109/B

Fluorescence spectra of native PDC-109/B in presence of increasing concentrations of acrylamide and cesium ion are shown in Fig. 6.3A and 6.3C, respectively. Fluorescence spectra of PDC-109/B bound to DMPC SUVs in the absence and in the presence of increasing concentrations of acrylamide and cesium ion are shown in Fig. 6.3B and 6.3D respectively. In each case (Fig. 6.3), spectrum 1 corresponds to PDC-109/B (in the absence and presence of DMPC SUVs) in the absence of quencher, the remaining spectra with decreasing emission intensities correspond to samples containing increasing concentrations of the quencher; the spectrum with lowest intensity corresponds to that recorded in the presence of 0.5 M quencher. Fig. 6.3A and 6.3C show that acrylamide quenches the protein fluorescence significantly in the native state and upon binding to DMPC SUVs whereas quenching with the ionic Cs$^+$ is considerably lower when compared to acrylamide.
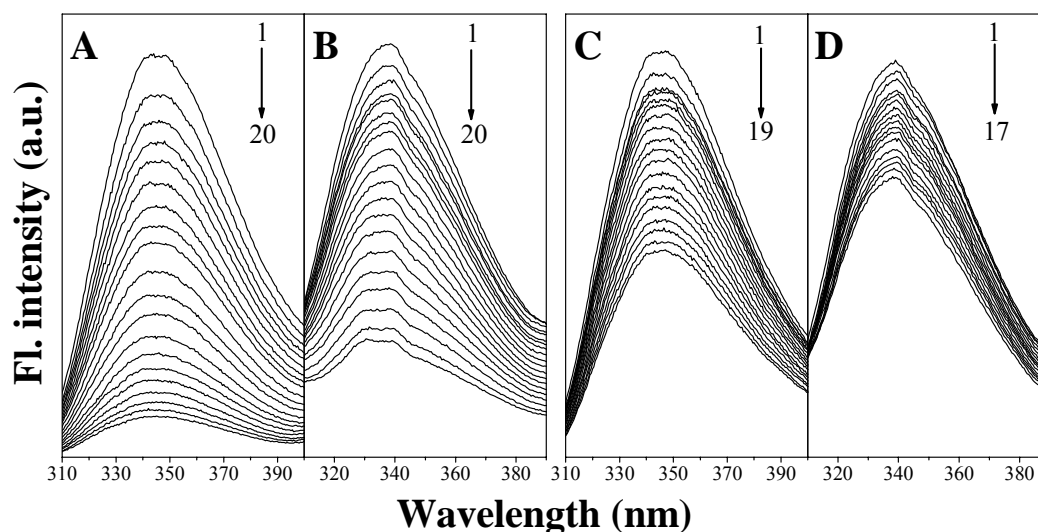
Fig. 6.3. Quenching of PDC-109/B fluorescence by acrylamide (A and B) and CsCl (C and D) in the native and upon binding to DMPC membranes. A and C, native PDC-109/B; B and D, PDC-109/B bound to DMPC membranes.

At 0.5 M concentration of the quencher, the extent of quenching by acrylamide and cesium ion of the native protein are 88.4% and 46.2% respectively, whereas upon binding to DMPC SUVs, acrylamide and Cs^+ quenched about 63.9% and 26.7% of the fluorescence emission of domain B, respectively. Quenching studies with succinimide and iodide yielded qualitatively similar spectra (not shown), and the extent of quenching observed with them at 0.5 M concentration was 83.9% and 62.4% of native protein, which decreased considerably to 50.2% and 46.4% upon binding to DMPC SUVs.

Table 6.1: Extent of quenching of tryptophan fluorescence of PDC-109/B observed with different quenchers, at a quencher concentration of 0.5 M.

Quencher	Quenching (%)			
	Native	With 20 mM PrC	With 0.15 mM Lyso-PC	With 0.15 mM DMPC
Acrylamide	88.4	77.3	70.0	63.9
Succinimide	83.9	69.9	58.8	50.2
Iodide (I^-)	62.1	50.8	48.4	46.4
Cesium ion (Cs^+)	46.2	37.8	29.4	26.7

The degree of quenching achieved in each case, at a resultant quencher concentration of 0.5 M, is shown in Table 6.1. Of the four quenchers used, acrylamide was the most effective, quenching 88.4% of the total intrinsic fluorescence of the protein, whereas succinimide, which is also neutral, quenched 83.9% of the total fluorescence because it is bulkier when compared to acrylamide. The ionic quenchers, I^- and Cs^+ could quench only 62.1% and 46.2% respectively, as these ionic quenchers can not penetrate into the protein matrix and can quench only surface exposed tryptophan residues.

6.4.2. Stern-Volmer analysis of quenching data

The quenching data obtained with different quenchers were analysed by the Stern-Volmer equation (Eq. 1) and Modified Stern-Volmer equation (Eq. 2) [Lehrer, 1971]:

$$F_o/F_c = 1 + K_{SV}[Q] \tag{1}$$

$$F_o/\Delta F = f_a^{-1} + (K_a f_a)^{-1} \cdot [Q]^{-1} \tag{2}$$

where F_o and F_c are the representative fluorescence intensities, corrected for dilution, in the absence and in the presence of quencher, [Q] is the resultant quencher concentration and K_{SV} is the Stern-Volmer constant of the protein for a given quencher. ΔF ($=F_o-F_c$) is the change in fluorescence intensity at any point in the quenching titration, f_a refers to the fraction of the total fluorophores accessible to the quencher and K_a is the corresponding Stern-Volmer constant for the accessible fraction of the fluorophore. A plot of F_o/F_c *versus* [Q] is known as a Stern-Volmer plot and a plot of $F_o/\Delta F$ as a function of $[Q]^{-1}$ is referred to as a Modified Stern-Volmer plot. Slopes of Stern-Volmer plots yield K_{SV} values, whereas slopes of modified Stern-Volmer plots give $(K_a f_a)^{-1}$ and their ordinate give the values of f_a.
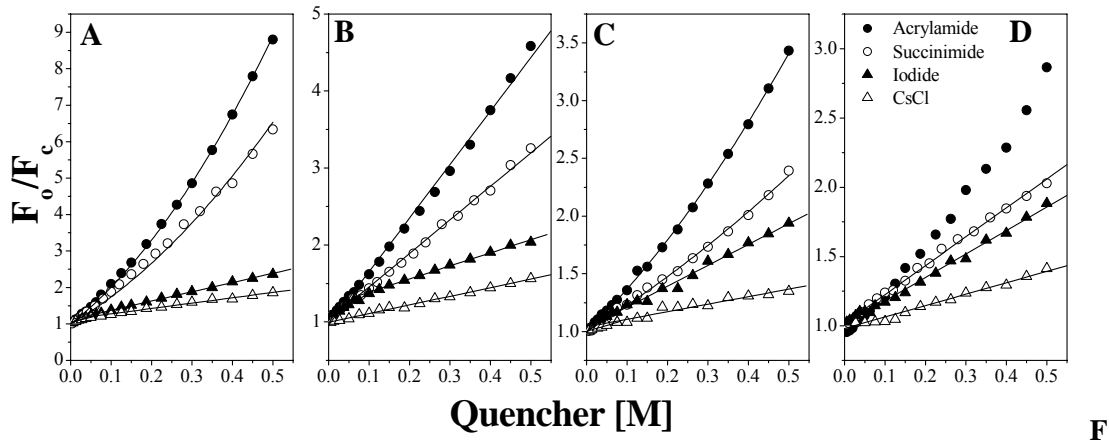
ig. 6.4. Stern-Volmer plots of fluorescence quenching data for PDC-109/B under different conditions. A) Native PDC-109/B, B) PDC-109/B with phosphorylcholine, C) PDC-109/B with Lyso-PC, D) PDC-109/B in the presence of DMPC. Quenchers used are: (●) acrylamide, (O) succinimide, (▲) iodide, (△) cesium ion.

Stern-Volmer plots for the quenching of PDC-109/B alone and PDC-109/B in presence of PrC, Lyso-PC and DMPC SUVs are shown in Fig. 6.4.A, 6.4.B, 6.4.C and 6.4.D, respectively. Each panel represents the Stern-Volmer plots for all the four quenchers used. From the figure it is seen that under all conditions except in the presence of PrC, Stern-Volmer plots for acrylamide quenching exhibit upward curvature, whereas succinimide also exhibited upward curvature for the native protein and in presence Lyso-PC, indicating that the quenching has both dynamic and static components. These data have been analyzed using equation 3, which allows the resolution of static and dynamic components and give corresponding quenching constants [Lakowitcz, 1999]:

$$F_o/F_c = (1 + K_{SV}[Q]) (1 + K_S[Q]) \tag{3}$$

Where K_{SV} is the Stern-Volmer (dynamic) quenching constant, K_S is the static quenching constant and [Q] is the concentration of quencher. The solid curved lines shown in Fig. 6.4 clearly indicate that the data fit very well to Eq.3. The K_{SV} (dynamic) values were determined from time resolved fluorescence studies by using equation (4):

$$\tau_o/\tau = 1 + K_{SV} [Q] \tag{4}$$

where τ_o and τ are the average lifetime of the fluorophore in the absence and in the presence of the quencher at a concentration, [Q]. From this analysis K_{SV} values obtained for native protein for acrylamide and succinimide are 2.22 and 2.02 M^{-1} respectively. Using this K_{SV} values in eq.3, K_S values were calculated as 6.27 and 4.34 M^{-1} for acylamide and succinimide, respectively. These values are listed in Table 6.2.

The Stern-Volmer plots obtained with cesium ion show linear dependence with quencher concentration for PDC-109/B in the presence of PrC and DMPC vesicles, but exhibit a biphasic pattern with the native protein and in the presence of Lyso-PC. In addition, biphasic plots are also seen with iodide for the native protein and its complex with PrC and Lyso-PC. The biphasic patterns (Stern-Volmer plot containing two linear plots that differ in the slope) indicate heterogeneity in the environment of accessible tryptophan residues to the quencher. From the slopes of the two linear components of biphasic plots obtained with the different quenchers, corresponding Stern-Volmer quenching constants, K_{SV1} and K_{SV2}, were determined. The bimolecular quenching constants, K_q ($K_q = K_{SV}/\tau_o$, where τ_o is the average lifetime of fluorescence decay) for acrylamide and succinimide were also calculated from the K_{SV} values and the average lifetimes were obtained from the time resolved fluorescence measurements. All these values are also listed in Table 6.2.
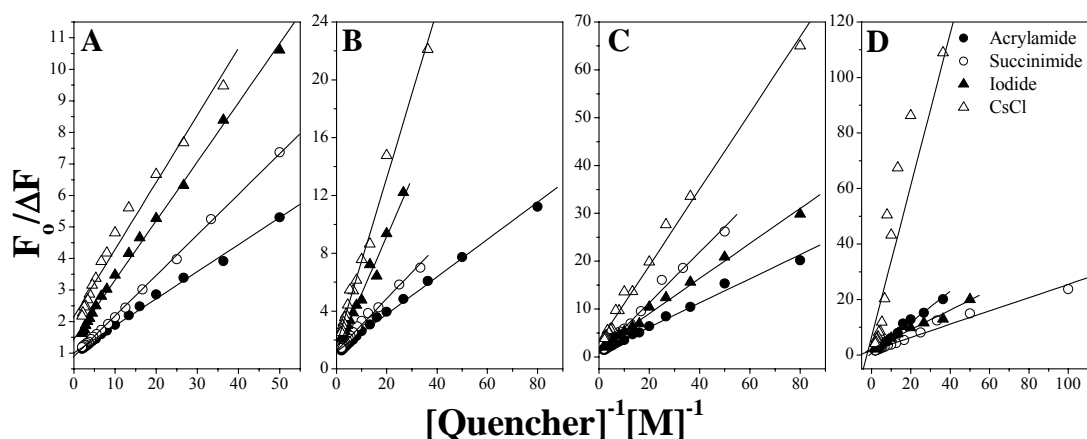
Fig. 6.5. Modified Stern-Volmer plots fluorescence quenching data for PDC-109/B under different conditions. A) Native PDC-109/B, B) PDC-109/B with *O*-phosphorylcholine, C) PDC-109/B with Lyso-PC, D) PDC-109/B in the presence of DMPC. Quenchers used are: (●) acrylamide, (O) succinimide, (▲) iodide, (△) cesium ion.

Table 6.2: Summary of parameters obtained from intrinsic fluorescence quenching and time resolved fluorescence on domain B of PDC-109

Sample description	K_S (M^{-1})	K_{SV1} (M^{-1})	K_{SV2} (M^{-1})	K_q (M^{-1}S^{-1})	f_a (%)	K_a (M^{-1})
Acrylamide						
Native PDC-109/B	6.27	2.22	-	1.53	99.5	11.75
With 20 mM PrC	-	6.64	-	-	83	9.15
With 0.15 mM Lyso-PC	1.83	1.45	-	0.83	57.3	4.58
With 0.15 mM DMPC	-	3.04	-	1.97	-	1.08
Succinimide						
Native PDC-109/B	4.34	2.09	-	1.33	94.6	8.88
With 20 mM PrC	-	4.46	-	-	80.4	6.86
With 0.15 mM Lyso-PC	1.43	0.77	-	0.44	84	3.47
With 0.15 mM DMPC	-	2.46	-	-	67.4	2.75
Iodide						
Native PDC-109/B	-	5.08	3.1	-	74	7.43
With 20 mM PrC	-	3.02	1.73	-	68.4	6.06
With 0.15 mM Lyso-PC	-	2.7	1.81	-	67	4.06
With 0.15 mM DMPC	-	1.66	-	-	65.8	3.11
Cesium ion						
Native PDC-109/B	-	2.75	1.47	-	66.6	4.28
With 20 mM PrC	-	1.2	-	-	60	2.88
With 0.15 mM Lyso-PC	-	1.27	0.57	-	30.4	2.61
With 0.15 mM DMPC	-	0.77	-	-	15.6	2.34

The modified Stern-Volmer plots for the quenching of PDC-109/B alone and in presence of PrC, Lyso-PC and DMPC SUVs are shown in Fig. 6.5.A, 6.5.B, 6.5.C, and 6.5.D, respectively. Each panel represents the modified Stern-Volmer plots for all the four quenchers used. From the Y-intercept of these plots, f_a, the fraction of accessible Trp residues to the quencher in each case has been determined and corresponding Stern-Volmer constant for the accessible portion, K_a, was calculated using Eq.2. The obtained values are listed in Table 6.2.

It is clearly seen from the data given in the Table 6.2 that in native PDC-109/B about 99.5% and 94.6% fluorescence intensity is accessible to acrylamide and succinimide respectively, whereas only 74% and 66.6% of the intensity is accessible for iodide and cesium ion, respectively. In the presence of different ligands, namely PrC, Lyso-PC and DMPC vesicles, values of f_a, the fraction of accessible fluorescence intensity decreased noticeably, in which PDC-109/B bound to DMPC has shown less values when compared to other ligands used. Under native condition, the K_a values for acrylamide and succinimide are 11.75 M^{-1}, and 8.88 M^{-1} respectively, indicating a higher quenching efficiency for acrylamide than succinimide, whereas the K_a values of I$^-$ and Cs$^+$ were 7.43 M^{-1} and 4.23 M^{-1}, respectively. Values of the association constant, K_a decreased markedly by ligand binding to PDC-109/B, where the values are much lower in the presence of DMPC (Table 6.2).

6.4.3. Lifetime measurements of fluorescence emission

The fluorescence decay curves of native domain B of PDC-109, in the presence of 0.15 mM Lyso-PC and 0.15 mM DMPC, obtained from the time resolved measurements are given in Fig. 6.6. In addition, fluorescence lifetime measurements were also carried out in the presence of acrylamide and succinimide at different

concentrations in each case. The decay curves were analysed by multi-exponential iterative program supplied by IBH. In each case, the decay curve could be best fitted to a biexponential decay function, i.e., two different lifetimes of the excited tryptophan residues could be observed. For native PDC-109/B, the lifetime values obtained were 1.03 and 3.16 ns ($\chi^2 \leq 1.31$) while in the presence of 0.15 mM Lyso-PC the lifetimes obtained were 1.24 and 3.31 ns ($\chi^2 \leq 1.17$), whereas for the protein in presence of 0.15 mM DMPC, the biexponential fits yielded lifetime value of 1.07 and 3.19 ns ($\chi^2 \leq 1.15$). These values, together with the values obtained in the presence of acrylamide and succinimide at 0.5 M concentration are listed in Table 6.3.
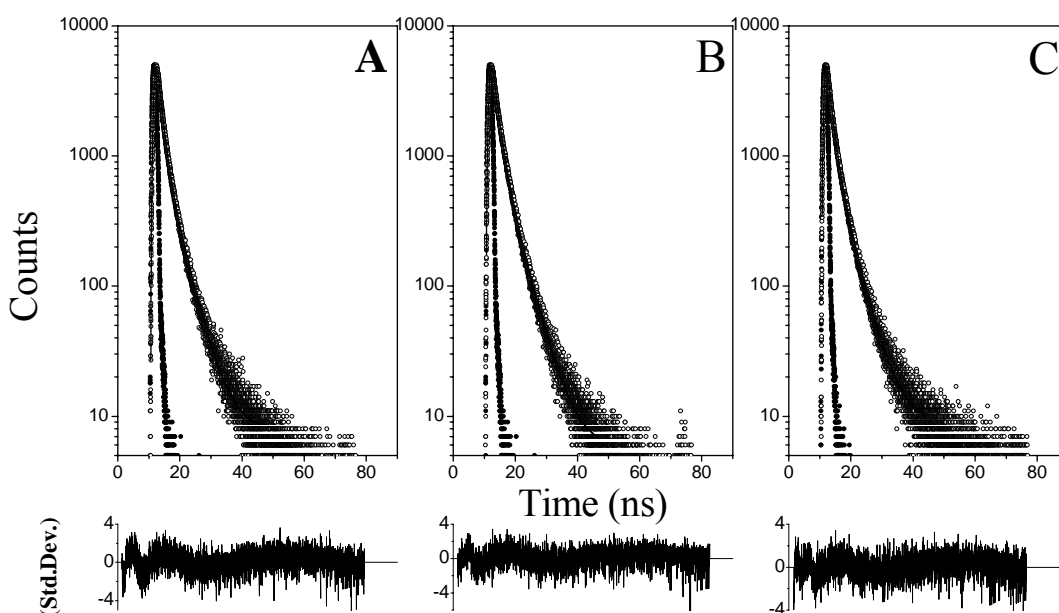
Fig. 6.6. Time-resolved fluorescene decay profiles of PDC-109 domain B. **(A)** Native PDC-109/B **(B)** in the presence of 0.15 mM Lyso-PC **(C)** in the presence of 0.15 mM DMPC. The fluorescence decay data and lamp profile are shown. Solid lines correspond to nonlinear least square fits of the experimental data to biexponential functions. The lower panels represent residuals.

Values of average lifetime of fluorescence decay for PDC-109/B under different conditions were calculated from the values of lifetime, τ_i and the corresponding pre-

exponential weighting factors, α_i (Table 6.3) using the following expressions [Grinwald & Steinberg, 1976]:

$$\tau = \Sigma_i \alpha_i \tau_i / \Sigma_i \alpha_i \qquad (4)$$

$$\langle\tau\rangle = \Sigma_i \alpha_i \tau^2_i / \Sigma_i \alpha_i \tau_i \qquad (5)$$

where τ and $\langle\tau\rangle$ are the average fluorescence lifetimes estimated by two different approaches. For native PDC-109/B, values of τ and $\langle\tau\rangle$ are obtained as 1.56 and 2.05 ns, respectively. Corresponding values obtained in the presence of 0.15 mM Lyso-PC are 1.74 and 2.2 ns, respectively, whereas the values obtained in the presence of 0.15 mM DMPC are 1.54 and 2.04 ns, respectively (Table 6.3).

Table 6.3: Results of time-resolved fluorescence studies on PDC-109/B under different conditions. Lifetimes of fluorescence decay, corresponding pre-exponential factors and calculated average lifetimes obtained with native PDC-109/B and in the presence of different ligands and quenchers are presented.

Sample description	α_1	τ_1 (ns)	α_2	τ_2 (ns)	τ	$\langle\tau\rangle$	χ^2
Native PDC-109/B	0.81	1.03	0.19	3.16	1.56	2.05	1.31
With 0.15 mM Lyso-PC	0.75	1.24	0.25	3.31	1.74	2.20	1.17
With 0.15 mM DMPC	0.78	1.07	0.22	3.19	1.54	2.04	1.15
PDC-109/B + 0.5 M acrylamide under different conditions							
Native PDC-109/B	0.99	0.55	0.01	5.39	0.62	1.2	1.23
With 0.15 mM Lyso-PC	0.87	0.87	0.13	2.54	1.01	1.21	1.28
With 0.15 mM DMPC	0.99	0.18	0.003	1.62	0.022	0.35	1.80
PDC-109/B + 0.5 M succinimide under different conditions							
Native PDC-109/B	0.98	0.25	0.01	1.12	0.43	0.71	1.20
With 0.15 mM Lyso-PC	0.88	1.01	0.19	2.80	0.13	1.70	1.13

6.4.4. Red-edge excitation shift studies (REES)

The effect of changing excitation wavelength on the wavelength of maximum emission for PDC-109/B in the native state and under different conditions is shown in Fig. 6.7. As the excitation wavelength is changed from 280 nm to 307 nm, the emission maximum of native PDC-109/B shifted from 344.25 nm to 347.75 nm, which corresponds to a REES of 3.5 nm. Further red shift is likely to be observed if the sample can be excited at wavelengths beyond 307 nm; however, reliable spectra could not be obtained for excitation beyond 307 nm due to low signal-to-noise ratio and artifacts due to the presence of residual intensity from the solvent Raman peak that sometimes remained even after background subtraction.
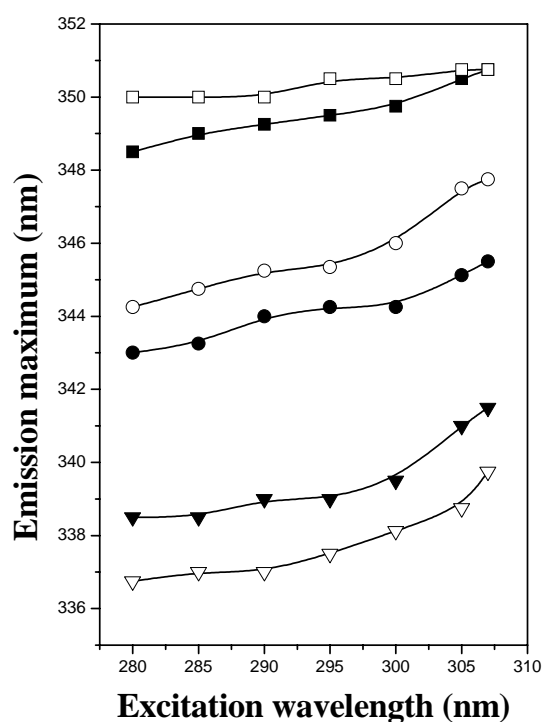
Fig. 6.7. Effect of changing excitation wavelength on the emission maximum of PDC-109/B. (O) Native PDC-109/B, (●) in presence of 0.15 mM DMPC, (▼) in presence of 20 mM PrC, (∇) in presence of 0.15 mM Lyso-PC, (■) upon denaturation with 6 M Gdn.HCl. (□) upon denaturation with 6 M Gdn.HCl and 10 mM β-ME.

Upon excitation at 280 nm, binding of PrC to PDC-109/B resulted in a blue shift of the emission maximum from 344.25 nm to 338.5 nm. As the excitation wavelength is changed from 280 nm to 307 nm, the emission maximum shifted from 338.5 nm to 341.5 nm, with REES of 3 nm. Upon binding to Lyso-PC micelles also the REES observed is 3 nm. Binding of PDC-109/B to DMPC SUVs led to a decrease in the REES to 2.5 nm. Upon denaturation with Gdn.HCl, the emission maximum of PDC-109/B shifted from 348.5 nm to 350.75 nm with the REES of 2.25 nm, while upon denaturation and reduction with β-ME, the emission λmax shifted from 350 nm (ex: 280 nm) to 350.75 nm (ex: 307 nm), that is, a REES of only 0.75 nm is observed.

6.5. Discussion

Previous studies have shown that the fluorescence properties of PDC-109 exhibit considerable changes upon interaction with choline phospholipids and the soluble ligands, phosphorylcholine and choline, which are part of the head group of choline phospholipids [Müller et al., 1998; Anbazhagan et al., 2008]. While ligand binding resulted in a significant blue shift with enhancement of the fluorescence intensity, denaturation led to substantial red shift. In addition, red edge excitation shift (REES) studies suggested that upon binding of PDC-109 to DMPC vesicles and Lyso-PC micelles some of the Trp residues of PDC-109 are located in the hydrophobic interior of the membrane. Since binding of PDC-109 to sperm plasma membrane results in an efflux of cholesterol and phospholipids, whereas domain B of this protein can bind to choline phospholipids, but can not induce lipid efflux, it may be expected that by investigating the binding of intact PDC-109 and domain B to lipid membranes, one can understand the differences between the effects induced by these two proteins on

the membranes, which can give us clues to understanding the mechanism of cholesterol efflux. With this objective, in this study the interaction of domain B of PDC-109 (PDC-109/B) with different phospholipids as well as soluble ligands such as choline and phosphorylcholine has been investigated using fluorescence approaches such as steady-state fluorescence quenching with neutral and charged quenchers, time-resolved fluorescence measurements and red-edge excitation shift studies. The results obtained have been compared with those obtained earlier with full PDC-109 and the functional implications, especially with respect to cholesterol efflux have been discussed here.

The emission λ_{max} of PDC-109/B observed at 345 nm (Fig. 6.1) indicates that Trp residues are the major contributors to the fluorescence of the protein and that the indole side chains are largely exposed to the aqueous environment. Binding of phosphorylcholine and phospholipids result in a blue shift of the emission maximum with increase in the emission intensity. Binding of phosphorylcholine and choline-containing phospholipids, viz., Lyso-PC and DMPC led to larger shifts than other phospholipids such as DMPG and DMPA. The shift indicates that the microenvironment of the indole side chains of the Trp residues becomes more hydrophobic, which, for the soluble ligand, PrC may be ascribed to the removal of bound water molecules in the binding site. For DMPC and Lyso-PC, the observed blue shift in the emission maximum may result from removal of water molecules from the ligand binding site and also due to a partial penetration of segments of the protein into the hydrophobic interior of the lipid membrane/micelle.

The red shift in the emission maximum of PDC-109/B to 350.5 nm (351 nm in the presence of β-ME) upon denaturation with 6 M Gdn.HCL indicates greater exposure of the Trp residues to the polar aqueous environment. These values

compare well with the emission λ_{max} of tryptophan alone in water [Lakowicz, 1999] and indicate the complete exposure of Trp residues in PDC-109/B to polar aqueous environment.

The tryptophan exposure, environment and accessibility of PDC-109/B in the absence and presence of ligands (PrC, Lyso-PC and DMPC membranes) were studied using four quenchers, namely acrylamide, succinimide, iodide and cesium ion. Acrylamide and succinimide are neutral quenchers and can diffuse into the protein interior and quench the fluorescence of partially buried Trp residues. The quenching efficiency of acrylamide is greater than the succinimide because of the bulkier size of latter. The charged quenchers, I^{P-} and Cs^+ generally show lower quenching when compared to neutral quenchers, as these can quench only surface-exposed Trp residues. Presence of charged residues in the neighbourhood of the Trp affects their quenching efficiency.

Binding of ligands to PDC-109/B alters the accessibility of tryptophan residues to the quenchers, indicating that ligand-induced conformational changes modify the penetration of quencher into the protein matrix. In the case of binding to lipid membranes, it is also possible that parts of the protein containing tryptophan residues may go into the hydrophobic regions of the lipids resulting in the decreased accessibility of the fluorophores to quenchers. Quenching profiles obtained with acrylamide and succinimide for native protein and protein in presence of different ligands showed an upward curvature towards Y-axis, clearly indicate the involvement of both dynamic and static quenching components. Stern-Volmer plots obtained with iodide and cesium ion with native protein and protein in presence of PrC, Lyso-PC are biphasic (Fig. 6.3). This clearly indicates that the charged quenchers experience

heterogeneity in Trp environment and all Trp residues are not completely accessible to the ionic quenchers.

Time resolved fluorescence studies showed the presence of two components in the fluorescence decay profiles of PDC-109/B. This suggests the heterogeneity of the environments of Trp residues.

For the native protein, The REES of 3.5 nm was observed (corresponding to a shift in the excitation wavelength from 280 nm to 307 nm). Such shift in the wavelength of emission maximum with change in excitation wavelength is characteristic of the red edge effect and indicates that the tryptophan residues are localized in a motionally restricted region, which offers considerable resistance to solvent reorientation in the excited state. The REES of 2.5 nm observed upon binding of PDC-109/B to DMPC vesicles shows that upon binding to DMPC, parts of the protein are partially embedded into the hydrophobic region of the membrane. However, as the reduction in REES due to binding to DMPC vesicles and Lyso-PC micelles is considerably smaller for PDC-109/B as compared to the full protein, it is likely that segments of domain B do not penetrate into the membrane interior to the same extent as compared to the whole protein. This could be the reason why domain B cannot induce cholesterol effect despite binding to choline phospholipids present in the membranes, whereas binding of the whole PDC-109 readily induces cholesterol efflux.

In summary, the intrinsic fluorescence properties of PDC-109/B have been investigated in the present study by quenching and REES experiments. Quenching studies indicate that ligand binding resulted in the shielding of tryptophan residues from different quenchers, with shielding ability in the following order: PrC < Lyso-

PC < DMPC. These results are similar with the results obtained with PDC-109. PDC-109/B binds to phosphorylcholine moiety specifically and the acyl chains of the lipids also interact with the protein, resulting in further stabilization of the protein structure. The quenching efficiency of the four quenchers used is in the following order: acrylamide > succinimide > iodide > cesium ion.

Chapter 7

General Discussion and Conclusions

7.1. General discussion and conclusions

The major objective of the present study (as mentioned in Chapter 1) was to investigate the interaction of PDC-109, the major bovine seminal plasma protein, and its domain B (PDC-109/B) with phospholipid membranes and soluble ligands, to study the effect of their binding on the phase properties of lipid membranes and to characterize the thermodynamic forces that govern its interaction with different lipids and other ligands. The studies reported in Chapters 2-6 clearly show that these objectives are mostly fulfilled. The results obtained in these studies are discussed in the following paragraphs and the implications are discussed in terms of the role of PDC-109 in cholesterol efflux and sperm capacitation.

Previous studies have reported that PDC-109 specifically binds to choline containing phospholipids present on sperm surface and that the binding leads to removal of cholesterol and phospholipids from membrane (referred to as cholesterol efflux). But the phase structure of the lipid/protein particles formed upon binding of PDC-109 to lipid membranes was unknown. In this direction we have investigated the effect of PDC-109 binding on the phase structure of membranes made up of dimyristoylphosphatidylcholine (DMPC), DMPC with 40 mol% cholesterol, dipalmitoylphosphatidylglycerol (DPPG), dimyristoylphosphatidylethnolamine (DMPE) and lysophosphatidylcholine (Lyso-PC) at various temperatures (10–50°C) by ^{31}P-NMR spectroscopy. It was observed that binding of PDC-109 to DMPC and DPPG results in a disruption of the multilamellar vesicles and induces the formation of small unilamellar vesicles or micelles, which is supported by the formation of isotropic signal in ^{31}P-NMR spectrum. The isotropic signal further indicates the absence of hexagonal structures and suggests that the aggregates are structures with high curvature. Addition of cholesterol at 40 mol% led to a partial stabilization of the lamellar phase in that the

fraction of the isotropic signal was less in the presence of cholesterol for the same PDC-109/DMPC ratio.   In addition, effect of binding of PDC-109 to dimyristoylphosphatidyletholamine (DMPE) at lipid/protein ratio of 1:1 was studied by ^{31}P-NMR spectroscopy.   In presence of PDC-109 there was no change in ^{31}P-NMR spectrum (bilayer) of DMPE, indicating a very weak binding of PDC-109 to DMPE. This is consistent with the results of Tannert et al. (2007), which show that PDC-109 disturbed membranes containing PC and SM, and perturbation was diminished in PE-containing membranes. The above results are also consistent with the weaker affinity exhibited by PDC-109 towards phosphatidylethanolamine and phosphatidylglycerol as compared to phosphatidylcholine [Thomas et al., 2003]. Hemolytic studies suggest that PDC-109 binds to the surface of erythrocyte membrane and causes the breakdown of the membrane similar to the action of PDC-109 on sperm plasma membrane.

Thermodynamic parameters characterizing the interaction of PDC-109 with heparin were obtained from isothermal titration calorimetric (ITC) studies. Interaction of heparin with PDC-109 resulted in large endothermic peaks, indicating that the binding process is associated with positive enthalpy change. The positive values of change in enthalpy and change in entropy for the binding of heparin to PDC-109 indicate that binding of heparin to PDC-109 is driven by entropic factors rather than enthalpy. The positive value of ΔS^o obtained for the binding of PDC-109 to heparin indicates an increase in entropy suggesting that the entropy of the system increases upon binding. This may be explained as resulting from the release of ordered water molecules that may be associated with the protein or the ligand or both from the interacting surfaces. The interaction of PDC-109 with heparin was also monitored by fluorescence spectroscopic studies, which showed that fluorescence intensity of PDC-109 decreases upon binding to heparin. Similarly, addition of chondroitin-6-sulfate to PDC-109 also resulted in a decrease in the fluorescence intensity of the protein. When

heparin was added to PDC-109 containing PrC, weak binding to PDC-109 was observed. On the other hand, when PrC was added to PDC-109 containing heparin, a significant increase was observed in the fluorescence intensity of the protein, suggesting strong binding of PrC to PDC-109. These results support that PDC-109 binds strongly to choline containing phospholipids than the other ligands. CD spectroscopic studies clearly indicate that binding of heparin induces conformational changes in both secondary and tertiary structure of PDC-109.

Interaction of PDC-109 with synthetic, *O*-acyl derivatives of choline, namely *O*-lauroylcholine and *O*-myristoylcholine was studied by isothermal titration calorimetry, fluorescence spectroscopy and CD spectroscopy. Such studies can lead to the development of new synthetic molecules with high affinity to PDC-109. Thermodynamic parameters obtained from the ITC studies indicate that PDC-109 – *O*-acylcholine interaction is enthalpically driven with negative contribution from entropy. At 25°C interaction of PDC-109 with OLC is favoured by both enthalpy and entropy, but at higher temperatures the entropic factors do not favour binding as the $\Delta S°$ value which is positive at 25°C becomes negative at 30°C, although very small in magnitude (-0.09 cal.mol^{-1}.K^{-1}) and the magnitude of the (negative) entropy of binding increases further as the temperature is increased further. These values outweigh the larger (negative) values of enthalpy of binding, which results in a decrease in the association constants. In fluorescence studies, the emission maximum for PDC-109 was observed at 340.5 nm, which upon addition of OLC exhibits a blue shift to 333 nm. This could be due to interaction of PDC-109 with the hydrophobic region of OLC. CD studies showed that binding of *O*-lauroylcholine induced changes in far-UV and near-UV CD spectra PDC-109, which is similar to the changes observed upon binding of phosphorylcholine or Lyso-PC with previous results. These changes could be due to the changes in the secondary and tertiary structure of the protein, as PDC-109 which exist

as a polydisperse aggregate in solution dissociates into dimeric form upon ligand binding.

Although PDC-109 binds to the choline head group of phospholipids such as phosphatidylcholine and sphingomyelin, several studies indicate that upon membrane binding parts of the protein interact with the hydrophobic interior of the membrane [Müller et al., 1998; Ramakrishnan et al., 2001; Greube et al., 2001]. This suggested that PDC-109 may have some hydrophobic regions on the surface. In order to investigate this aspect, the interaction of three hydrophobic ligands, namely ANS, TNS, and bis-ANS to PDC-109 and its domain B has been investigated by fluorescence spectroscopy. Binding of ANS, TNS and bis-ANS to PDC-109 and PDC-109/B resulted in a decrease in the fluorescence intensity of protein with successive addition of ligand. From the K_a values obtained for ANS, TNS, and bis-ANS it is clear that the interaction of bis-ANS with PDC-109 is characterized by a stronger affinity than that of ANS and TNS, the K_a values for the former ligand being 3.66 and 9.54 times higher, respectively than the latter two ligands. Similarly bis-ANS binds to PDC-109/B with an affinity that is 8.8 and 13 times higher than ANS and TNS, respectively. These observations indicate that the surface of PDC-109 has considerably hydrophobic region(s). Circular dichroism (CD) spectroscopic studies with both intact PDC-109 and its domain B indicate that hydrophobic ligand binding lead to significant changes in the secondary and tertiary structures of PDC-109 and PDC-109/ B.

The microenvironment and accessibility of the tryptophan residues present in domain B of PDC-109 in the native state and in the presence of PrC, Lyso-PC and DMPC was investigated by fluorescence quenching experiments. Two neutral quenchers (acrylamide and succinimide), and two charged quenchers, iodide (I^-) and cesium ion (Cs^+) were employed in these experiments. Binding of PrC, Lyso-PC and DMPC to PDC-109/B resulted in a progressive decrease in the degree of quenching.

Among these, the minimum degree of quenching was observed in the presence of DMPC and maximum quenching was seen in the presence of PrC, suggesting that, in addition to the choline head group, presence of acyl chains stabilize the binding and thus promote tightening of the protein structure, leading to decreased accessibility of the tryptophan residues to the different quenchers. The quenching efficiency of the four quenchers used is in the following order: acrylamide > succinimide > iodide > cesium ion. A red-edge excitation shift (REES) of 3.5 nm was observed with native PDC-109/B, suggesting that the microenvironment surrounding the Trp residues in this protein has a reduced mobility and that the reorientation of the solvent water molecules around them is considerably restricted. Upon binding of PDC-109/B to lyso-PC and DMPC membranes the REES value decreased slightly to 3.0 nm and 2.5 nm, respectively, suggesting moderate changes in the solvent water relaxation. A comparison with previous studies on the complete PDC-109 protein [Anbazhagan, 2005; Anbazhagan et al., 2008], where the REES value of 4.0 nm for the native protein decreased to 2.5 and 1.5 nm, in the presence of DMPC and lyso-PC, respectively, suggests that domain B interacts primarily at the membrane interface whereas the whole PDC-109 protein inserts into the non polar region of the membrane, where the red edge effects are significantly reduced. This suggests that domain B is probably unable to induce cholesterol efflux because it does not penetrate deep into the hydrophobic interior of the membrane.

The studies presented in this thesis will aid in understanding more about the interaction of PDC-109 and its domain B with lipid membranes and various soluble ligands. Several events occur at the sperm plasma membrane from ejaculation to fertilization, in which PDC-109 plays a crucial role in sperm capacitation which is an important step before fertilization can occur. PDC-109 binds to phospholipids and a variety of other molecules (given in Chapter 1); therefore studies on the molecular

events involved in the interaction of PDC-109 with lipid membranes and other ligands will facilitate better understanding of mechanisms involved in the sperm capacitation. Such an understanding will be useful to resolve the causes of infertility, in birth control and to aid in developing improved methods of sperm cryopreservation.

References

148 *References...*

REFERENCES

Abraham, T., Lewis, R.N.A.H., Hodges, R.S. & McElhaney, R.N. (2005) Isothermal titration calorimetric studies of the binding of a ration designed analogue of the antimicrobial peptide gramicidin S to phospholipids bilayer membranes. *Biochemistry* **44:** 2103-2112.

Anbazhagan, V. & Swamy, M.J. (2005) Thermodynamics of phosphorylcholine and lysophosphatidylcholine binding to major protein of bovine seminal plasma, PDC-109. *FEBS Lett*. **579:** 2933-2938.

Anbazhagan, V. (2005) Biophysical investigations on the interaction of the major bovine seminal plasma protein, PDC-109 with model membranes. *Ph. D. Thesis.* Submitted to University of Hyderabad.

Anbazhagan, V., Damai, R.S., Paul, A. & Swamy, M.J. (2008) Interaction of the major protein from bovine seminal plasma, PDC-109 with phospholipid membranes and soluble ligands investigated by fluorescence approaches. *Biochim. Biophys. Acta* (Published online) doi:10.1016/j.bbapap.2008.03.002.

Arnoult, C., Zeng, Y. & Florman, H.M. (1996) ZP3-dependent activation of sperm cation channels regulates acrosomal secretions during mammalian fertilization. *J. Cell. Biol.* **134:** 637-645.

Arora, A., Abildgaard, F., Bushweller, J.H. & Tamm, L.K. (2001) Structure of outer membrane protein A transmembrane domain by NMR spectroscopy. *Nat. Struct. Biol.* **8:** 334-338.

Arnulphi, C., Jin, L., Tricerri, M.A. & Jonas, A. (2004) Enthalpy-driven apolipoprotein A-I and lipid bilayer interaction indicating protein penetration upon lipid binding. *Biochemisry* **43:** 12258-12264.

Austin, C.R. (1952) The capacitation of the mammalian sperm. *Nature* **170:** 326.

Baker, M.E. (1985) The PDC-109 protein from bovine seminal plasma is similar to the gelatin-binding domain of bovine fibronectin and a kringle domain of human tissue-type plasminogen activator. *Biochem. Biophys. Res. Commun.* **130:** 1010-1014.

Banarjee, T. & Kishore, N. (2006) Binding of 8-anilinonaphthalene sulfonate to dimeric and tetrameric Concanavalin A: Energetics and Its implications on saccharide binding studied by isothermal titration calorimetry and spectroscopy. *J. phys. Chem.* **110:** 7022-7028.

Bányai, L., Trexler, M., Koncz, S., Gyenes, M., Sipos, G. & Patthy, L. (1990) The collagen-binding site of type-II units of bovine seminal fluid protein PDC-109 and fibronectin. *Eur. J. Biochem.* **193:** 801-806.

Bányai, L., Tordai, H. & Patthy, L. (1996) Structure and domain-domain interactions of the gelatin-binding site of human 72-kilodalton type IV collagenase (Gelatinase A, matrix metalloproteinase 2). *J. Biol. Chem.* **271:** 12003-12008.

Baxa, U., Cooper, A., Weintraub, A., Pfeil, W. & Seckler, R. (2001) Enthalpic barriers to the hydrophobic binding of oligosaccharides to phage P22 tailspike protein. *Biochemistry* **40:** 5144-5150.

Bleil, J.D. & Wasserman, P.M. (1983) Sperm-egg interaction in the mouse: sequence of events and induction of the acrosome reaction by a zona pellucida glycoprotein. *Dev. Biol.* **95:** 317-324.

Branton, D. (1966) Fracture faces of frozen membranes. *Proc. Natl. Acad. Sci. USA* **55:** 1048-1056.

Branton, D. (1971) Freeze-etching studies of membrane structure. *Phil. Trans. Roy. Soc. London B.* **261:** 133-138.

Bullivant, S. (1974) Freeze-etching techniques applied to biological membranes. *Phil. Trans. Roy. Soc. London B.* **268:** 5-14.

Calvete, J.J., Paloma, F.V., Sanz, L. & Romero, A. (1996a) A procedure for the large-scale isolation of major bovine seminal plasma proteins. *Protein Expr. Purif.* **8:** 48 –56.

Calvete, J.J., Mann, K., Sanz, L., Raida, M. & Töpfer-Petersen, E. (1996b) The primary structure of BSP-30 K, a major lipid-, gelatin-, and heparin-binding glycoprotein of bovine seminal plasma. *FEBS Lett.* **399:** 147-152.

Calvete, J.J., Raida, M., Sanz, L., Wempe, F., Scheit, K-H., Romer, A. & Töpfer-Petersen, E. (1994) Localization and structural characterization of an oligosaccharide *O*-linked to bovine PDC-109. Quantitation of the glycoprotein in seminal plasma and on the surface of ejaculated and capacitated spermatozoa. *FEBS Lett.* **350:** 203-206.

Calvete, J.J., Campanero-Rhodes, M.A., Raida, M. & Sanz, L. (1999) Characterisation of the conformational and quaternary structure-dependent heparin-binding region of bovine seminal plasma protein PDC-109. *FEBS Lett.* **444:** 260-264.

Chang, M.C. (1951) Fertilizing capacity of spermatozoa deposited into the fallopian tubes. *Nature* **168:** 697-698.

Chandonnet, L., Roberts, K.D., Chapdelaine, A. & Manjunath, P. (1990) Identification of heparin-binding proteins in bovine seminal plasma. *Mol. Reprod. Dev.* **26:** 313-318.

Chattopadhyay, A. & Mukherjee, S. (1999a) Red edge excitation of a deeply embedded membrane probe: Implications in water penetration. *J. Phys. Chem. B.* **103:** 8180-8185.

Chattopadhyay, A. & Mukherjee, S. (1999b) Depth-dependent solvent relaxation in membranes: wavelength-selective fluorescence as a membrane dipstick. *Langmuir* **15:** 2142-2148.

Cheifetz, S., Boggs, J.M. & Moscarello, M.A. (1985) Increase in vesicle permeability mediated by myelin basic protein: Effect of phosphorylation of basic protein. *Biochemistry* **24:** 5170-5175.

Chipman, D.M., Grisaro, V. & Sharon, N. (1967) The binding of oligosaccharides containing *N*-acetylglucosamine and *N*-acetylmuramic acid to lysozyme. *J. Biol. Chem.* **242:** 4388-4394.

Clermont, Y., Oko, R. & Hermo, L. (1993) Cell biology of mammalian spermiogenesis. *In* Cell and molecular biology of the testis (ed. Desjardans, C. & Ewing, J.) Oxford university Press. New York. pp. 332-376.

Collier, I.E., Wilhem, S.M., Eisen, A.Z., Marmer, B.L., Grant, G., Seltzer, A., Kronberger, J.L., He, A., Bauer, E.A. & Goldber, G.I. (1988) H-ras oncogene-transformed human bronchial epithelial cells (TBE-1) secrete a single metalloprotease capable of degrading basement membrane collagen. *J. Biol. Chem.* **263:** 6579-6587.

Constantine, K.L., Madrid, M., Bányai, L., Trexler, M., Patthy, L. & Linás, M. (1992) Refined solution structure and ligand-binding properties of PDC-109 domain b. A collagen-binding type II domain. *J. Mol. Biol.* **223:** 281-98.

Cullis, P.R., de Kruijff, B., Hope, M.J., Verkleji, A.J., Nayar, R., Farren, S.B., Tilcock, C., Madden, T.D. & Bally, M.B. (1983) Structural properties of lipids and their functional roles in biological membranes. Membrane fluidity in biology (Aloia, R.C. Ed.), Academic press, New York. Vol. 1, pp. 39-81

Cullis, P.R., Hope, M.J. & Tilcock, C.P.S. (1986) Lipid polymorphism and the roles of lipids in membranes. *Chem. Phys. Lipids* **40:** 127-144.

Danielli, J.F. & Davson, H. (1935) A contribution to the theory of permeability of thin films. *J. Cell. Comp. Physiol.* **5:** 495-508.

Darszon, A., Lievano, A. & Beltran, C. (1996) Ion channels: Key elements in gamate signaling. *Curr. Topics. Dev. Biol.* **34:** 117-167.

Davis, B.K., Byrne, R. & Bedigian, K. (1980) Studies on the mechanism of cpacitation: albumin-mediated changes in plasma membrane lipids during in vitro incubation of rat sperm cells. *Proc. Natl. Acad. Sci. USA* **77:** 1546-1550.

Dejter-Juszynski, M., Harpaz, N., Flowers, H.M. & Sharon, N. (1978) Blood group ABH-specific macroglycolipids of human erythrocytes: Isolation in high yield from a crude membrane glycoprotein fraction. *Eur. J. Bioch.* **83:** 363-378.

De Krester, D.M. & Kerr, J.B. (1994) The cytology of the testis. *In* physiology of reproduction (ed. Knobil, E & J. Neil), pp. 117-290, Raven Press, New York.

De Kruijff, B. (1987) Polymorphic regulation of membrane lipid composition. *Nature* **329:** 587-588.

Desnoyers, L. & Manjunath, P. (1992) Major proteins of bovine seminal plasma exhibit novel interactions with phospholipids. *J. Biol. Chem.* **267:** 10149-10155.

Desnoyers, L. & Manjunath, P. (1993) Interaction of a novel class of phospholipids-binding proteins of bovine seminal fluid with different affinity matrices. *Arch. Biochem. Biophys.* **305:** 341-349.

Eddy, E.M. & O'Brein, D.A. (1994) The spermatozoon. *In* The physiology of Reproduction, (Knobil, E and J.D. Neill J.D. eds.), Raven Press, New York, pp.29-78.

Eads, J.C., Mahoney, N.M., Vorobiev,S., Bresnick, A.R., Wen, K.K., Rubenstein, P.A., Haarer, B.K. & Almo, S.C. (1998) Structure determination and characterization of Saccharomyces cerevisiae profilin. *Biochemistry* **37:** 11171-11181.

Ehrenwald, E., Parks, J.E. & Foote, R.H. (1990) Bovine oviductal fluid components and their potential role in sperm cholesterol efflux. *Mol. Reprod. Dev.* **25:** 195-204.

Engelman, D.M., Goldman, A. & Steitz, T.A. (1982) The identification of helical segments in the polypeptide chain of Bacteriorhodospin. *Methods Enzymol.* **88:** 81-89.

Evans, G.D. & Hardison, W.G.M. (1985) Phospholipid, cholesterol, polypeptide and glycoprotein composition of hepatic endosome subfractions. *Biochem. J.* **232:** 33-36.

Esch, F.S., Ling, N.C., Bohlen, P., Ying, S.Y. & Guillemin, R. (1983) Primary structure of PDC-109, a major protein constituent of bovine seminal plasma. *Biochem. Biophys. Res. Commun.* **113:** 861-867.

Fawcett, D.W. (1975) The mammalian spermatozoon. *Dev. Biol.* **44:** 394-436.

Florman, H.M. (1994) Sequential focal and global elevations of sperm intracellular Ca^{2+} are initiated by the zona pellucida during acrosomal exocytosis. *Dev. Biol.* **165:** 152-164.

Florman, H.M., Arnoult, C., Kazan, I.G., Li, C. & O'Toole, C.M.B. (1998) A perspective on the control of mammalian fertilization by egg-activated ion channels in sperm: a tale of two channels. *Biol. Reprod.* **59:** 12-16.

Foster, D.L., Boublik, M. & Kaback, H.R. (1983) Structure of the lac carrier protein of *Escherichia coli. J. Biol. Chem.* **258:** 31-34.

Fraser, L.R. (1995) Cellular biology of capacitation and acrosome reaction. *Hum. Reprod. Suppl.* **10:** 22-30.

García-Hernández, E., Zubillaga, R.A., Chavelas-Adame, E.A., Vázquez-Contreras, E., Rojo-Domínguez, A. & Costas, M. (2003) Structural energetics of protein-carbohydrate interactions: Insights derived from the study of lysozyme binding to its natural saccharide inhibitors. *Protein Sci.* **12:** 135-142.

Gardas, A. (1976) A structural study on a macroglycolipid containing 22 sugars isolated from human erythrocytes. *Eur. Bioch.* **68:** 177-183.

Gasset, M., Saiz, J. L., Sanz, L., Gentzel, M., Töpfer-Petersen, E. & Calvete, J.J. (1997) Conformational features and thermal stability of bovine seminal plasma protein PDC-109 oligomers and phosphorylcholine-bound complexes. *Eur. J. Biochem.* **250:** 735–744.

Gasset, M., Magdaleno, L. & Calvete, J.J. (2000) Biophysical study of the perturbation of model membrane structure caused by seminal plasma protein PDC-109. *Arch. Biochem. Biophys.* **374:** 241–247.

Gennis, R.B. (1989) Biomembranes: Molecular Structure and Function. Springer-Verlag, New York.

Gerwig, G.L., Calvete, J.J., Töpfer-Petersen, E. & Vliegenthart, J.F. (1996) The structure of the *O*-linked carbohydrate chain of bovine seminal plasma protein PDC-109 revised by ^{1}H-NMR spectroscopy. A correction. *FEBS Lett.* **387:** 99-100.

Gledhill B.L. (1985) Cytometry of mammalian sperm. *Gamate Res.* **12:** 423-438.

Go, K.J. & Wolf, D.P. (1983) The role of sterols in sperm capacitation. *Adv. Lipid Res.* **20:** 317-330.

Gómez, J., Hilser, V. J., Xie, D. and Freire, E. (1995) The heat capacity of proteins. *Proteins* **22:** 404-412.

Gorter, E. & Grendel, F. (1925) On bimolecular layers of lipid on the chromacytes of the blood. *J. Exp. Med*. **41:** 439-443.

Green, D.E. & Fleischer, S. (1963) The role of lipids in mitochondrial electron transfers and oxidative phosphorylation. *Biochim. Biophys. Acta.* **70:** 554-582.

Greube, A., Müller, K., Töpfer-Petersen, E., Herrmann, A. & Müller, P. (2001) Influence of the bovine seminal plasma protein PDC-109 on the physical state of membranes. *Biochemistry* **40:** 8326-8334.

Grinvald, A. & Steinberg, I.Z. (1976) The fluorescence decay of tryptophan residues in native and denatured proteins. *Biochim. Biophys. Acta* **427:** 663-678.

Gross, R.W. (1985) Identification of plasmalogen as the major phospholipid constituent of cardiac sarcoplasmic reticulum. *Biochemistry* **24:** 1662-1668.

Guraya, S.S. (1965) Histochemical studies on spermateleosis in sheep, goat and buffalo. *Cellule* **65:** 367-378.

Guraya, S.S. (1971) Morphological and histochemical changes in the mitochondria during spermiogenesis in the opossum. *Acta Anat.* **179:** 120-125.

Guraya, S.S. (1973) Correlative histochemical and ultrastructural observations on the mitochondria of ram spermiogenisis. *Acta Anat.* **84:** 552-558.

Gwatkin, R.B.L. (1997) Fertilization mechanisms in man and mammals. New York: Plenum Press.

Harlos, K. & Eibl, H. (1980) Influence of calcium ions on phosphatidylglycerol. Two separate lamellar structures. *Biochemistry* **19:** 895-899.

Helenius, A. & Simons, K. (1975) Solubilization of membranes by detergents. *Biochim. Biophys. Acta* **415:** 29-79.

Harrison, R.A.P. (1996) Capacitation mechanisms, and the role of capacitation as seen in eutherian mammals. *Reprod. Fertil. Dev.* **8:** 581-596.

Henderson, R. & Unwin, P.N.T. (1975) Three-dimensional model of purple membrane obtained by electron microscopy. *Nature* **257:** 28-32.

Hirschberg, C.B. & Snide, M.D. (1987) Topography of glycosylation in the rough endoplasmic reticulum and golgi apparatus. *Ann. Rev. Biochem.* **56:** 63-87.

ITC data analysis in Origin®, Tutorial guide 7.0, Microcal™, Northampton, MA, USA, 2002, 99 pp.

Jacobson, K. (1983) Lateral diffusion in membranes. *Cell Motility* **3:** 367-373.

Jain, M.K. & White, H.B. 3rd. (1977) Long-range order in biomembranes. *Adv. Lipid Res.* **15:** 1-60.

Jain, M.K. (1983) Nonrandom lateral organization in bilayers and biomembranes. *In* Membrane fluidity in Biology (Aloia, R.C. Ed.), Academic press, New York. Vol. 1, pp. 1-37.

Jain, M.K. (1988) Introduction to biological membranes. Wiley, New York.

Johnson, M.H. (1970) Selective damage to spermatogenic cells of high antigenicity during auto-allergic aspermatogenisis. *J. Pathol*. **102:** 131-138.

Katz, D.F. & Drobnis, E.Z. (1990) Analysis and interpretation of the forces generated by spermatozoa. *In:* Bavister, B.D., Commins, J., Roldan, E.R.S., eds. Fertilization in mammals. Norwell, MA: Sereno symposium: pp. 125-137.

Kemme, M. & Scheit, K.H. (1988) Cloning and sequence analysis of a cDNA from seminal vesicle tissue. *Nucleosides Nucleotides* **7:** 693-697.

Knowles, P.F. & Marsh, D. (1991) Magnetic resonance of membranes. *Biochem. J.* **264:** 625-641.

Lakowicz, J. R. (1999) Principles of Fluorescence Spectroscopy, 2nd Edition, Kluwer Academic Publishers, New York..

Langlais, J. & Roberts, K.D. (1985) A molecular membrane model of sperm capacitation and the acrosome reaction of mammalian spermatozoa. *Gamete Res.* **12:** 183-224.

Lefebvre, R. & Suarez, S.S. (1996) Effect of capacitation on bull sperm binding to homologous oviductal epithelium. *Biol. Reprod.* **54:** 575-582.

Lehrer, S. S. (1971) Solute perturbation of protein fluorescence. The quenching of the tryptophyl fluorescence of model compounds and of lysozyme by iodide ion. *Biochemistry* **10:** 3254-3263

Lenard, J. & Singer, S.J. (1966) Protein conformation in cell membrane preparations as studied by optical rotatory dispersion and circular dichroism. *Proc. Natl. Acad. Sci. USA* **56:** 1828-1835.

Lievano, A., Santi, C.M., Serrano, J., Trevano, C.L., Bellve, A.R., Hernandez-Cruz, A. & Dorszon. A. (1996) A T-type Ca^{2+} channels and α_{1E} expression in spermatogenic cells and their possible relevance to the sperm acrosome reactions. *FEBS Lett.* **388:** 150-154.

Lobel, P., Dahms, N.M. & Kornfeld, S. (1988) Cloning and sequence analysis of the cation-independent mannose 6-phosphate receptor. *J. Biol. Chem.* **263:** 2563-2570.

Makhatadze, G.I. & Privalov, P.L. (1990) Heat capacity of proteins. I. Partial molar heat capacity of individual amino acid residues in aqueous solution: hydration effect. *J. Mol. Biol.* **213:** 375-384.

Manjunath, P., Sairam, M.R. & Uma, J. (1987a) Purification of four gelatin-binding proteins from bovine seminal plasma by affinity chromatography. *Biosci. Rep.* **7:** 231-238.

Manjunath, P. & Sairam, M.R. (1987b) Purification and biochemical characterization of three major acidic proteins (BSP-A1, BSP-A2 and BSP-A3) from bovine seminal plasma. *Biochem. J.* **241:** 685-692.

Manjunath, P., Baillargeon, L., Marcel, Y.L., Seidah, N.G., Chretien, M. & Chapdelaine, A. (1988) Diversity of novel proteins in gonadal fluids. In: McKerns K.W, Chrétien M (eds) Molecular biology of brain and endocrine peptidergic systems. Plenum Press, New York, pp. 259-273.

Manjunath, P., Marcel, Y.L., Uma, J., Seidah, N.G., Chretien, M. & Chapdelaine, A. (1989) Apolipoprotein A-I binds to a family of bovine seminal plasma proteins. *J. Biol. Chem.* **264:** 16853-16857.

Manjunath, P., Chandonnet, L., Leblond, E. & Desnoyer, L. (1994) Major proteins of bovine seminal vesicles bind to spermatozoa. *Biol. Reprod.* **50:** 27-37.

Manjunath, P., Nauc, V., Bergeron, A. & Menard, M. (2002) Major proteins of bovine seminal plasma bind to the low density lipoprotein fraction of hen's egg yolk. *Biol. Reprod.* **67:** 1250-1258.

Manjunath, P. & Thérien, I. (2002) Role of seminal plasma phospholipid-binding proteins in sperm membrane lipid modification that occurs during capacitation. *J. Reprod. Immunol.* **53:** 109-119.

Mann, T. & Lutwalk-Mann, C. (1981) Male reproductive function and semen, Springer, Berlin Heidelberg, New York.

Marsh, D. (1990) Lipid-protein interactions in membranes. *FEBS Lett.* **268:** 371-375.

Mathews, C.K., van Holde, K.E. & Ahern, K.G. (2003) Biochemistry, 3 rd edition, Pearson education. Chapter 10, pp: 320.

Matulis, D. & Lovrien, R.E. (1998) 1-anilino-8-naphthalene sulfonate anion-protein binding depends primarily on ion pair formation. *Biophys. J.* **74:** 1-8.

McMullen, B.A. & Fujikawa, K. (1985) Amino acid sequence of the heavy chain of human alpha-factor XIIa (activated Hageman factor). *J. Biol. Chem.* **260:** 5328-5341.

Meizel, S. (1985) Molecules that initiate or help stimulate the acrosome reaction by their interaction with the mammalian sperm surface. *Am. J. Anat.* **174:** 285-302.

Miller, D.J., Winer, M.A. & Ax, R.L. (1990) Heparin-binding proteins from seminal plasma bind to bovine spermatozoa and modulate capacitation by heparin. *Biol. Reprod.* **42:** 899-915.

Moreau, R., Thérien, I., Lazure, C. & Manjunath, P. (1998) Type II domains of BSP-A1/-A2 proteins: binding properties, lipid efflux, and sperm capacitation potential. *Biochem. Biophys. Res. Commun.* **246:** 148-154.

Moreau, R. and Manjunath, P. (1999) Characterization of lipid efflux particles generated by seminal phospholipid-binding proteins. *Biochim. Biophys. Acta* **1438:** 175-184.

Morgan, D.O., Edman, J.C., Standring., D.N., Fried, V.A., Smith, M.C., Roth, R.A. & Rutter, W.J. (1987) Insulin-like growth factor II receptor as a multifunctional binding protein. *Nature* **329:** 301-307.

Müller, P., Erlemann, K-R., Müller, K., Calvete, J.J., Töpfer- Petersen, E., Marienfeld, K. & Herrmann, A. (1998) Biophysical characterization of the interaction of bovine seminal plasma protein PDC-109 with phospholipid vesicles. *Eur. Biophys. J.* **27:** 33–41.

Müller, P., Greube, A., Töpfer-Petersen, E. & Herrmann, A. (2002) Influence of the bovine seminal plasma protein PDC-109 on cholesterol in the presence of phospholipids. *Eur. Biophys. J.* **31:** 438–447.

O'Brien, R., Ladbury, J.E. & Chowdry, B.Z. (2000) Isothermal titration calorimetry of biomolecules. *In* Protein-ligand interactions: hydronomics and calorimetry Ed, Harding, S. E. & Chowdry, B. Z, Oxford Iniversity Press.

Oliphant, G., Reynold, A.B. & Thomas, T.S. (1985) Sperm surface components involved in the control of the acrosome reaction. *Am. J. Anat.* **174:** 269-283.

Oshima, A., Nolan, C.M., Kyle, J.W., Grubb, J.H., & Sly, W.S. (1988) The human cation-independent mannose 6-phosphate receptor. Cloning and sequence of the full-length cDNA and expression of functional receptor in COS cells. *J. Biol. Chem.* **263:** 2553-2562.

Patrat, C., Serres, C. & Jouannet, P. (2000) The acrosome reaction in human spermatozoa. *Biol. Cell* **92:** 255-266.

Phillips, D.M. (1975) In: Hamilton D.W, Greep R.O (eds) Handbook of physiology, Sect 7: Endocrinology, vol V. Am Physiol Soc, Washington DC. pp 405-420.

Ramakrishnan, M., Anbazhagan, V., Pratap, T.V., Marsh, D. & Swamy, M.J. (2001) Membrane insertion and lipid-protein interactions of bovine seminal plasma protein, PDC-109 investigated by spin label electron spin resonance spectroscopy. *Biophys. J.* **81:** 2215-2225.

Richardson, S.H., Hultin, O.H. & Fleischer, S. (1964) Interactions of mitochondrial structural protein with phospholipids. *Arch. Biochem. Biophys.* **105:** 254-260.

Robertson, J.D. (1959) The ultrastructure of cell membranes and their derivatives. *Biochemical Society Symposium* **16:** 3-43.

Roldan, E.R.S., Murase, T. & Shi, Q.X. (1994) Exocytosis in spermatozoa in response to progesterone and zona pellucida. *Science* **266:** 1578-1581.

Roth, J. (1987) Subcellular organization of glycosylation in mammalian cells. *Biochim. Biophys. Acta* **906:** 405-436.

Sato, N. & Oura, C. (1984) The fine structure of the neck region of cat spermatozoa. *Okajimas Folica Anat Jpn.* **61:** 267-285.

Scheit, A.K.H., Kemme, M., Aumuller, G., Seitz, J., Hagendorff, G. & Zimmer, M. (1988) The major protein of bull seminal plasma: biosynthesis and biological function. *Biosci. Rep.* **8:** 589-608.

Segrest, J.P., Kahane, I.., Kackson, R.L. & Marchesi, V.T. (1973) Major glycoprotein of the human erythrocyte membrane: Evidence for an amphipathic structure. *Arch. Biochem. Biophys.* **155:** 167-183.

Seidah, N.G., Manjunath, P., Rochemont. J., Sairam, M.R. & Chretien, M. (1987) Complete amino acid sequence of BSP-A3 from bovine seminal plasma. Homology to PDC-109 and to the collagen-binding domain of fibronectin. *Biochem. J.* **243:** 195-203.

Shivaji, S., Scheit, K.H. & Bhargava, P.M. (1990) Proteins of seminal plasma. Wiley, New York.

Sidhu, K.S. & Guraya, S.S. (1985) Buffalo Bull Semen Morphology. USG Ludhiana, India, pp 27-28.

Simons, K. & van Meer, G. (1988) Lipid sorting in epithelial cells. *Biochemistry* **23:** 6197-6202.

Simons, K., and Toomre, D. (2000) Lipid rafts and signal transduction. *Nat. Rev. Mol. Cell Biol.* **1**: 31-39.

Singer, S.J. (1974) The molecular organization of membranes. *Ann. Rev. Bioch.* **43:** 805-833.

Singer, S.J. & Nicolson, G.L. (1972) The fluid mosaic model of the structure of cell membrane. *Science* **175:** 720-731.

Skudlarek, M.D., Tulsiani, D.R.P., & Orgebin-Crist, M.-C. (1992) Rat epididymal luminal fluid acid beta-D-galactosidase optimally hydrolases glycoprotein substrate at neutral pH. *Biochem J.* **286:** 907-914.

Snell, W.J. & White, J.M. (1996) The molecules of mammalian fertilization. *Cell* **85:** 629-637.

Srinivas, V. R., Reddy, G. B. and Surolia, A. (1999) A predominantly hydrophobic recognition of H-antigenic sugars by winged bean acidic lectin: a thermodynamic study. *FEBS Lett.* **450:** 181-185.

Sultan, N.A.M. & Swamy, M.J. (2005) Energetics of carbohydrate binding to *Momordica charantia* (bitter gourd) lectin: An isothermal titration calorimetric study. *Arch. Biochem. Biophys.* **437:** 115-125.

Swamy, M.J., Marsh, D., Anbazhagan, V. & Ramakrishnan, M. (2002) Effect of cholesterol on the interaction of seminal plasma protein, PDC-109 with phosphatidylcholine membranes. *FEBS Lett.* **528:** 230-234.

Swamy, M.J. (2004) Interaction of bovine seminal plasma proteins with model membranes and sperm plasma membranes. *Curr. Sci.* **87:** 203-211.

Swamy, M.J., Tarafdar, P.K. & Damai, R.S. (2007) Structure of Biological Membranes and Lipid-Protein Interactions. *Annual Convention Souvenir of the Andhra Pradesh Akademi of Sciences*, pp. 18-21.

Tanford, C. & Reynolds, J.A. (1976) Characterization of membrane proteins in detergent solutions. *Biochim. Biophys. Acta* **457:** 133-170.

Tannert, A., Kurz, A., Erlemann, K.R., Müller, K., Herrmann, A., Schiller, J., Manjunath, P. & Müller, P. (2007) The bovine seminal plasma protein PDC-109 extracts phosphorylcholine-containing lipids from the outer membrane leaflet. *Eur. Biophys. J.l* **36:** 461-475.

Tannert, A., Töpfer-Petersen, E., Herrmann, A., Müller, K., & Müller, P. (2007) The lipid composition modulates the influence of the bovine seminal plasma protein PDC-109 on membrane stability. *Biochemistry* **46:** 11621-11629.

Terstappen, G.C. & Reggiani A. (2001) In silico research in drug discovery. *Trends. Pharmacol. Sci.* **22:** 23-26.

Thérien, I., Bleau, G. & Manjunath, P. (1995) phosphatidylcholine-binding proteins of bovine seminal plasma modulate sperm capacitation of spermatozoa by heparin. *Biol. Reprod.* **52:** 1372-1379.

Thérien, I., Moreau, R. & Manjunath, P. (1998) Major proteins of bovine seminal plasma and high-density lipoprotein induce cholesterol efflux from epididymal sperm. *Biol. Reprod.* **59:** 768-776.

Thomas, C.J., Anbazhagan, V., Ramakrishnan, M., Sultan, N., Surolia, I. & Swamy, M.J. (2003) Mechanism of membrane binding by the bovine seminal plasma protein, PDC-109. A surface plasmon resonance study. *Biophys. J*. **84:** 3037-3044.

Thompson, T.E. & Tillack, T.W. (1985) Organization of glycosphingolipids in bilayers and plasma membranes of mammalian cells. *Annu. Rev. Biophys. Biophys. Chem.* **14:** 361-386.

Torrecillas, A., Laynez, J., Menédez., Corbálan-García, S. & Gomez-Fernández. (2004) Calorimetric study of the interaction of the C2 domains of classical protein kinase C isoenzymes with Ca^{2+} and phospholipids. *Biochemistry* **43:** 11727-11739.

Tulsiani, D.R.P., Abou-Haila, A., Loeser, C.R. & Pereira, B.M.J. (1998a) The biological and functional significance of the sperm acrosome and acrosomal enzymes in mammalian fertilization. *Exp. Cell. Res.* **240:** 151-164.

Tulsiani, D.R.P., Orgebin-Crist, M.-C, & Skudlarek, M.D. (1998b) The epididymis: cellular and molecular aspects. *J. Reprod. Fertil. suppl.* **53:** 85-97.

VP-ITC Instruction manual (2001) MicroCal Inc, Northampton, MA, USA.

Wah, D.A., Fernández-Tornero, C., Sanz, L., Romero, A. & Calvete, J.J. (2002) Sperm coating mechanism from the 1.8 Å crystal structure of PDC-109-phosphorylcholine complex. *Structure* **10:** 505–514.

Wallach, D.F.H. & Zahler, P.H. (1966) Protein conformation in cellular membranes. *Proc. Natl. Acad. Sci. USA* **56:** 1552-1559.

Ward, C.R. & Kopf, G.S. (1993) Molecular events mediating sperm activation. *Dev. Biol.* **104:** 287-296.

Ward, C.R., Storey, B.T. & Kopf, G.S. (1992) Activation of Gi protein in mouse sperm membrane by solubilized proteins of the zona pellucida, the ovum's extracelular matrix. *J. Biol. Chem.* **267:** 14061-14607.

Ward, C.R., Storey, B.T. & Kopf G.S. (1994) Selective activation of Gi1 and Gi2 in mouse sperm by the zona pellucida the ovum's extracellular matrix. *J. Biol. Chem.* **269:** 13254-13258.

Wassarman, P.M. (1987) The biology and chemistry of fertilization. *Science* **235:** 553-560.

Wassarman, P.M. (1999) Mammalian fertilization: Molecular aspects of gamete adhesion, exocytosis, and fusion. *Cell* **96:** 175-183.

Watson, P.E. (1981) The effects of cold shock on sperm cell membranes, in *Effects of low temperature on biological membranes* (Morris, G.J. & Clarke, D., eds) pp-189-219, Academic press, London.

Wieprecht, T., Beyermann, M. & Seelig, J. (1999) Binding of antibacterial magainin peptides to electrically neutral membranes: Thermodynamics and structure. *Biochemistry* **38**: 10377-10387.

Wilhelm, S.M., Collier, I.E., Marner, B.L., Eisen, A.Z., Grant, G.A. & Goldberg, G.I. (1989) SV40-transformed human lung fibroblasts secrete a 92-kDa type IV

collagenase which is identical to that secreted by normal human macrophages. *J. Biol. Chem*. **264:** 17213-17221.

Wiseman, T., Williston, S., Brandts, J.F. & Lin, L.N. (1989) Rapid measurement of binding constants and heats of binding using a new titration calorimeter. *Anal. Biochem.* **179:** 131-137.

Visconti, P.E., Bailey, J.L., Moore, G.D., Pan. D., Olds-Clarke, P. & Kopf, G.S. (1995) Capacitation of mouse spermatozoa: Correlation between the capacitation state and protein tyrosine phosphorylation. *Development* **121:** 1129-1137.

Visconti, P.E., Calantino-Hormer, H., Moore, G. D., Bailey, J.L., Ning, X., Fornes, M. and Kopf, G. S. (1998) The molecular basis of sperm capacitation. *J. Androl.* **19:** 242–248.

Yanagamachi, R. (1994) Mammalian fertilization. In: Knobil, E., Neill J. D. (eds.), the physiology of reproduction. 2nd ed. New York: Raven Press, pp.189-317.

Curriculum vitae

Curriculum vitae

Rajani Swarnalatha,. D. was born in Sullurpeta in 1978. She did her schooling at Sullurpet, and Jawahar Navodaya Vidyalaya (Class VI to XII), Nellore. She joined Sri VLCC Govt. Degree Ccollege, Sullurpeta, and obtained her B.Sc. degree (Chemistry, Botany and Zoology) in 1999. She received her M.Sc. degree (Biochemistry) in 2001 from Sri Venkateswara University, Tirupati. She joined for Ph.D at School of Chemistry, University of Hyderabad in 2002. She was qualified as JRF (2001) and SRF (2004) by Council of Scientific and Industrial Research, India. Besides lipid-protein interactions, her areas of research interests include vaccine development and extraction of drugs from natural products.

List of Publications

1. Goel**,** M., **Damai**, **R.S**., Sethi, D.K., Kaur, K.J., Maiya, B.G., Swamy, M.J. &. Salunke, D.M (2005) Crystal structures of the PNA-porphyrin complex in the presence and absence of lactose: Mapping the conformational changes on lactose binding, interacting surfaces, and supramolecular aggregations. *Biochemistry* **44:** 5588-5596.

2. Swamy, M.J., Tarafdar, P.K. & **Damai, R.S.** (2007) Structure of Biological Membranes and Lipid-Protein Interactions. *Annual Convention Souvenir of the Andhra Pradesh Akademi of Sciences*, pp. 18-21.

3. Anbazhagan, V., **Damai, R.S.,** Paul, A. & Swamy, M.J. (2008) Interaction of the major protein from bovine seminal plasma, PDC-109 with phospholipids membranes and soluble ligands investigated by fluorescence approaches, *Biochim. Biophys. Acta* (2008), doi:10.1016/j.bbapap.2008.03.002.

4. **Damai, R.S.** & Swamy, M.J. (2008) Fluorescence spectroscopic studies on the interaction of domain B of PDC-109 with phospholipid membranes and soluble ligands. (*to be communicated*).

5. Anbazhagan, V., **Damai**, **R.S.** & Swamy, M.J. (2008) Interaction of the major protein from bovine seminal plasma, PDC-109 with heparin. Isothermal titration calorimetric and fluorescence spectroscopic studies. (*Manuscript under preparation*).

6. **Damai**, **R.S**., Anbazhagan, V. & Swamy, M.J. (2008) A ^{31}P-NMR study of interaction of PDC-109, a choline-specific protein from bovine seminal plasma, with phospholipid membranes. (*Manuscript under preparation*).

7. **Damai**, **R.S**., Tarafdar, P.K &. Swamy, M.J. (2008) Isothermal titration calorimetric studies of the binding of *O*-acylcholines to PDC-109, the major protein from bovine seminal plasma. (*Manuscript under preparation*).

8. **Damai**, **R.S.** & Swamy, M.J. (2008) Fluorescence and CD spectroscopic studies on the interaction hydrophobic ligands to PDC-109 and its domain B. (*Manuscript under preparation*).

Symposia attended

1. Paper presented (**Poster**) at the second Indian Symposium of the Protein Society- Protein Structure and Function, October 28-30, (2004) held at Indian institute of Technology, Mumbai (IITB), India. "Modulation of the structure of DMPC membranes by PDC-109, the major protein from bovine seminal plasma. A ^{31}P-NMR Study"
Rajani S. Damai, V. Anbazaghan and M. J. Swamy

2. Paper presented (**Poster**) in the CHEMFEST-2005, School of Chemistry, University of Hyderabad in March (2005). "Interaction of bovine seminal plasma protein, PDC-109 with dimyristoylphosphatidylcholone. A ^{31}P-NMR Study".
Rajani S. Damai, V. Anbazaghan and M. J. Swamy

3. Paper presented (**Poster**) in the CHEMFEST-2006, School of Chemistry, University of Hyderabad in 04, March (2006). "Isothermal titration Calorimetric studies of the binding of heparin to PDC-109, a major protein from bovine seminal plasma".
Rajani S. Damai, V. Anbazaghan and M. J. Swamy

4. Paper presented **(Oral & Poster)** in the CHEMFEST-2007, School of Chemistry, University of Hyderabad in 09-10, March (2006). "Biophysical studies of the interaction of PDC-109, the major protein from bovine seminal plasma with choline phospholipids and heparin".
    Rajani S. Damai and M. J. Swamy

5. Participated in International conference on "Molecular Cellular Biology & Therapeutics of HIV and Associated Viral Infections" held at University of Hyderabad, Hyderabad, India. (January 12-14, 2007).